Explosions

Phenomenology, Dynamics and Mitigation

Dr Arief Dahoe

Explosion, Hydrogen Safety and Combustion Scientist

Dutch Armed Forces

Knowledge Center for Explosion and Hydrogen Safety

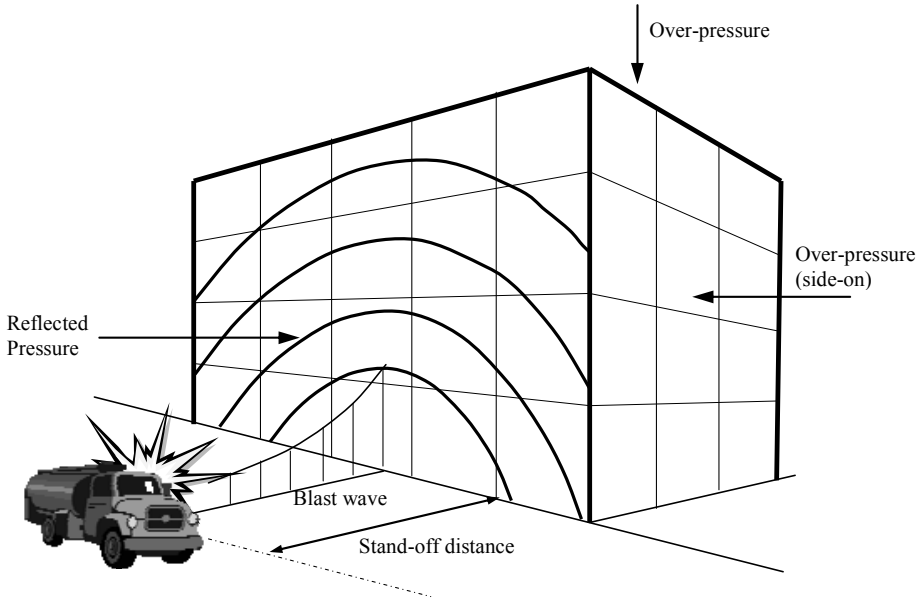
http://www.explosionsolutions.org/kcehs/

ACKNOWLEDGEMENTS

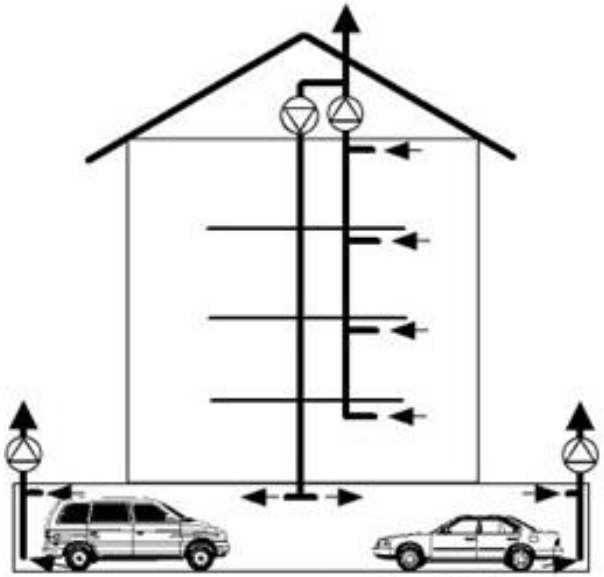
UNIVERSITY OF CAMBRIDGE

TU Delft

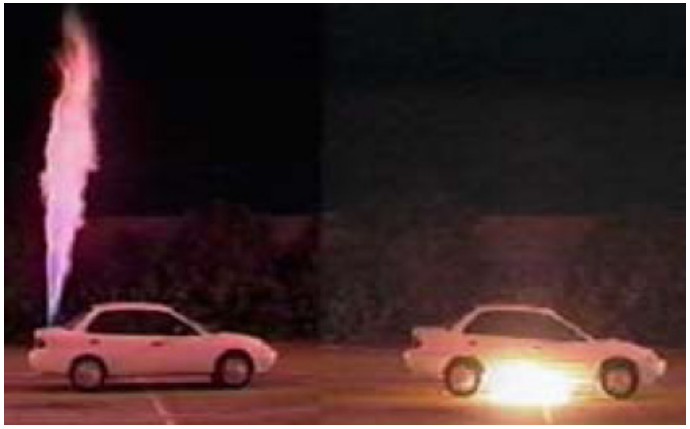
Delft University of Technology



Unconfined explosion: Blast-structure interaction [1].

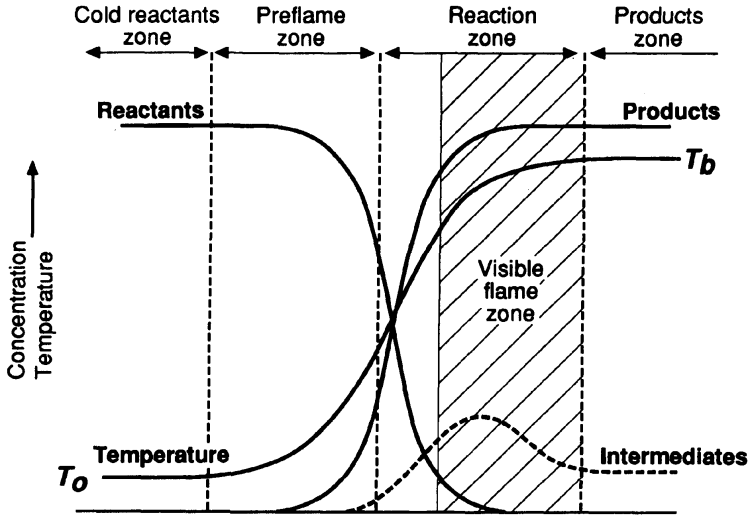


Confined explosion:
Garage beneath building.

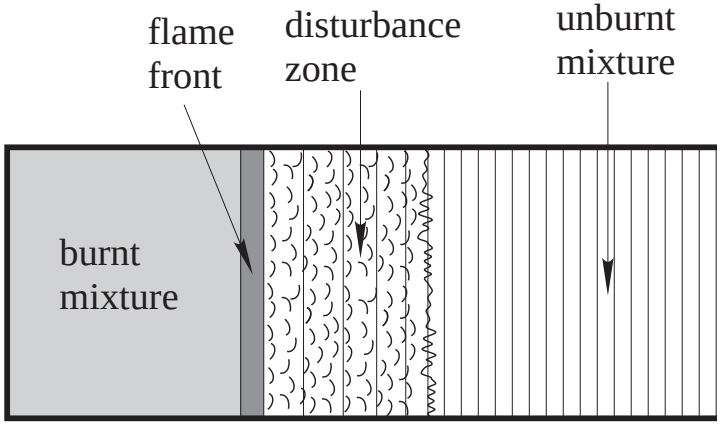


Hydrogen versus Gasoline.

Deflagration and Detonation

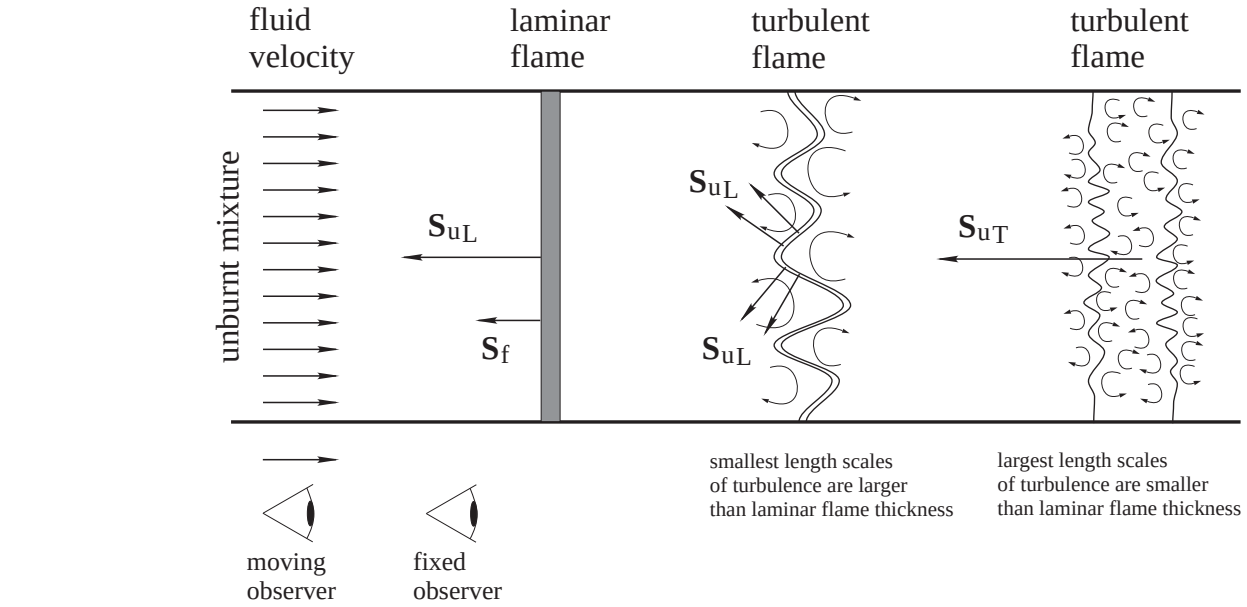


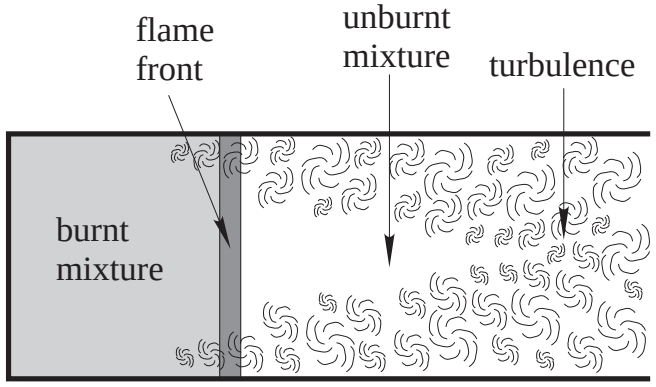
Deflagration

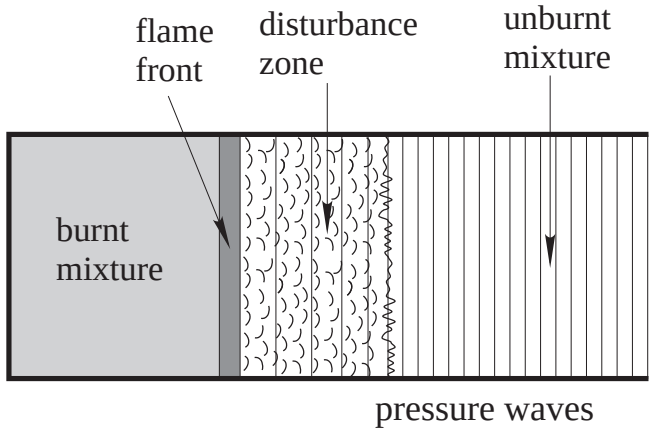


Detonation

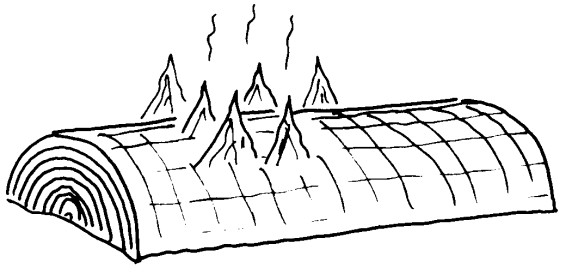
Flame Propagation: Laminar and Turbulent



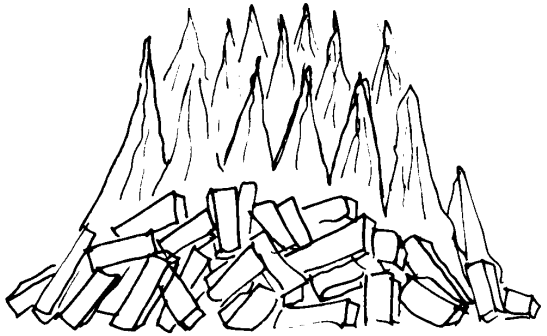




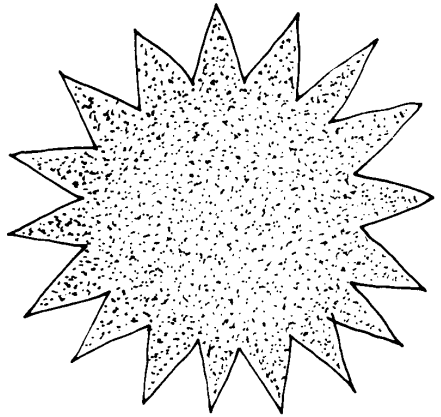
Gas Explosions versus Dust Explosions



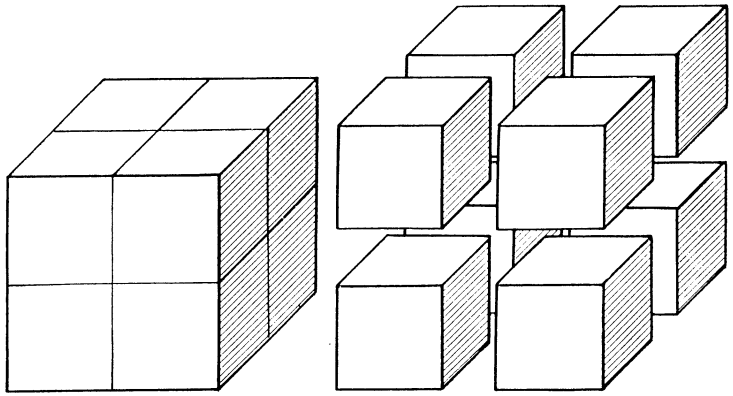
(a) SLOW COMBUSTION



(b) FAST COMBUSTION



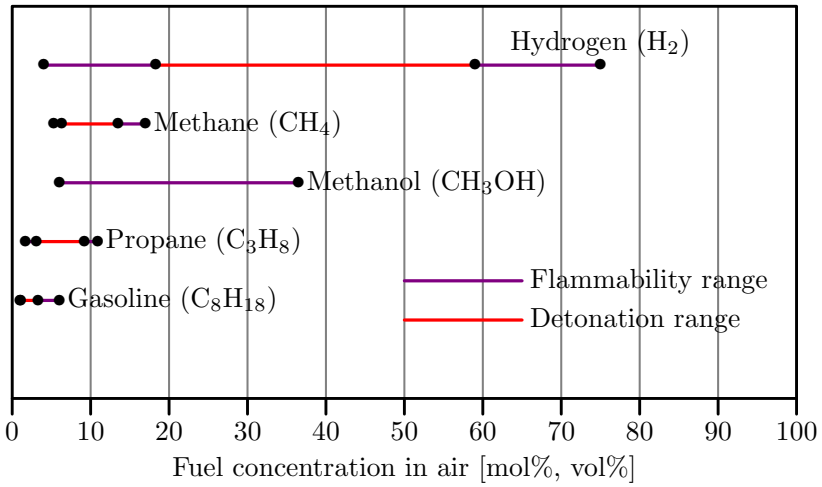
(c) EXPLOSION



From Ref. [2].

Ignition and combustion properties. Initial conditions: 25 °C and 101.325 kPa.

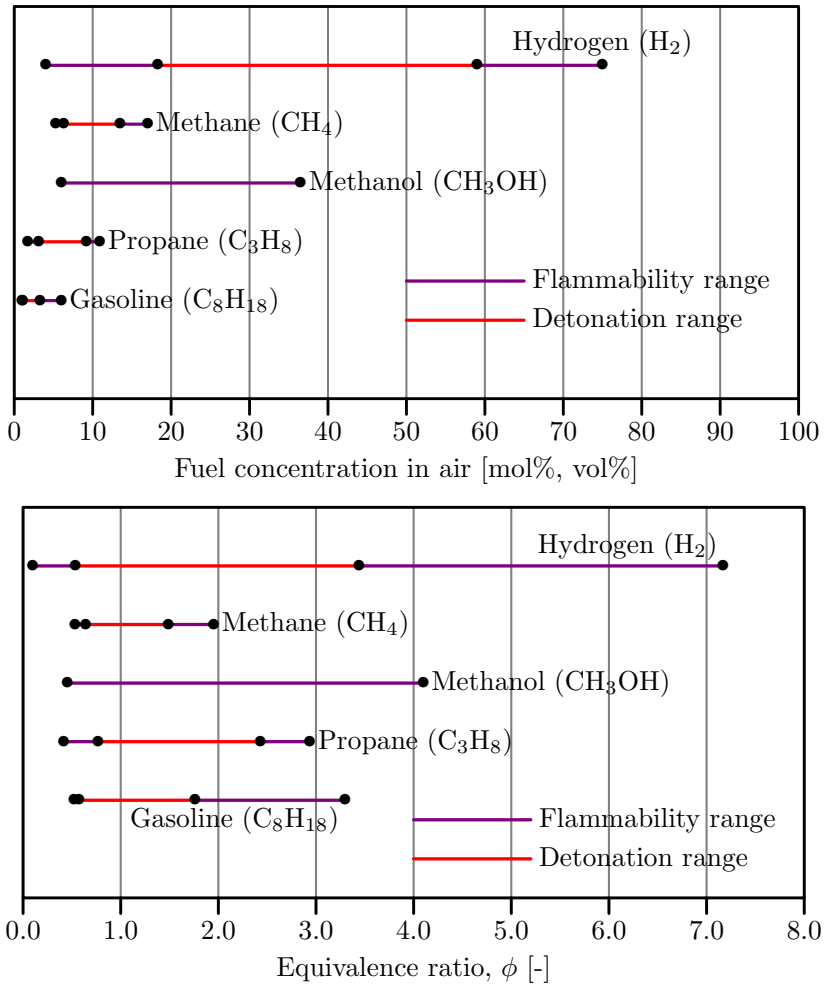
Fuel	**Lower flamm. limit vol. %**	**Lower deton. limit vol. %**	**Stoich. fuel conc. vol. %**	**Upper deton. limit vol. %**	**Upper flamm. limit vol. %**	**Minim. ign. energy mJ**	**Auto-ign. temp. °C**	**Lamin. burn. veloc. cm s^{-1}**
Hydrogen (H_2)	4.0	18.3	29.5	59.0	75.0	0.017	585	225
Methane (CH_4)	5.3	6.3	9.5	13.5	17.0	0.274	537	37
Methanol (CH_3OH)	6.0	-	12.3	-	36.5	0.174	385	48
Propane (C_3H_8)	1.7	3.1	4.0	9.2	10.9	0.240	450	47
Gasoline (C_8H_{18})	1.0	1.1	1.9	3.3	6.0	0.240	215	30



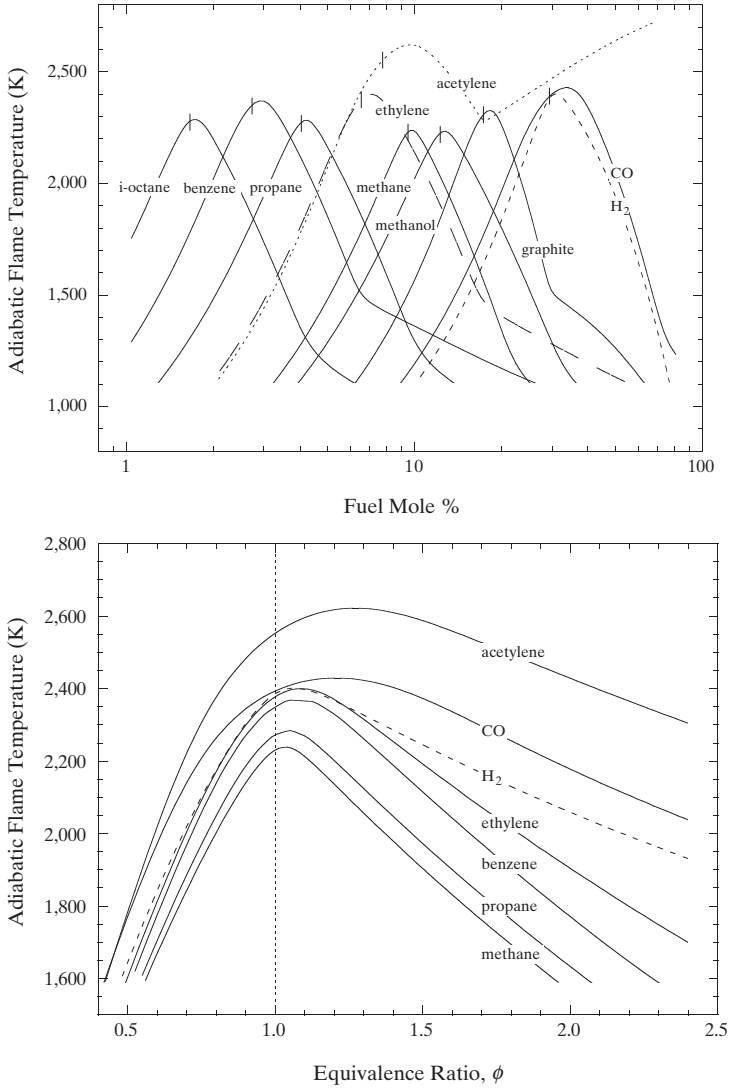
Flammability and detonation limits [3].



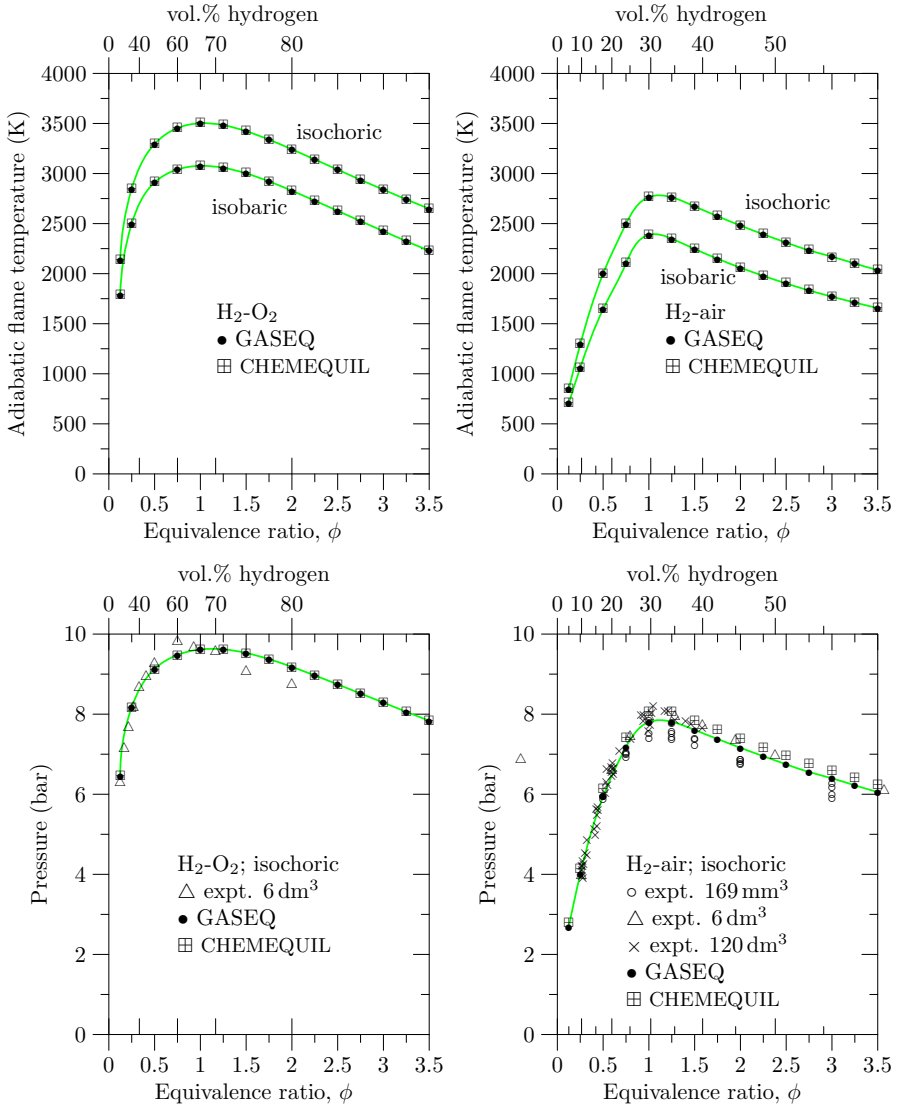
Domestic hydrogen boiler.



Flammability and detonation limits [3].
Initial conditions: 1 bar and 298.15 K.



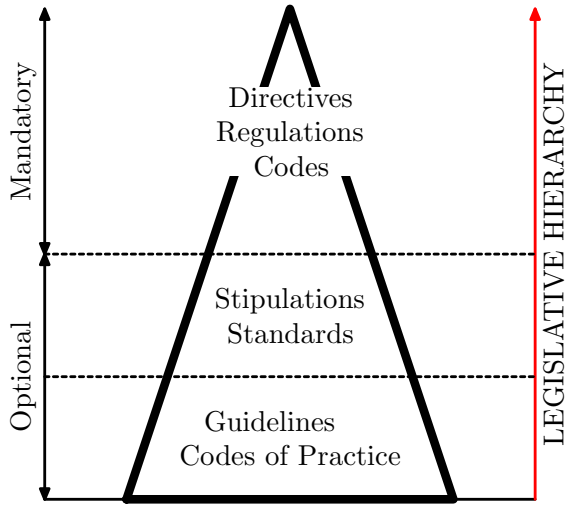
Adiabatic flame temperature as a function of mixture composition [4].
Initial conditions: 1 bar and 298.15 K.



Isobaric Flame Temperature
Isochoric Flame Temperature

Comparison between the adiabatic flame temperature, T_f^{ad}, of hydrogen-oxygen and hydrogen-air mixtures calculated by CHEMEQUIL and GASEQ. Experimental data: $\times$ 120 dm^3 explosion vessel [5]; $\triangle$ 6 dm^3 explosion vessel [6]; $\circ$ 169 cm^3 explosion vessel [7].

Regulations, Codes and Standards



• Directives and regulations are the law. They represent the State's position on what is acceptable and what is not. They impose duties, responsibilities and accountabilities on people and organisations. Consequently, regulations are at the top of the hierarchy of things of which you need to take heed. Make sure that you are aware of the regulations pertaining to the work that you are proposing to carry out.

Directive 2014/34/EU: ATEX 114 [8]
Directive 1999/92/EC: ATEX 153 [9]

• Codes are laws written and enacted by the legislative branch of government. But unlike directives and regulations they require industry consensus or approval by a knowledgeable body to be put into effect.
• Standards are intended to aid designers and engineers with ensuring that the piece of technology needed to fulfil a certain function is appropriate and has been properly designed and manufactured.
• There is an additional, special form of guidance issued by the State: the so-called 'Approved Code of Practice' (e.g. COMAH [10]). If you follow this guidance then you will comply with the law. If you don't do it this way, then the onus is on you to prove that your way assures at least the same level of safety as that achieved through following the guidance.

ATEX 114
Objectives Pertaining to Gas and Dust Explosion Hazards

PREVENT FORMATION EXPLOSIVE MIXTURES	ELIMINATE IGNITION SOURCES	MINIMIZE INJURY AND DAMAGE
• Implement a hazardous dust inspection, housekeeping, testing and control program • Use proper dust collection systems and filters • Apply inertization • Minimize the escape of flammable gases and dust from process equipment or ventilation systems • Use surfaces that minimize dust accumulation and facilitate cleaning • Provide access to all hidden areas to permit inspection • Inspect for dust residues in open and hidden areas at regular intervals • If ignition sources are present, use cleaning methods that do not generate dust clouds • Use only vacuum cleaners approved for dust collection • Locate relief valves away from dust deposits	• Use appropriate electrical equipment and wiring methods • Control static electricity, including bonding of equipment to ground • Control smoking, open flames, and sparks • Control mechanical sparks and friction • Use separator devices to remove foreign materials capable of igniting combustibles from process materials • Separate heated surfaces and heating systems from dusts • Separate heated surfaces and heating systems from flammable gas mixtures • Select and use industrial trucks properly • Use cartridge-activated tools properly • Use an ignition preventive maintenance program	• Separation of the hazard (isolate with distance) • Segregation of the hazard (isolate with a barrier) • Deflagration isolation/venting • Pressure relief venting for equipment • Direct vents away from work areas • Specialized fire suppression systems • Explosion protection systems • Spark/ember detection for suppression activation • Develop an emergency action plan • Maintain emergency exit routes

ATEX 114
Equipment Groups and Catergories [8]

	Group I		Group II		
	Category M1	Category M2	Category 1	Category 2	Category 3
Level of protection	Very High	High	Very High	High	Normal
Endangered by firedamp and/or combustible dust	Is endangered	Is likely to be endangered			
Danger by gas, vapour, mist or air/dust mixtures			Long periods or frequently	Likely to occur	Unlikely to occur, and if they do occur, only infrequently and for a short period
Required protection	2 independent means / Or assured for 2 faults occuring independently	Also in case of more severe operating conditions	2 independent means / Or assured for 2 faults occuring independently	Even in the event of frequently occuring disturbances of fault	Only during normal operation
Usage	Mining & mining surface installations	Mining & mining surface installations	Gas: Zone 0, 1 & 2	Gas: Zone 1 & 2	Gas: Zone 2
			Dust: Zone 20, 21 & 22	Dust: Zone 21 & 22	Dust: zone 22

ATEX 114
Gas Groups and Dust Groups [8]

Explosion Group	Temperature Class / Maximum Surface Temperature Allowed					
Ignition Temp	T1	T2	T3	T4	T5	T6
	>450°	>300°	>200°	>135°	>100°	>85°
I	Methane	l-amyl acetate	Amyl alcohol	Acetaldehyde		
IIA Ignition energy higher than 0.18mJ	Acetone	n-butane	Petrols			
	Ammonia	n-butanol	Diesel Oils			
	Benzene	1-butene	Heating Oils			
	Ethylacetate	Propylacetate	n-hexane			
	Methane	l-propanol				
	Methanol	Vinyl Chloride				
	Propane					
	Toluene					
IIB Ignition energy lower than 0.18mJ	Cyanide Hydrogen	Butadleno	Dimethylether	Diethylether		
	Dioxane	Ethyloglicol				
	Coal Gas (lighting gas)	Ethylene Oxide	Sulfide Hydrogen			
IIC Ignition energy lower than 0.18mJ	Hydrogen	Acetylene				Carbon Disulphur

Dust Group	Types of Dust	Representative Dust
IIIC	Conductive Dusts	Graphite Powder
		Toner
IIIB	Non-Conductive Dusts	Milk Powder
		Powdered Sugar
		Flour
IIIA	Fibers	Saw Dust
		Tobacco

EXPLOSION SEVERITY CLASSIFICATION

Class	K_{St}-value ($\mathrm{bar\,m\,s^{-1}}$)	Severity
St 3	$K_{St} > 300$	Extremely explosive
St 2	$200 < K_{St} \leq 300$	Strongly explosive
St 1	$100 < K_{St} \leq 200$ $0 < K_{St} \leq 100$	Moderately explosive Weakly explosive
St 0	$K_{St} = 0$	Not explosive

ATEX 153
HAZARDOUS AREA CLASSIFICATION

Hazardous places are classified in terms of zones on the basis of the frequency and duration of the occurrence of an explosive atmosphere. The extent of the measures to be taken in accordance with Annex II, Part A, is determined by this classification.

GAS EXPLOSIONS

Zone 0 A place in which an explosive atmosphere consisting of a mixture with air of flammable substances in the form of gas, vapour or mist is present continuously or for long periods or frequently.

Zone 1 A place in which an explosive atmosphere consisting of a mixture with air or flammable substances in the form of gas, vapour or mist is likely to occur in normal operation occasionally.

Zone 2 A place in which an explosive atmosphere consisting of a mixture with air of flammable substances in the form of gas, vapour or mist is not likely to occur in normal operation but, if it does occur, will persist for a short period only.

DUST EXPLOSIONS

Zone 20 A place in which an explosive atmosphere in the form of a cloud of combustible dust in air is present continuously, or for long periods or frequently.

Zone 21 A place in which an explosive atmosphere in the form of a cloud of combustible dust in air is likely to occur in normal operation occasionally.

Zone 22 A place in which an explosive atmosphere in the form of a cloud of combustible dust in air is not likely to occur in normal operation but, if it does occur, will persist for a short period only.

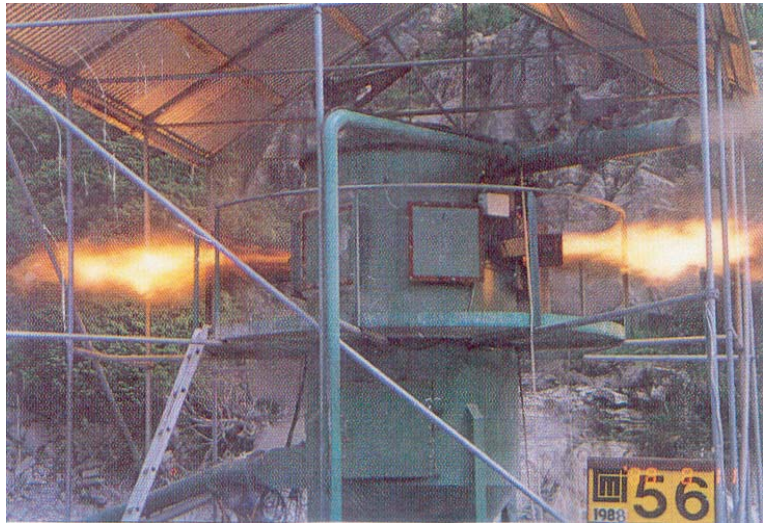
Approved Code of Practice [10]
Health and Safety Executive. Control of Major Accident Hazards (COMAH). Hazardous Area Classification and Control of Ignition Sources.

Zone 0 / 20: Explosive mixture for more than 1000h/yr. Category 1 equipment. One year equals 8760 hours.

Zone 1 / 21: Explosive mixture for more than 10, but less than 1000 h/yr. Category 1 or 2 equipment.

Zone 2 / 22: Explosive mixture for less than 10h/yr, but still sufficiently likely. Category 1, 2 or 3 equipment. Require controls over ignition sources.

Categorization into the three zones is based upon release calculations according to EN 60079-10-1 [11] and EN 60079-10-2 [12].



Codes and Standards Pertaining to Dust Explosion Hazards

• NFPA 68. Standard on Explosion Protection by Deflagration Venting, 2013 Edition. National Fire Protection Association, Quincy, MA, United States of America, 2013 [13].
• NFPA 654. Standard for the Prevention of Fire and Dust Explosions from the Manufacturing, Processing, and Handling of Combustible Particulate Solids, 2017 Edition. National Fire Protection Association, Quincy, MA, United States of America, 2017 [14].
• NFPA 61. Standard for the Prevention of Fires and Dust Explosions in Agricultural and Food Processing Facilities, 2017 Edition. National Fire Protection Association, Quincy, MA, United States of America, 2017 [15].
• NFPA 484. Standard for Combustible Metals, 2015 Edition. National Fire Protection Association, Quincy, MA, United States of America, 2015. [16].
• NFPA 664. Standard for the Prevention of Fires and Explosions in Wood Processing and Woodworking Facilities, 2017 Edition. National Fire Protection Association, Quincy, MA, United States of America, 2017 [17].
• NFPA 655. Standard for Prevention of Sulfur Fires and Explosions, 2017 Edition. National Fire Protection Association, Quincy, MA, United States of America, 2017 [18].
• EN 13237. Potentially explosive atmospheres. Terms and definitions for equipment and protective systems intended for use in potentially explosive atmospheres, 2012 Edition. European Committee for Standardization (CEN), Brussels, Belgium, Europe, 2012 [19]
• EN 1437. Explosion suppression systems, 2005 Edition. European Committee for Standardization (CEN), Brussels, Belgium, Europe, 2005 [20]
• EN 14491. Dust explosion venting protective systems, 2012 Edition. European Committee for Standardization (CEN), Brussels, Belgium, Europe, 2012 [21]
• EN 14797. Explosion venting devices, 2006 Edition. European Committee for Standardization (CEN), Brussels, Belgium, Europe, 2006 [22]

• EN 13673-1. Determination of the maximum explosion pressure and the maximum rate of pressure rise of gases and vapours - Part 1: Determination of the maximum explosion pressure, 2003 Edition. European Committee for Standardization (CEN), Brussels, Belgium, Europe, 2003. European Standard, Prepared by Technical Committee CEN/TC 305 *Potentially explosive atmospheres - Explosion prevention and protection* [23]
• EN 13673-2. Determination of the maximum explosion pressure and the maximum rate of pressure rise of gases and vapours - Part 2: Determination of the maximum rate of explosion pressure rise, 2005 Edition. European Committee for Standardization (CEN), Brussels, Belgium, Europe, 2005. European Standard, Prepared by Technical Committee CEN/TC 305 *Potentially explosive atmospheres - Explosion prevention and protection* [24]
• EN 14034-1. Determination of explosion characteristics of dust clouds - Part 1: Determination of the maximum explosion pressure $p_{\max}$ of dust clouds, 2004 Edition. European Committee for Standardization (CEN), Brussels, Belgium, Europe, 2004. European Standard, Prepared by Technical Committee CEN/TC 305 *Potentially explosive atmospheres - Explosion prevention and protection* [25]
• EN 14034-1. Determination of explosion characteristics of dust clouds - Part 1: Determination of the maximum explosion pressure $p_{\max}$ of dust clouds, 2011 Edition. European Committee for Standardization (CEN), Brussels, Belgium, Europe, 2011. European Standard, Prepared by Committee EXL/23 *Explosion and fire precautions in industrial and chemical plant.* Amendment July 2011. Amends and replaces EN 14034-1:2004. [26]
• EN 14034-2. Determination of explosion characteristics of dust clouds - Part 2: Determination of the maximum explosion rate of explosion pressure rise $(dp/dt)_{\max}$ of dust clouds. 2006 Edition. European Committee for Standardization (CEN), Brussels, Belgium, Europe, 2006. European Standard, Prepared by Technical Committee CEN/TC 305 *Potentially explosive atmospheres - Explosion prevention and protection* [27]
• EN 14034-3. Determination of explosion characteristics of dust clouds - Part 3: Determination of the lower explosion limit LEL of dust clouds, 2006 Edition. European Committee for Standardization (CEN), Brussels, Belgium, Europe, 2006. European Standard, Prepared by Technical Committee CEN/TC 305 *Potentially explosive atmospheres - Explosion prevention and protection* [28]
• EN 14034-4. Determination of explosion characteristics of dust clouds - Part 4: Determination of the limiting

oxygen concentration LOC of dust clouds, 2004 Edition. European Committee for Standardization (CEN), Brussels, Belgium, Europe, 2004. European Standard, Prepared by Technical Committee CEN/TC 305 *Potentially explosive atmospheres - Explosion prevention and protection.* [29]

• EN 60079-10-2. Explosive atmospheres. Classification of areas. Explosive dust atmospheres, 2015 Edition. European Committee for Standardization (CEN), Brussels, Belgium, Europe, 2015 [12]

• ISO 6184-1. Explosion Protection Systems - Part 1: Determination of explosion indices of combustible dusts in air. The International Organization for Standardization (ISO), 1985. [30]

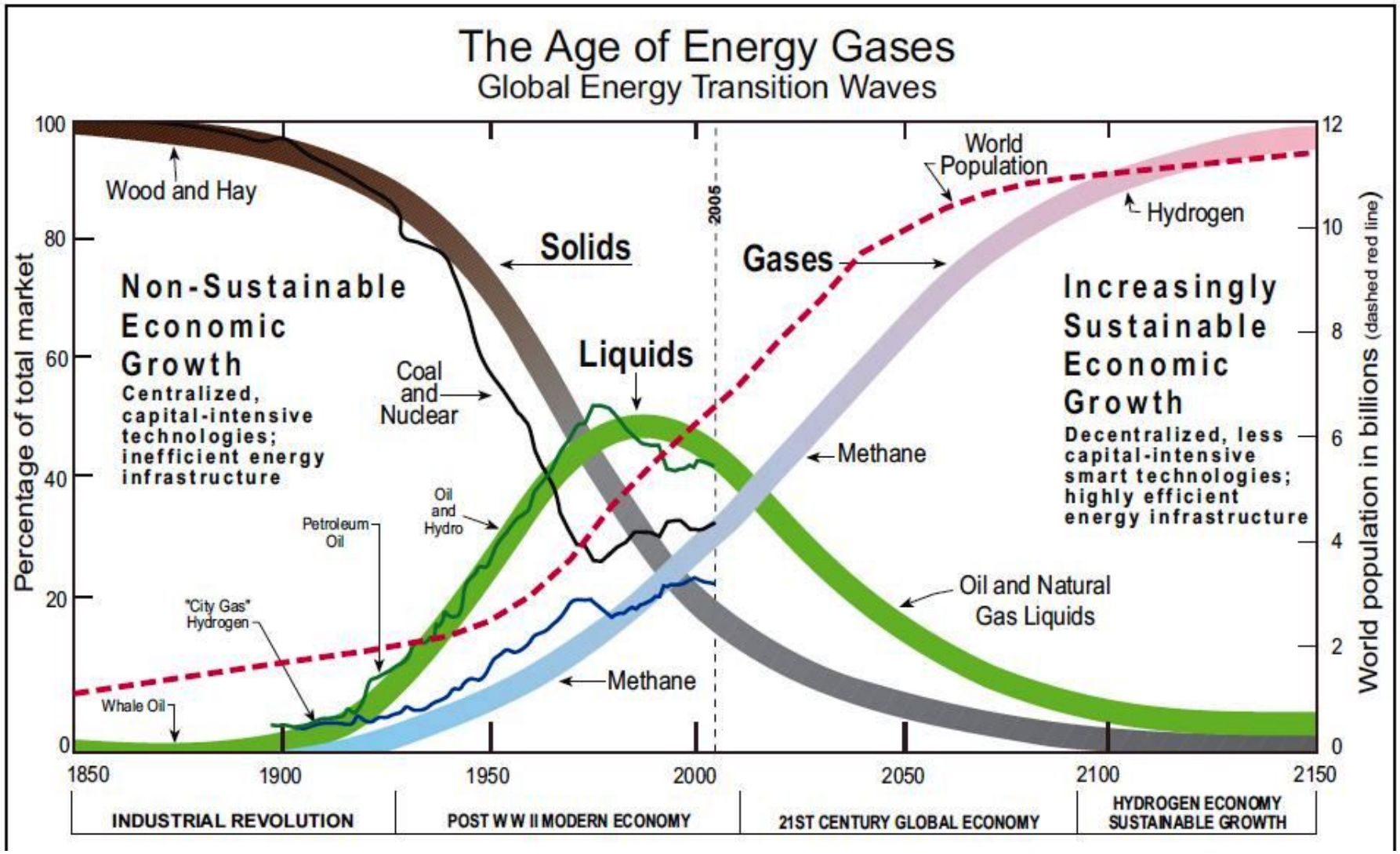
Regulations, Codes and Standards
ATEX Methodology

Hazardous Area Classification:
Determine whether hazardous places are present and, if so, where they are located.

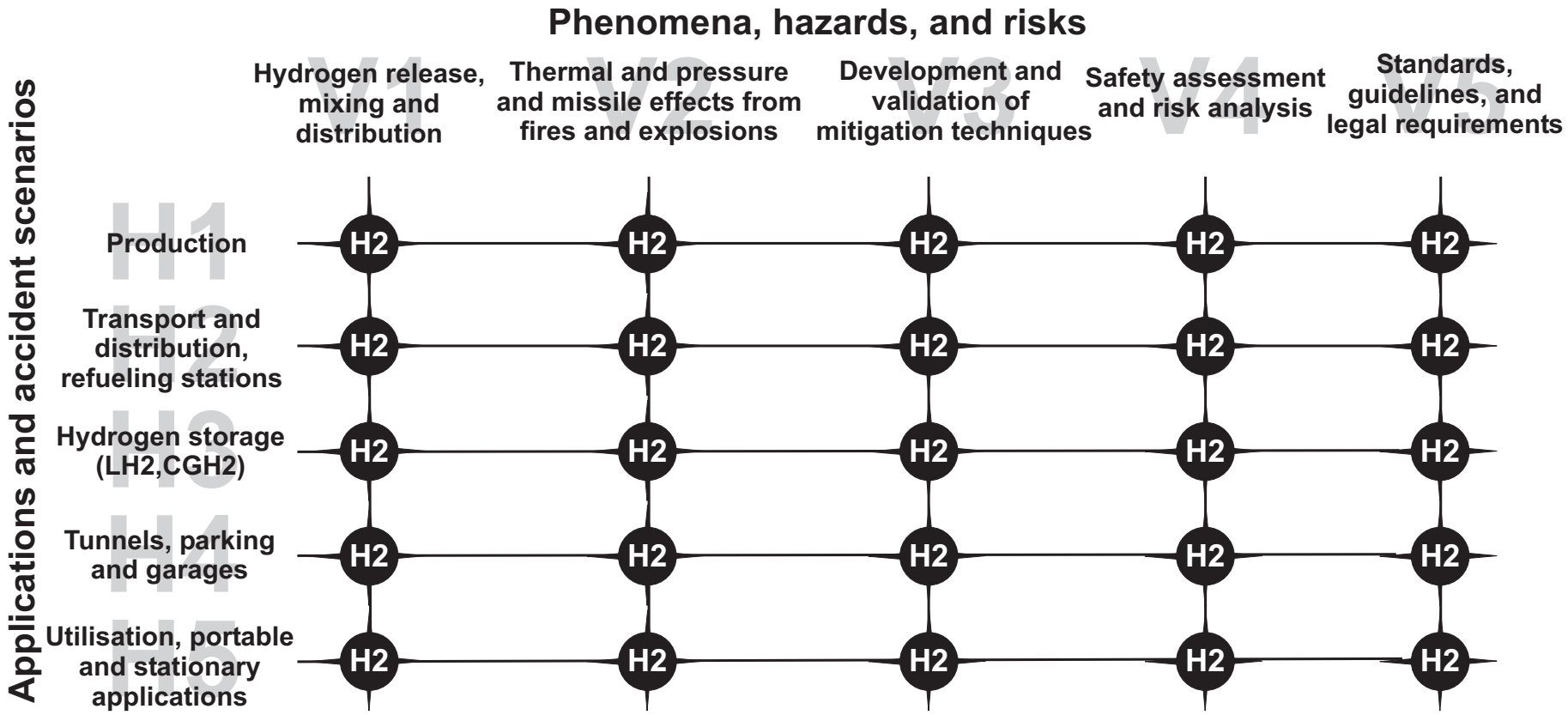
$$\begin{bmatrix}\text{Likelihood}\\ \text{of}\\ \text{explosion}\end{bmatrix} = \begin{bmatrix}\text{Likelihood of}\\ \text{explosive}\\ \text{atmosphere}\end{bmatrix} \times \begin{bmatrix}\text{Likelihood of}\\ \text{ignition source}\end{bmatrix} \tag{1}$$

Combustible gas and dust clouds in the explosive region are categorized into 3 zones, based upon the release (as per EN 60079-10-2 [12]):

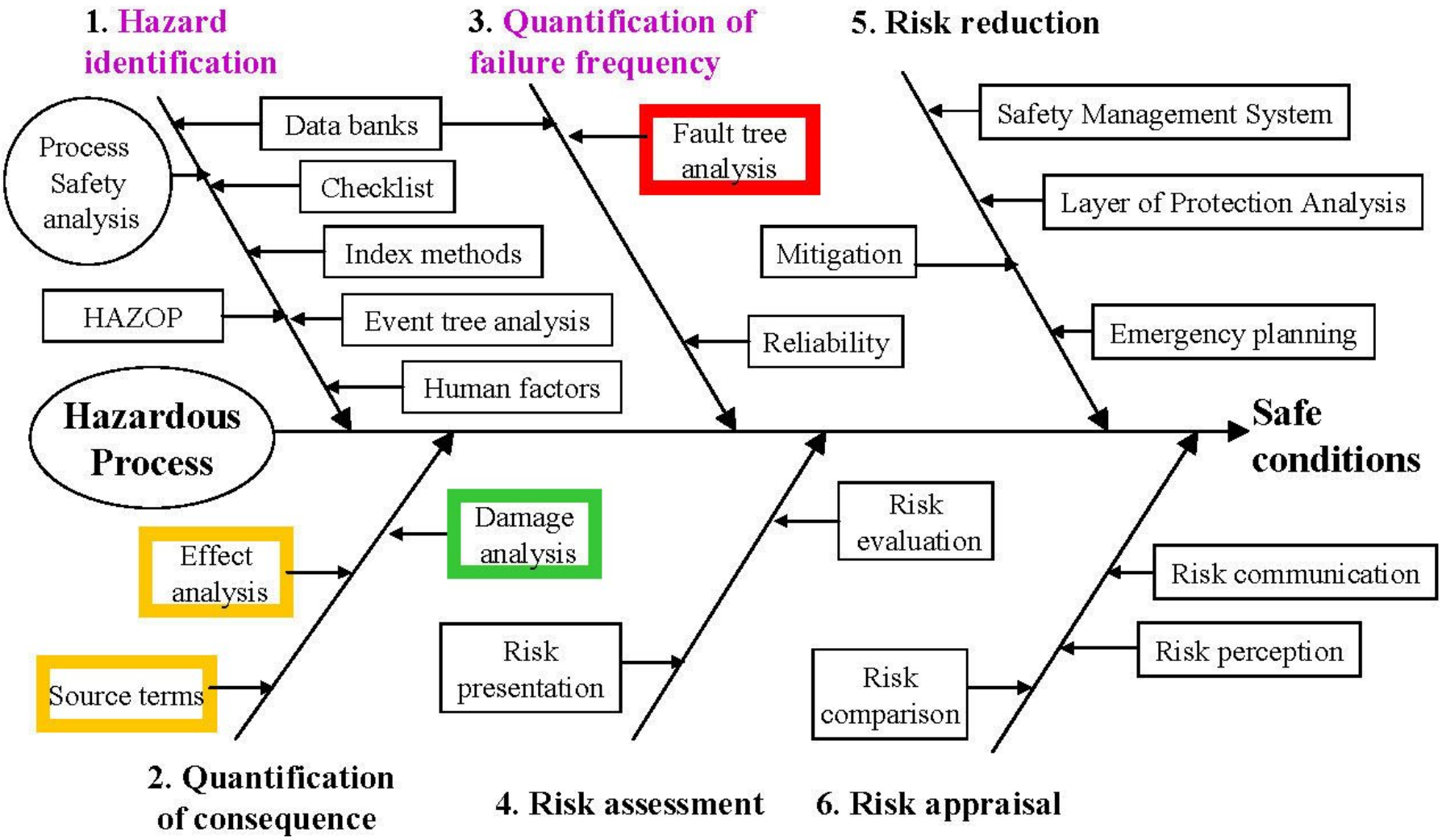
Zone 0 or 20: A continuous release inside a containment enclosure gives rise to Zone 0 (gas) or 20 (dust). A place in which an explosive mixture is continuously present (or for long periods, or, frequently for short periods).
E.g. a mill or pneumatic conveying system.
Zone 1 or 21: A primary instantaneous release gives rise to Zone 1 or 21. A place in which an explosive atmosphere is likely to occur occasionally under normal operating conditions. E.g., bagging points and inspection ports that are frequently opened, ventilation systems for flammable gases.
Zone 2 or 22: A secondary instantaneous release gives rise to Zone 2 or 22. A place where an explosive mixture is unlikely to occur under normal operation but, if it does occur, will persist for a short period only. E.g., leaks from incorrectly fitted lids, spillages.



Transition of the energy mix. From [31].



The HySafe Activity Matrix. From [32].



The Risk Analysis Fishbone Diagram.





Coverage: 200000 km/yr



Diesel: 35 kg/100 km $\longrightarrow$ 1 refueling/year



Hydrogen calamity (transportation)



LNG: 25 kg/100 km $\longrightarrow$ 4 refuelings/year



Hydrogen: 10 kg/100 km $\longrightarrow$ 35 refuelings/year

Impact energy transition on refueling operations. From [33].

GASEOUS HYDROGEN STORAGE – EXPLOSION HAZARDS

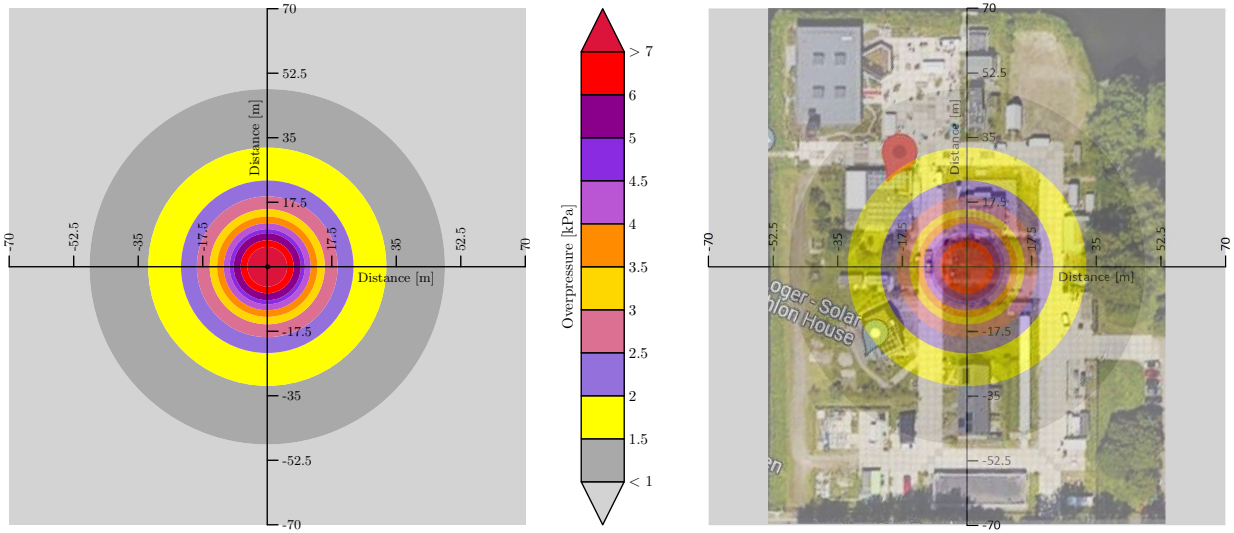


Kjorbo, Norway
Monday 10 June 2019 at 17:30 h
Hydrogen Explosion (3.0 – 3.5 kg H_2)
Glass damage at 60 – 70 m distance
Office at 60 m distance
Houses at > 225 m distance

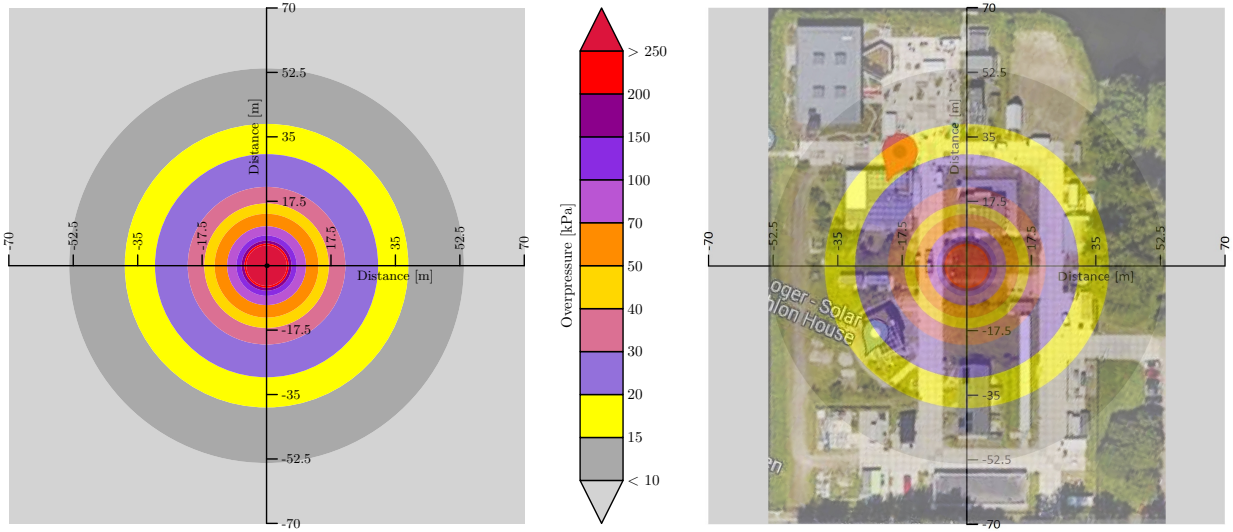


DELFT UNIVERSITY OF TECHNOLOGY – GREEN VILLAGE

Explosion involving 3.5 kg hydrogen Blast calculation according to Ref. [34].



Deflagration



Detonation

PRESSURE EFFECTS ON PEOPLE, STRUCTURES AND EQUIPMENT

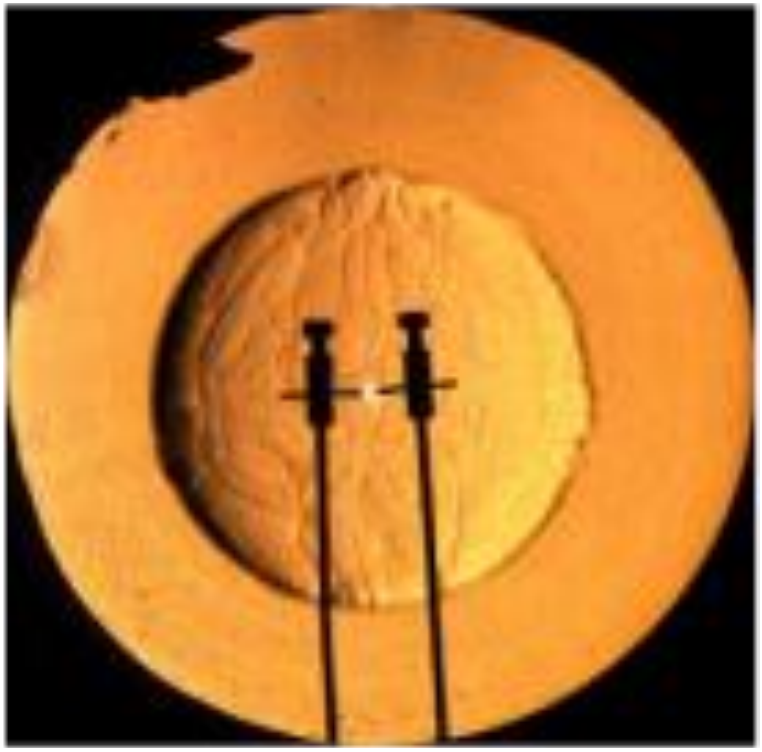
Entry	Overpressure (kPa)	Damage/injury
1	190	Occupants of unstrengthened building will be killed by direct action of blast, by being struck by building debris, or by impact against hard surfaces [35].
2	69–76	Occupants of unstrengthened building are expected to suffer severe injuries or death from direct blast, building collapse, or translation [35].
3	70	Probable total destruction of buildings; heavy machine tools moved and badly damaged [36].
4	60	Loaded train boxcars completely demolished [36].
5	55	Occupants of unstrengthened building will be killed or incur serious injuries by blast to eardrums and lungs, by being blown down or struck by fragments and building debris [35].
6	50–55	Unreinforced brick panels, 25–35 cm thick, fail by shearing or flexure [36].
7	50	Loaded tank cars/train wagons overturned; brick walls, 20–30 cm thick, collapse [36].
8	40–45	Collapse of pipe bridge [36].
9	35–40	Displacement of pipe bridge, failure of piping [36].
10	20–40	Large trees fall down [36].
11	35	Breakage of wooden telephone poles; most buildings destroyed, except for concrete reinforced shear wall buildings; *platting* of cars and trucks pressed inwards [36].
12	30–35	Near-complete destruction of houses [36].
13	30	Cladding of light industrial buildings ruptured. Panelling torn-off [36].
14	20–28	Frameless, self-framing steel panel building demolished; rupture of oil storage tanks [36].
15	24	Personnel injuries of a serious nature or possible death are likely from fragments, debris, firebrands or other objects. There is a 10% chance of eardrum rupture [35].
16	15–20	Unreinforced concrete or cinderblock walls shattered [36].
17	20	Heavy machines in industrial buildings suffer little damage; steel frame building distorted and pulled away from foundations [36].
18	18	Lower limit of serious structural damage; 50% destruction of brickwork of houses [36].

Table 1: Continued.

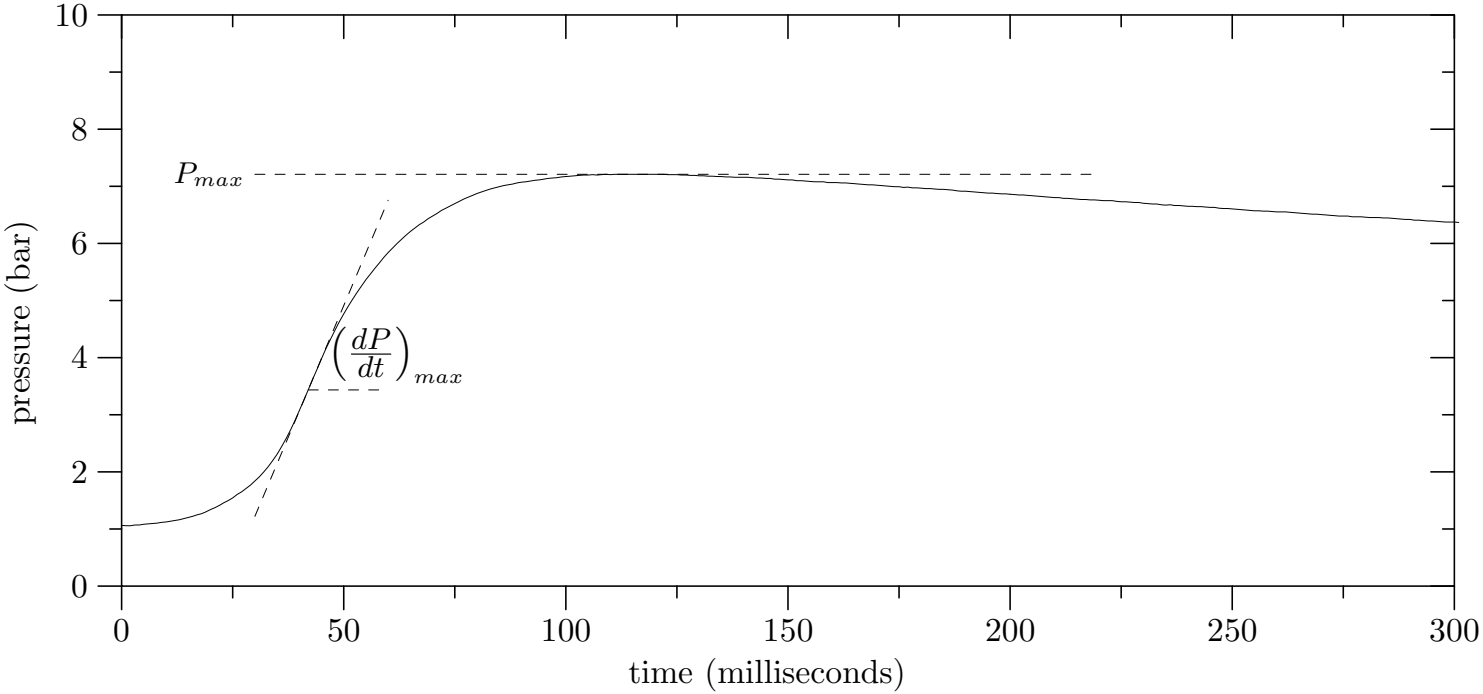
19	16	Personnel may suffer temporary hearing loss or injury from secondary blast effects such as building debris and the tertiary effect of displacement. No fatalities or serious injuries from direct blast are expected [35].
20	15	Partial collapse of walls and roofs of houses [36].
21	7–15	Corrugated asbestos shattered. Corrugated steel or aluminum panels fastenings fail, followed by buckling; wood panel fastenings fail, panels blown in [36].
22	10	Steel frame of clad buildings slightly distorted [36].
23	5.9–8.3	Personnel are provided a high degree of protection from death or serious injury with injuries that do occur being principally caused by glass breakage and building debris [1].
24	8	Partial demolition of houses, made uninhabitable [36].
25	7	Collapse of roof of a tank [36].
26	3.5–7	Windows usually shattered; occasional damage to window frames [36].
27	5	Minor damage to house structures [36].
28	3	Limited minor structural damage [36].
29	2	Probability of 0.95 of no serious damage beyond this value; some damage to house ceilings; 50% of window glass broken [36].
30	1	Typical threshold for glass breakage [36].
31	0.7	Breakage of small windows under strain [36].
32	0.3	Loud noise similar to sonic boom; occasional glass failure [36].
33	0.2	No structural damage; occasional breaking of large window panes already under strain [36].
34	0.15	Annoying noise [36].

Confined deflagrations: explosion severity parameters



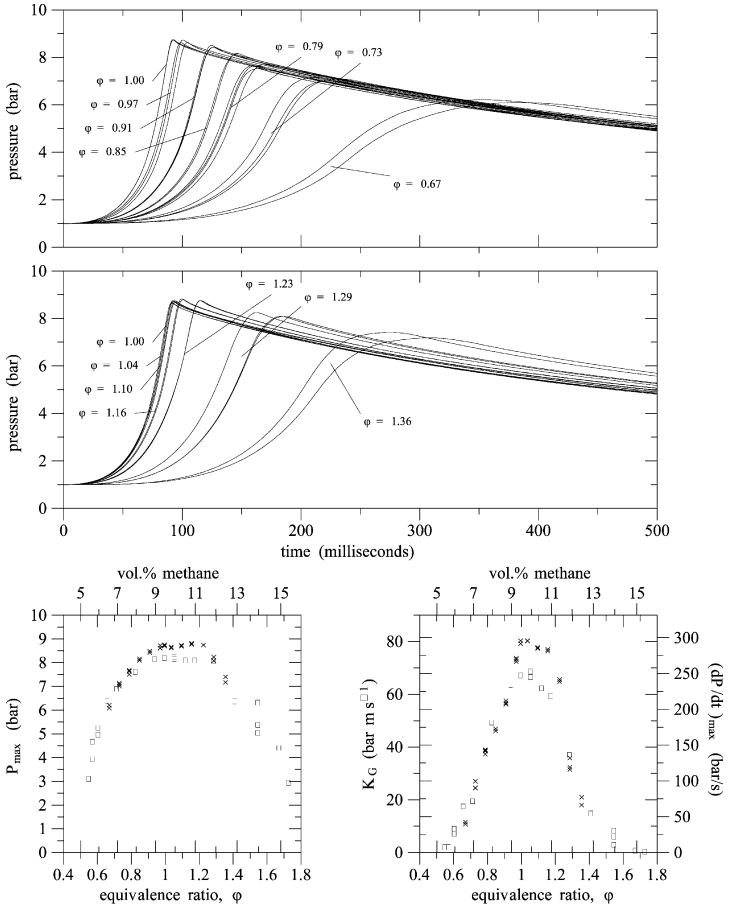


Confined deflagrations: explosion severity parameters

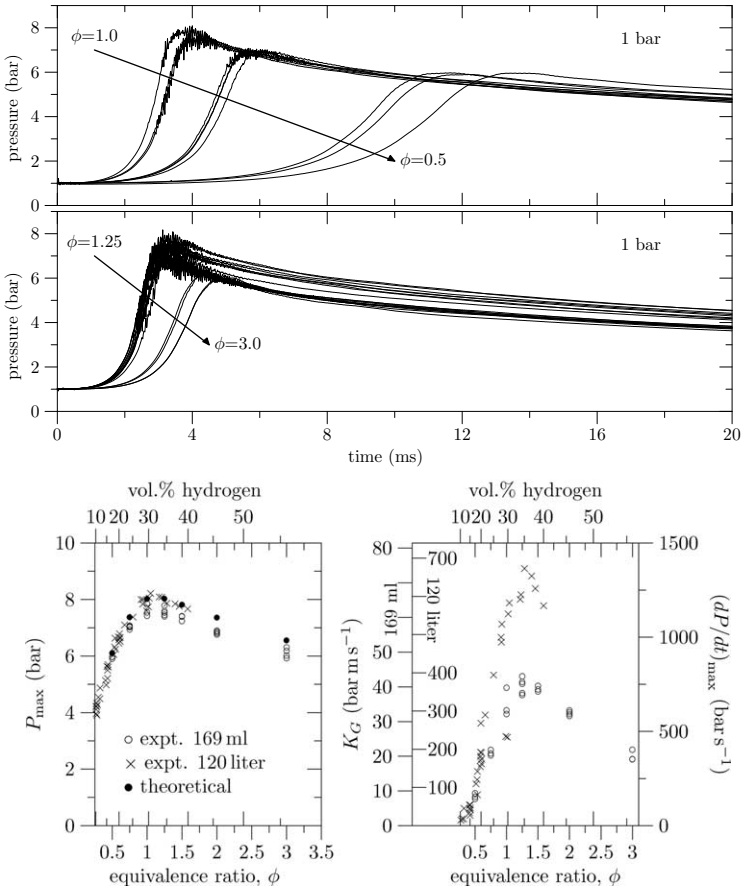


Experimental explosion pressure curve of a 500 $\mathrm{g\,m^{-3}}$ cornstarch-air mixture [37].

Confined deflagrations: explosion severity parameters



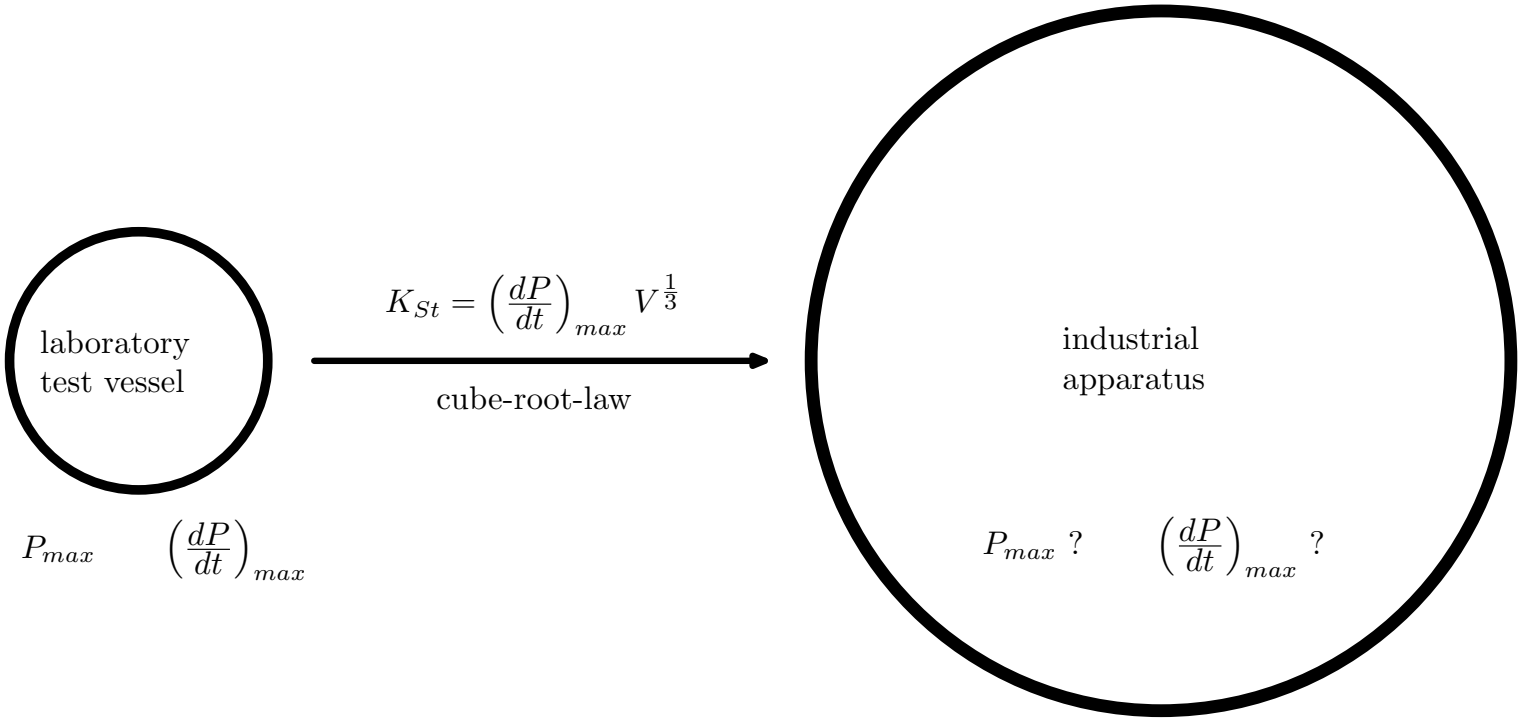
Methane-air



Hydrogen-air

Confined deflagrations: explosion severity parameters

Scaling an explosion: a matter of invariance across size?

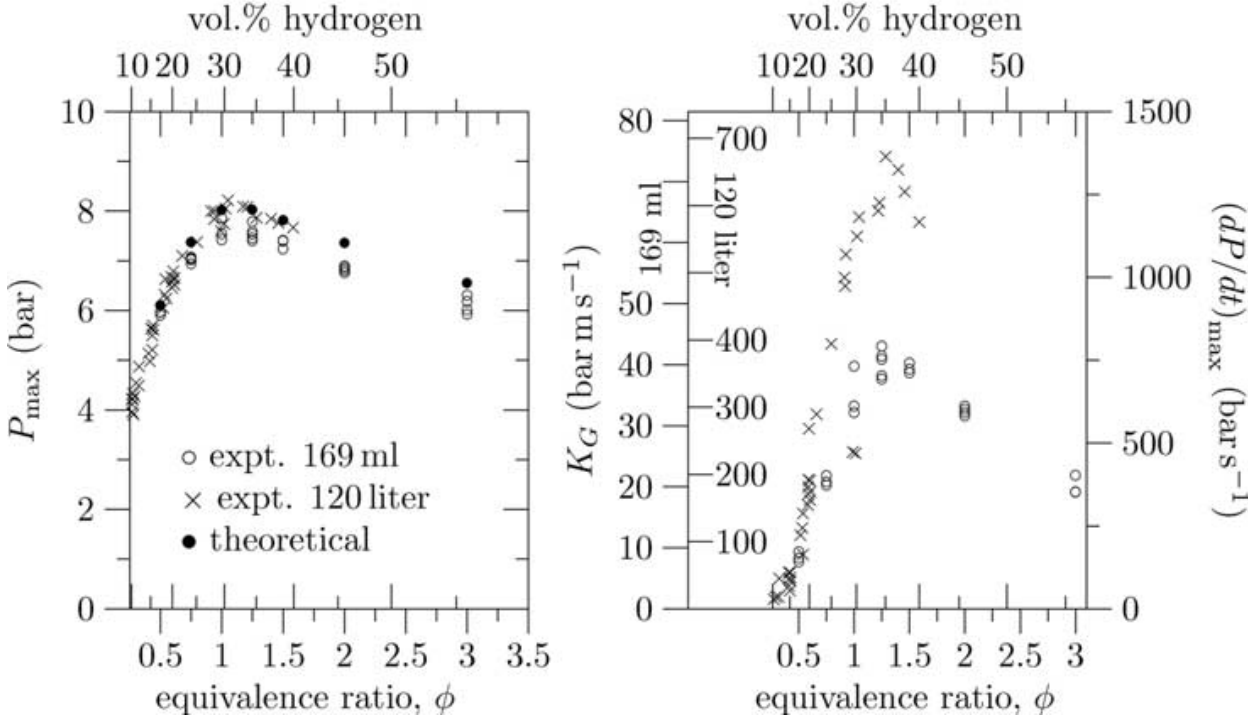


$$n_0\text{Reactants} \longrightarrow n_p\text{Products}: \qquad P_{\max} = \frac{n_p}{n_0}\frac{T_f}{T_0}P_0 \qquad \text{and} \qquad K_{\mathrm{St}} = \left(\frac{dP}{dt}\right)_{max} V^{1/3}$$

Deflagration parameters (hydrogen-air, laminar)

Theoretical maximum explosion pressure

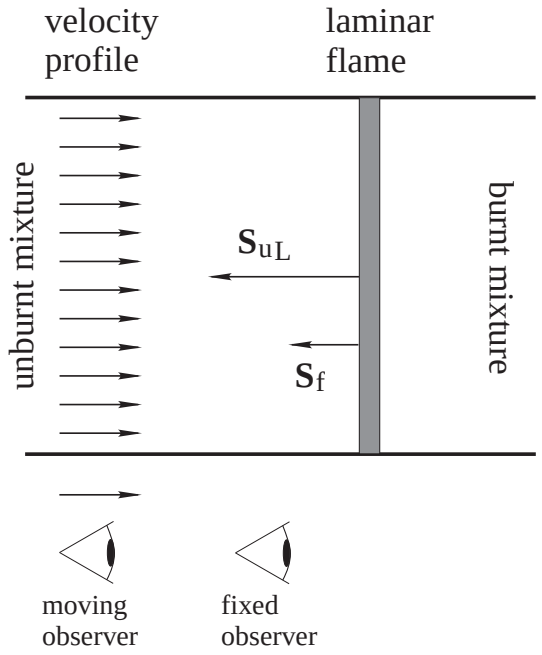
ϕ	0.5	0.75	1.0	1.25	1.5	2.0	3.0
P_{max} (bar)	6.096	7.366	8.011	8.016	7.807	7.35	6.546

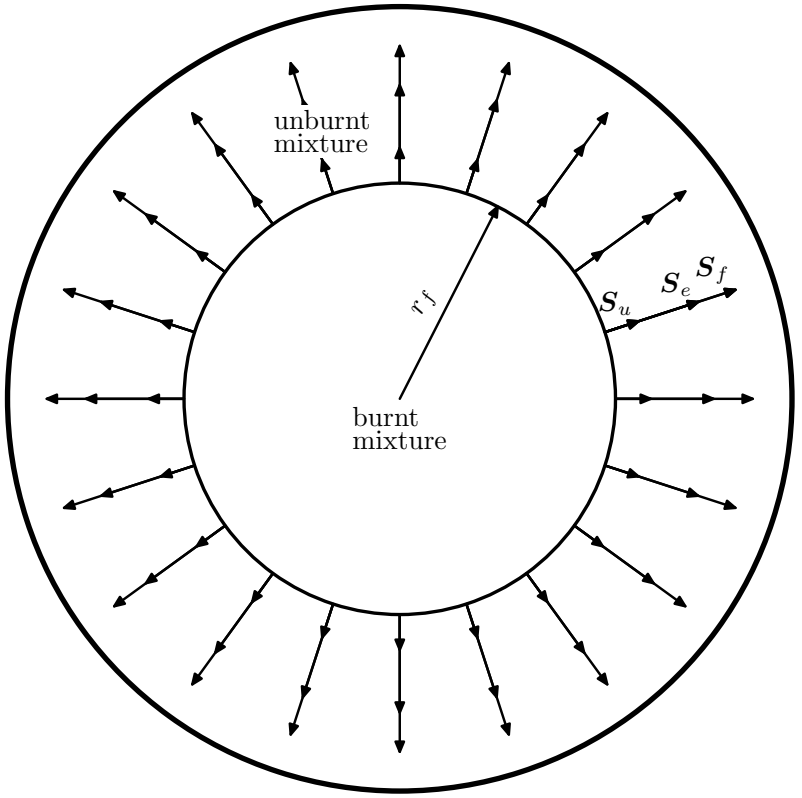


Comparison between P_{max}- and K_G-values: (○) 169-ml cylindrical vessel [7], (×) 120-litre explosion sphere [5].

Confined deflagrations: explosion severity parameters

Effect of compression on laminar burning velocity



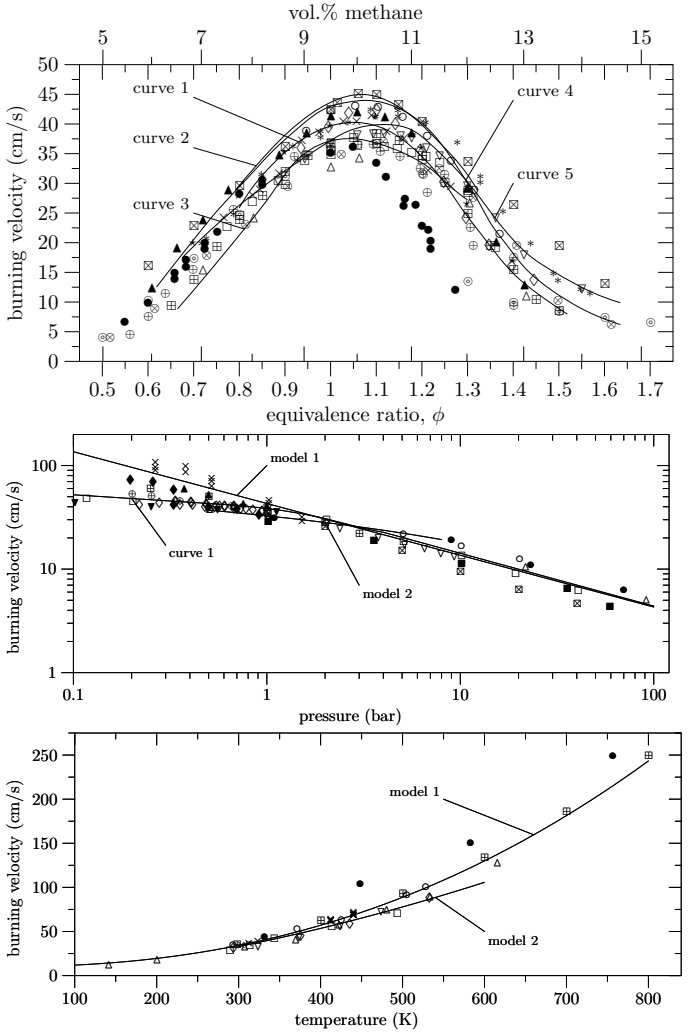


$\boldsymbol{S}_f = \text{flow velocity} + \boldsymbol{S}_u$

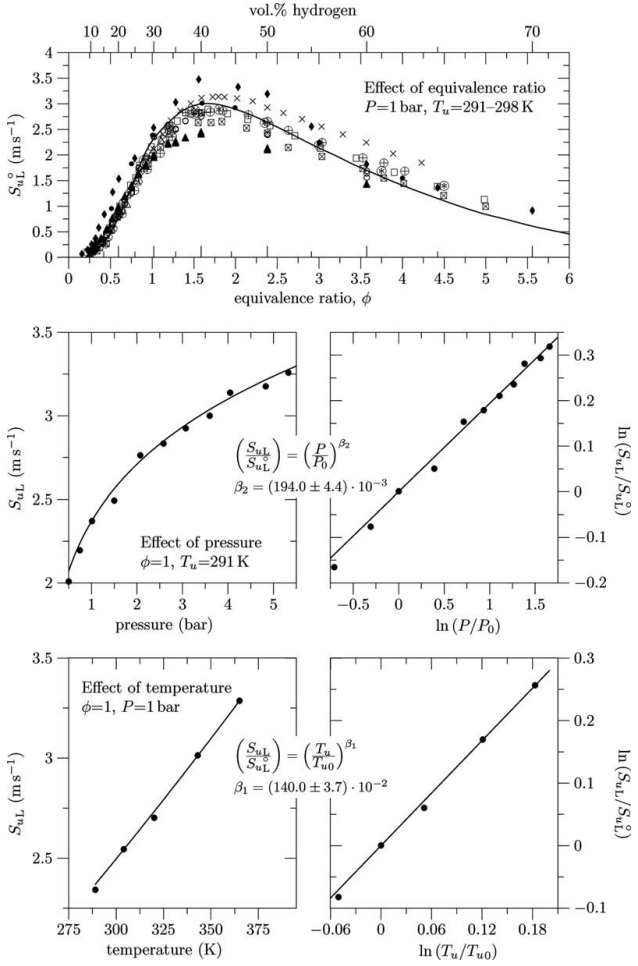
$\boldsymbol{S}_f = \boldsymbol{S}_e + \boldsymbol{S}_u$

Laminar burning velocity: effect of pressure and temperature

Methane-air [38]



Hydrogen-air [7]



Governing equations of a compressible reacting flow

Governing equations:

$$\frac{\partial \rho}{\partial t} + \nabla \cdot (\rho \boldsymbol{v}) = 0 \tag{2}$$

$$\frac{\partial (\rho \boldsymbol{v})}{\partial t} + \nabla \cdot (\rho \boldsymbol{v}\boldsymbol{v}) = -\nabla p + \nabla \cdot \boldsymbol{\tau} + \sum_{i=1}^{N} \rho Y_i \boldsymbol{g} \tag{3}$$

$$\frac{\partial (\rho Y_i)}{\partial t} + \nabla \cdot (\rho \boldsymbol{v} Y_i) = -\nabla \cdot [\rho Y_i \boldsymbol{V}_i] + \dot{w}_i \tag{4}$$

$$\begin{aligned} \frac{\partial (\rho h)}{\partial t} + \nabla \cdot (\rho \boldsymbol{v} h) = \frac{\partial p}{\partial t} + \boldsymbol{v} \cdot \nabla p + \boldsymbol{\tau} : \nabla \boldsymbol{v} - \nabla \cdot [\lambda \nabla T] + \nabla \cdot \boldsymbol{q} \\ + \nabla \cdot \left[\sum_{i=1}^{N} \rho Y_i h_i \boldsymbol{V}_i + \mathrm{R}T \sum_{i=1}^{N} \sum_{j=1}^{N} \left(\frac{X_j \alpha_i}{\mathcal{M}_i \mathcal{D}_{ij}} \right) (\boldsymbol{V}_i - \boldsymbol{V}_j) \right] + \sum_{i=1}^{N} \rho Y_i \boldsymbol{g} \cdot \boldsymbol{V}_i \end{aligned} \tag{5}$$

$$\frac{p}{\rho} = \frac{\gamma - 1}{\gamma} \sum_{i=1}^{N} Y_i \left[h_{f_i}^{\circ} + \int_{T^{\circ}}^{T} \mathrm{C}_{\mathrm{P}i}(T)\, dT \right] \tag{6}$$

$$\text{where} \quad \boldsymbol{\tau} = \mu \left[\nabla \boldsymbol{v} + (\nabla \boldsymbol{v})^{\dagger} \right] + \left(\kappa - \tfrac{2}{3}\mu \right) [\nabla \cdot \boldsymbol{v}]\, \boldsymbol{I} \tag{7}$$

$$\text{and} \quad \boldsymbol{q} = \epsilon \sigma T^4 \tag{8}$$

Assumptions:

- **Steady state**
- **Non-uniform pressure field**
- **Viscous dissipation in energy equation included**
- **Neglect effect of body forces in momentum and energy equation**
- **Soret and Dufour effect in species and energy equation included**

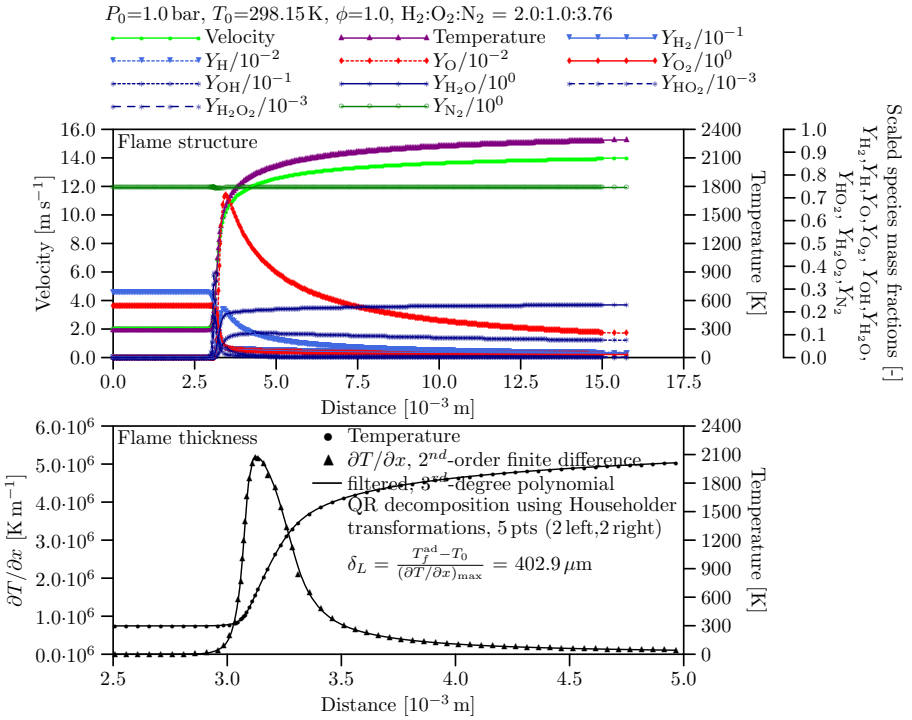
Governing equations of a compressible reacting flow: laminar flame solution

The reaction rate coefficients are in the form $k_f = \mathrm{A}T^{\beta}\exp\left(-\mathrm{E_a}/\mathrm{R}T\right)$. Units are in moles, cubic centimetres, seconds, Kelvins and calories.

	Reaction	A	β	$\mathrm{E_a}$
1	$H_2 + O_2 \rightleftharpoons 2OH$	$1.70 \cdot 10^{13}$	0.0	47780.
2	$OH + H_2 \rightleftharpoons H_2O + H$	$1.17 \cdot 10^{9}$	1.3	3626.
3	$H + O_2 \rightleftharpoons OH + O$	$5.13 \cdot 10^{16}$	-0.816	16507.
4	$O + H_2 \rightleftharpoons OH + H$	$1.80 \cdot 10^{10}$	1.0	8826.
5	$H + O_2 + M \rightleftharpoons HO_2 + M^a$	$2.10 \cdot 10^{18}$	-1.0	0.
6	$H + O_2 + O_2 \rightleftharpoons HO_2 + O_2$	$6.70 \cdot 10^{19}$	-1.42	0.
7	$H + O_2 + N_2 \rightleftharpoons HO_2 + N_2$	$6.70 \cdot 10^{19}$	-1.42	0.
8	$OH + HO_2 \rightleftharpoons H_2O + O_2$	$5.00 \cdot 10^{13}$	0.0	1000.
9	$H + HO_2 \rightleftharpoons 2OH$	$2.50 \cdot 10^{14}$	0.0	1900.
10	$O + HO_2 \rightleftharpoons O_2 + OH$	$4.80 \cdot 10^{13}$	0.0	1000.
11	$2OH \rightleftharpoons O + H_2O$	$6.00 \cdot 10^{8}$	1.3	0.
12	$H_2 + M \rightleftharpoons H + H + M^b$	$2.23 \cdot 10^{12}$	0.5	92600.
13	$O_2 + M \rightleftharpoons O + O + M$	$1.85 \cdot 10^{11}$	0.5	95560.
14	$H + OH + M \rightleftharpoons H_2O + M^c$	$7.50 \cdot 10^{23}$	-2.6	0.
15	$H + HO_2 \rightleftharpoons H_2 + O_2$	$2.50 \cdot 10^{13}$	0.0	700.
16	$HO_2 + HO_2 \rightleftharpoons H_2O_2 + O_2$	$2.00 \cdot 10^{12}$	0.0	0.
17	$H_2O_2 + M \rightleftharpoons OH + OH + M$	$1.30 \cdot 10^{17}$	0.0	45500.
18	$H_2O_2 + H \rightleftharpoons HO_2 + H_2$	$1.60 \cdot 10^{12}$	0.0	3800.
19	$H_2O_2 + OH \rightleftharpoons H_2O + HO_2$	$1.00 \cdot 10^{13}$	0.0	1800.

[a] Third body efficiencies: $k_5(H_2O) = 21\,k_5(Ar)$, $k_5(H_2) = 3.3\,k_5(Ar)$.
[b] Third body efficiencies: $k_{12}(H_2O) = 6\,k_{12}(Ar)$, $k_{12}(H) = 2\,k_{12}(Ar)$, $k_{12}(H_2) = 3\,k_{12}(Ar)$. [c] Third body efficiency: $k_{14}(H_2O) = 20\,k_{14}(Ar)$.

Detailed kinetic scheme for hydrogen-air combustion. From [39].



Solution of the governing equations for the laminar flame structure. From [40].

Confined deflagrations: a simple model

Objective:
Find a dynamic equation for the pressure evolution

Approximate expression relating the unburnt mixture mass fraction to the fractional pressure rise [38, 41, 42]:

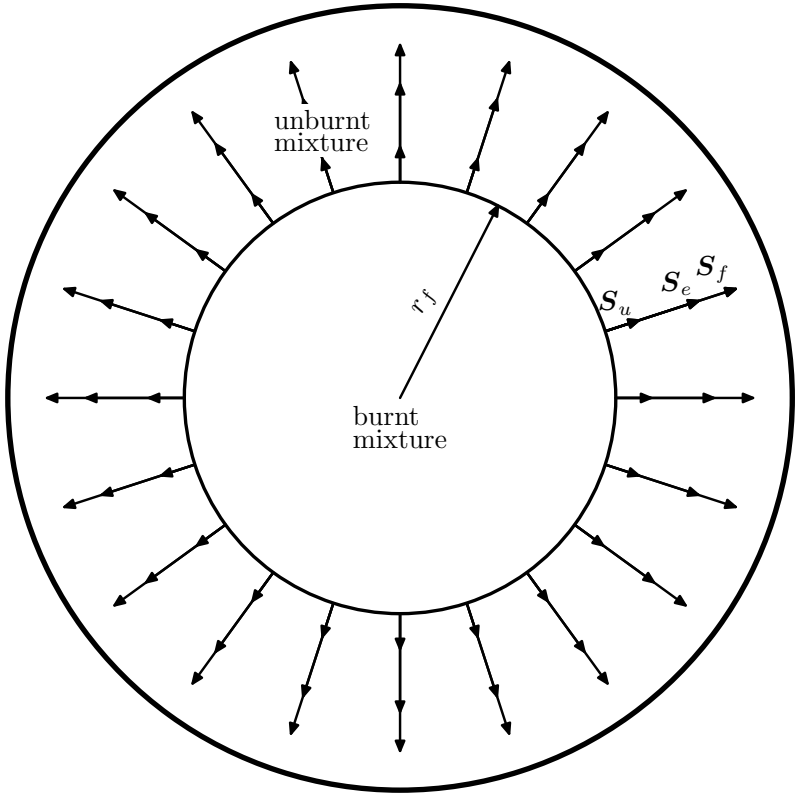
$$\frac{m_u}{m_{u0}} = \frac{P_{max} - P}{P_{max} - P_0} \tag{9}$$

Differentiation with respect to time:

$$\frac{dP}{dt} = -\frac{P_{max} - P_0}{m_{u0}} \frac{dm_u}{dt} \tag{10}$$

The combustion wave propagates with a velocity equalling the sum of the expansion velocity, S_e, the conversion velocity, S_n, and the burning velocity S_u. Since the unburnt mixture immediately ahead of the flame front moves with velocity $S_e + S_n$, the velocity at which the unburnt mixture enters the combustion wave is minus the burning velocity. Therefore, the mass consumption rate of the unburnt mixture can be expressed as

$$\frac{dm_u}{dt} = -4\pi r_f^2 \rho_u S_u \tag{11}$$



A relationship can be established between the rate of pressure rise and the burning velocity. By substitution of equation (11) into equation (10):

$$\frac{dP}{dt} = 4\pi \frac{P_{max} - P_0}{m_{u0}} r_f^2 \rho_u S_u \tag{12}$$

Confined deflagrations: a simple model

The next step is to express the density of the unburnt mixture, ρ_u, and the location of the flame front, r_f, in terms of known variables. For adiabatic compression of the unburnt mixture, $P\rho^{-\gamma} = \text{constant}$ and hence

$$\frac{\rho_{u0}}{\rho_u} = \left(\frac{P_0}{P}\right)^{\frac{1}{\gamma}} \tag{13}$$

Furthermore, $V_b = V_{vessel} - V_u$, which can be rewritten as

$$\frac{4}{3}\pi r_f^3 = V_{vessel} - \frac{m_u R T_u}{P} \tag{14}$$

Since $\rho^{-1} = \hat{\mathrm{R}}T/P$ where $\hat{\mathrm{R}}$ denotes the specific gas constant in $\mathrm{J\,kg^{-1}\,K^{-1}}$, the volume of the unburnt mixture can be expressed as

$$\begin{aligned} \frac{m_u \hat{\mathrm{R}} T_u}{P} &= V_{vessel}\rho_{u0}\frac{P_{max}-P}{P_{max}-P_0}\rho_u^{-1} = V_{vessel}\left(\frac{\rho_{u0}}{\rho_u}\right)\frac{P_{max}-P}{P_{max}-P_0} \\ &= V_{vessel}\left(\frac{P_0}{P}\right)^{\frac{1}{\gamma}}\frac{P_{max}-P}{P_{max}-P_0} \end{aligned} \tag{15}$$

and equation (14) yields the following expression for the location of the flame front:

$$r_f = R_{vessel}\left[1 - \left(\frac{P_0}{P}\right)^{\frac{1}{\gamma}}\frac{P_{max}-P}{P_{max}-P_0}\right]^{\frac{1}{3}} \tag{16}$$

Confined deflagrations: a simple model

By inserting equations (16) and (13) into equation (12) and by noting that $m_{u0} = \rho_{u0} V_{vessel}$, the following ordinary differential equation is obtained for the rate of pressure rise:

$$\frac{dP}{dt} = \frac{3\,(P_{max} - P_0)}{R_{vessel}} \left[1 - \left(\frac{P_0}{P} \right)^{\frac{1}{\gamma}} \frac{P_{max} - P}{P_{max} - P_0} \right]^{\frac{2}{3}} \left(\frac{P}{P_0} \right)^{\frac{1}{\gamma}} S_u \tag{17}$$

From equation (17) it can be seen that (dP/dt) increases monotonically with P and hence the maximum rate of pressure rise is attained when $P = P_{max}$. By substituting $P = P_{max}$ into equation (17) and multiplying both sides by the cube root of the vessel volume, the following expression is found for the $K_{G/St}$-value:

$$\boxed{K_{G/St} = \left(\frac{dP}{dt} \right) V^{1/3} = (36\pi)^{1/3} (P_{max} - P_0) \left(\frac{P_{max}}{P_0} \right)^{\frac{1}{\gamma}} S_u} \tag{18}$$

which is a normalization of the maximum rate of pressure rise with respect to the vessel volume.

Burning velocity: determination by solving inverse problem

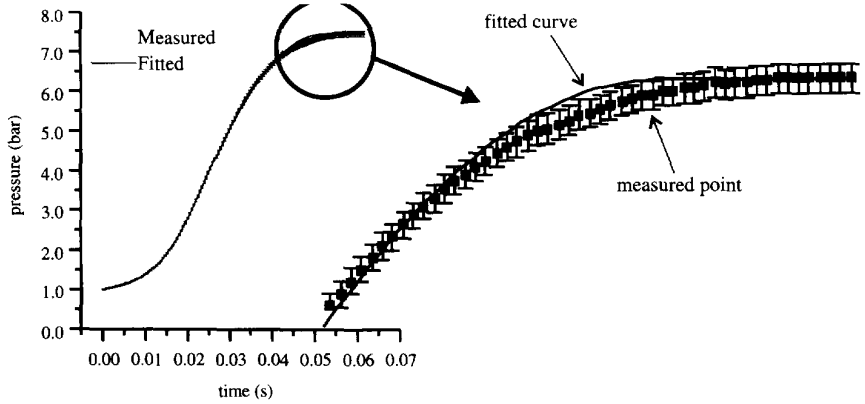


Table 3 Fitted results

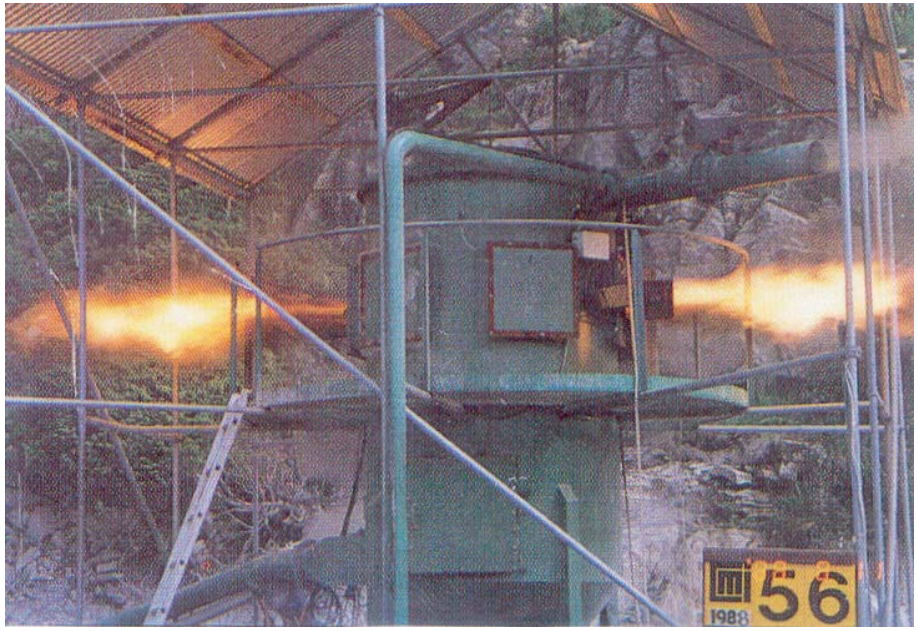
Parameter	Value ± s.e.
S_{u0}	(306.0 ± 4.3)E-02 m s^{-1}
α	(−93.4 ± 2.0)E-02
δ	(41.2 ± 1.6)E-03 m

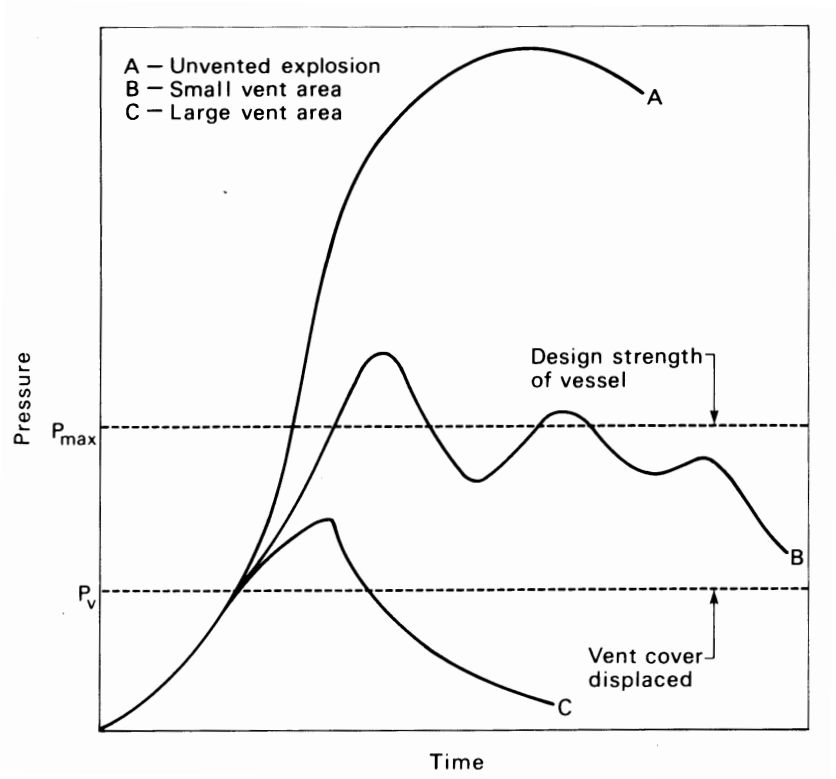
For a 95.0% confidence interval, multiply s.e. by 1.9793.
Fit method: Marquardt non-linear fit. Sum of Res. squared: 100.8282 with 124 degrees of freedom. This has a *P* value of 0.9372.

Determination of the burning velocity by solving the inverse problem for the pressure-time curve of a 500 g m^{-3} cornstarch-air mixture measured in the strengthened 20-litre explosion sphere. From [42].

$$\frac{S_u}{S_{u0}} = \left(\frac{P}{P_0}\right)^{\alpha} \left(\frac{T}{T_0}\right)^{\beta}$$

Vented deflagrations: pressure relief venting





A model for vented deflagrations

Bradley D. and Mitcheson A. The venting of gaseous explosions in spherical vessels. I - Theory. Combustion and Flame, 32:221-236, 1978 [43].
Bradley D. and Mitcheson A. The venting of gaseous explosions in spherical vessels. II - Theory and experiment. Combustion and Flame, 32:237-255, 1978 [44].

Model developed for centrally ignited fuel-air mixtures in a spherical vessel with vent flow expressions for the rate of change in the mass of unburnt mixture:

$$\frac{dm_u}{dt} = \begin{cases} -4\pi r_f^2 \rho_u S_u - C_d A_v \rho \left[\dfrac{\gamma P}{\rho} \left(\dfrac{\gamma+1}{2} \right)^{\frac{1+\gamma}{1-\gamma}} \right]^{1/2} & \text{if} \quad \dfrac{P_a}{P} \leq \left(\dfrac{2}{\gamma+1} \right)^{\frac{\gamma}{\gamma-1}} \quad \text{(sonic)} \\ -4\pi r_f^2 \rho_u S_u - C_d A_v \left\{ \dfrac{2\gamma P \rho}{\gamma-1} \left(\dfrac{P_a}{P} \right)^{\frac{2}{\gamma}} \left[1 - \left(\dfrac{P_a}{P} \right)^{\frac{\gamma-1}{\gamma}} \right]^{\frac{1+\gamma}{1-\gamma}} \right\}^{1/2} & \text{if} \quad \dfrac{P_a}{P} > \left(\dfrac{2}{\gamma+1} \right)^{\frac{\gamma}{\gamma-1}} \quad \text{(sub-sonic)} \end{cases} \tag{19}$$

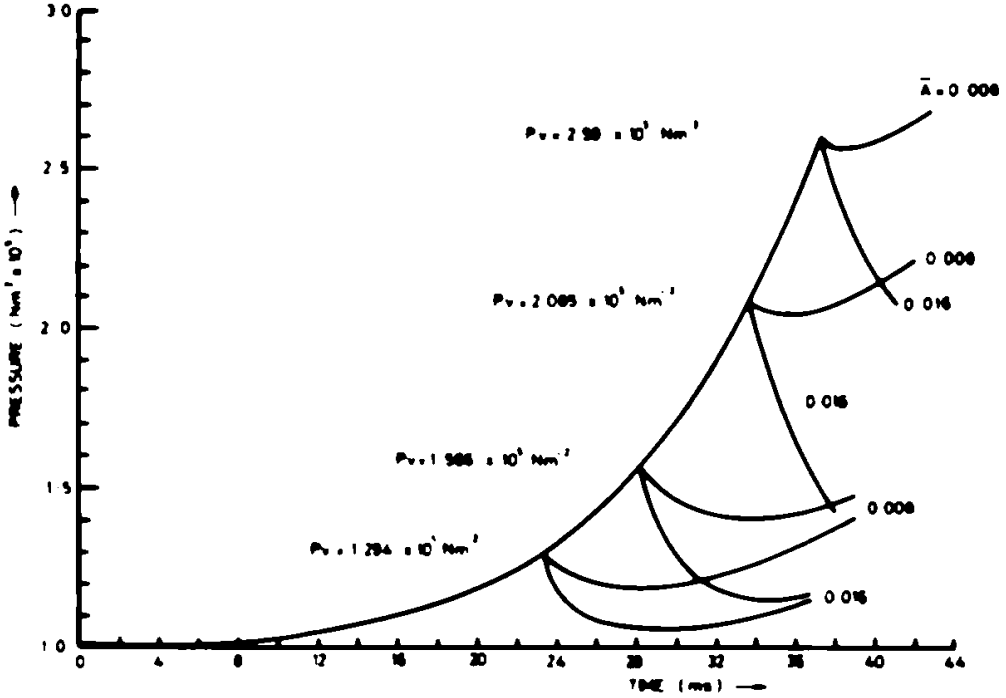
where ρ is the density of the vented mixture, P_a the ambient pressure, C_d a discharge coefficient and A_v the vent area. Substitution into (10), and repeating steps (11) to (17) results in

$$\frac{dP}{dt} = \begin{cases} \dfrac{3\left(P_{max} - P_0\right)}{R_{vessel}} \left[1 - \left(\dfrac{P_0}{P} \right)^{\frac{1}{\gamma}} \dfrac{P_{max} - P}{P_{max} - P_0} \right]^{\frac{2}{3}} \left(\dfrac{P}{P_0} \right)^{\frac{1}{\gamma}} S_u + C_d A_v \rho \left[\dfrac{\gamma P}{\rho} \left(\dfrac{\gamma+1}{2} \right)^{\frac{1+\gamma}{1-\gamma}} \right]^{1/2} \\ \dfrac{3\left(P_{max} - P_0\right)}{R_{vessel}} \left[1 - \left(\dfrac{P_0}{P} \right)^{\frac{1}{\gamma}} \dfrac{P_{max} - P}{P_{max} - P_0} \right]^{\frac{2}{3}} \left(\dfrac{P}{P_0} \right)^{\frac{1}{\gamma}} S_u + C_d A_v \left\{ \dfrac{2\gamma P \rho}{\gamma-1} \left(\dfrac{P_a}{P} \right)^{\frac{2}{\gamma}} \left[1 - \left(\dfrac{P_a}{P} \right)^{\frac{\gamma-1}{\gamma}} \right]^{\frac{1+\gamma}{1-\gamma}} \right\}^{1/2} \end{cases} \tag{20}$$

A model for vented deflagrations

Assume that the density of the vented mixture, ρ, is equal to that of the burnt mixture, ρ_b. With this assumption, the density of the vented mixture, ρ, in equation (20) can be computed from

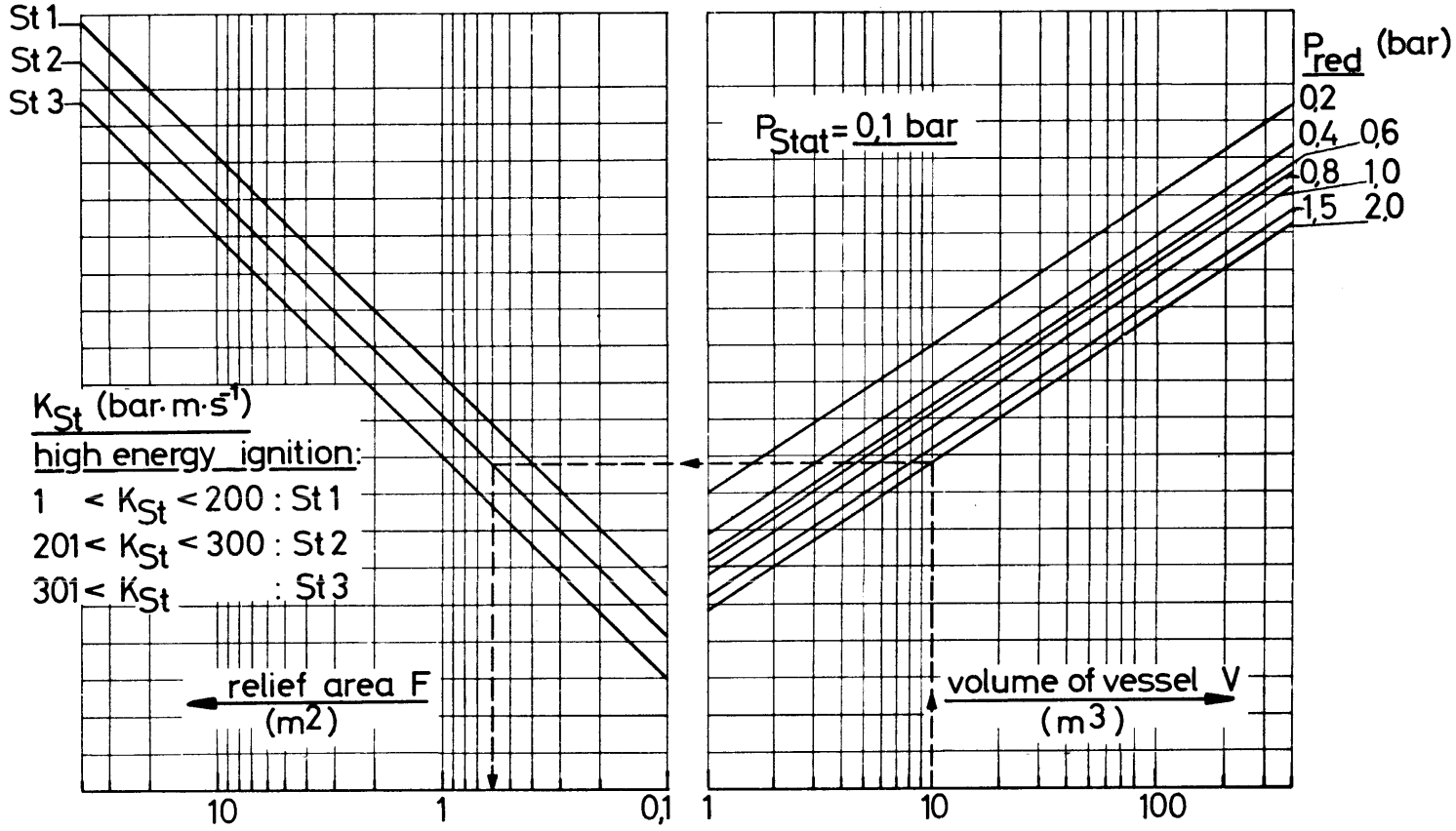
$$\rho \equiv \rho_b = \frac{T_u}{T_f}\rho_u = \rho_{u0}\frac{T_{u0}}{T_f}\left(\frac{P}{P_0}\right)^{\frac{\gamma-1}{\gamma}}\left(\frac{P}{P_0}\right)^{\frac{1}{\gamma}} \tag{21}$$



The figure shows the solution of equations (20) and (21) for two area ratios (vent area divided by total surface area of enclosure) and four different vent opening pressures.

From: Bradley D. and Mitcheson A. The venting of gaseous explosions in spherical vessels. I - Theory. Combustion and Flame, 32:221-236, 1978 [43].

Explosion severity
Pressure relief venting (VDI methodology)



From [45, 46].

Explosion severity
Pressure relief venting (NFPA methodology)

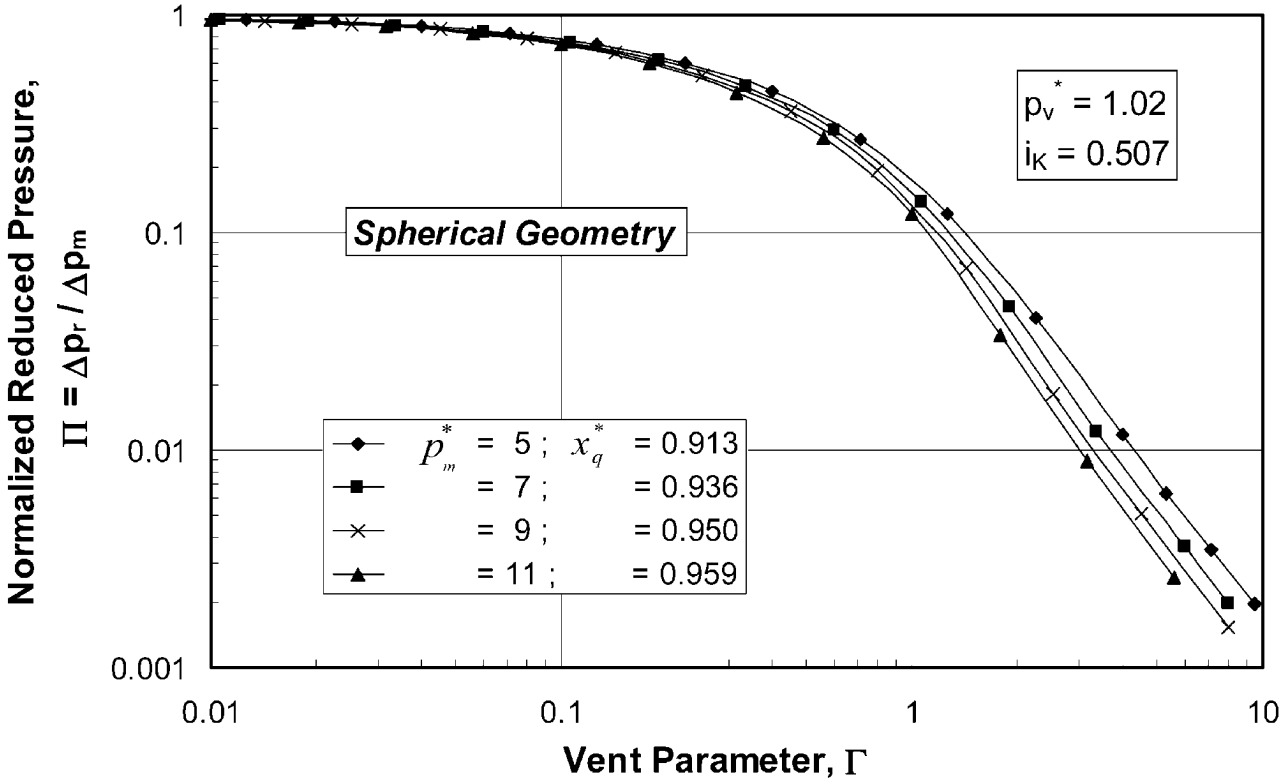
The NFPA 68 standard [13] proposes the following expression for the required venting area to protect an enclosure against a dust deflagration:

$$A_v = 10^{-4}\left(1 + 1.54\,P_{stat}^{4/3}\right) \times K_{\mathrm{St}} \times V^{3/4} \times \sqrt{\frac{P_{max}}{P_{red}} - 1}$$

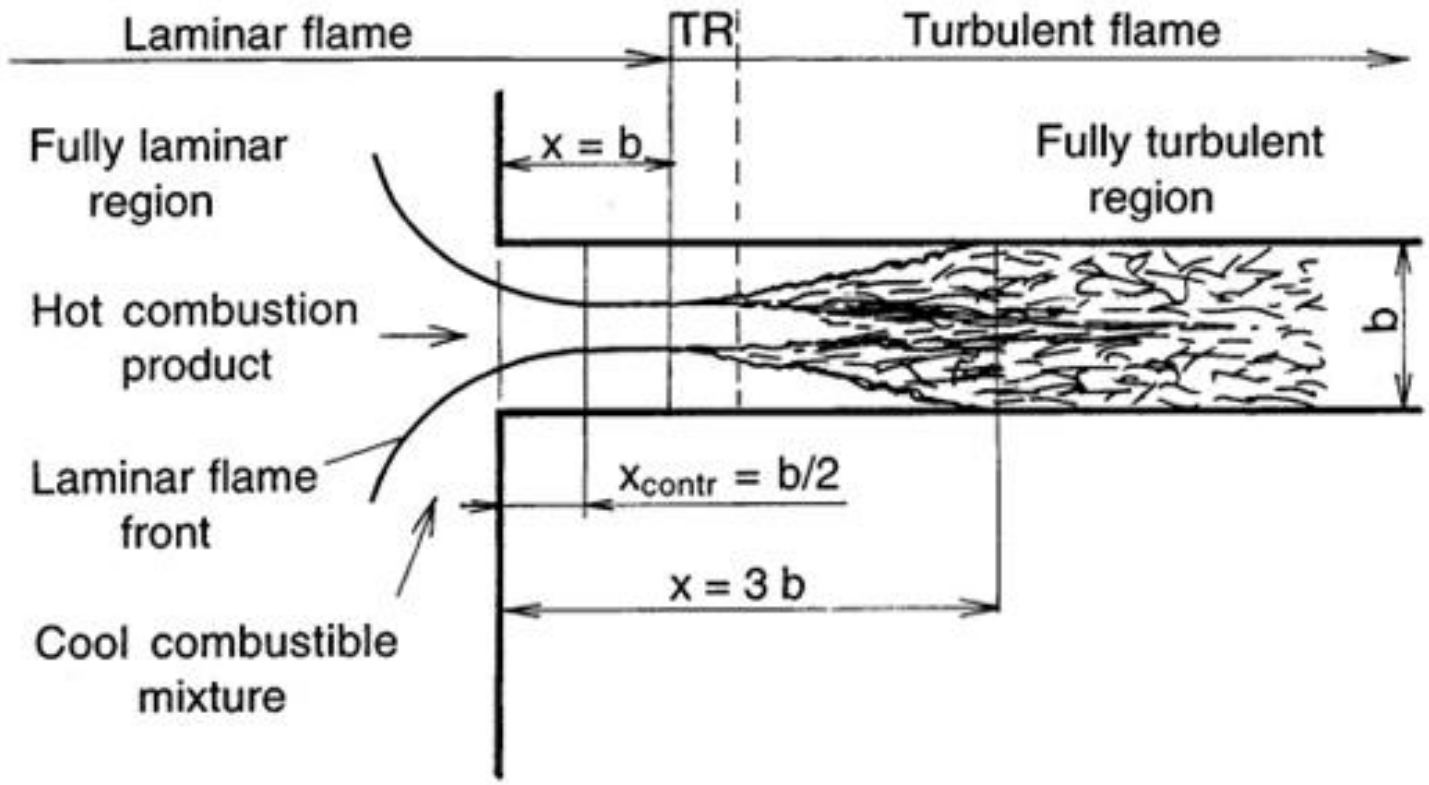
Explosion severity
Pressure relief venting (Other methodologies)

Tamanini F. Scaling parameters for vented gas and dust explosions. Journal of Loss Prevention in the Process Industries, 14:455–461, 2001. [47]

$$\text{Define} \qquad \Pi = \frac{P - P_0}{P_{max} - P_0} \qquad \text{and} \qquad \Gamma = C_d c_u \sqrt{\frac{\gamma + 1}{2}} \frac{A_v}{V^{2/3}} \frac{P_{max} - P_0}{K_G}$$

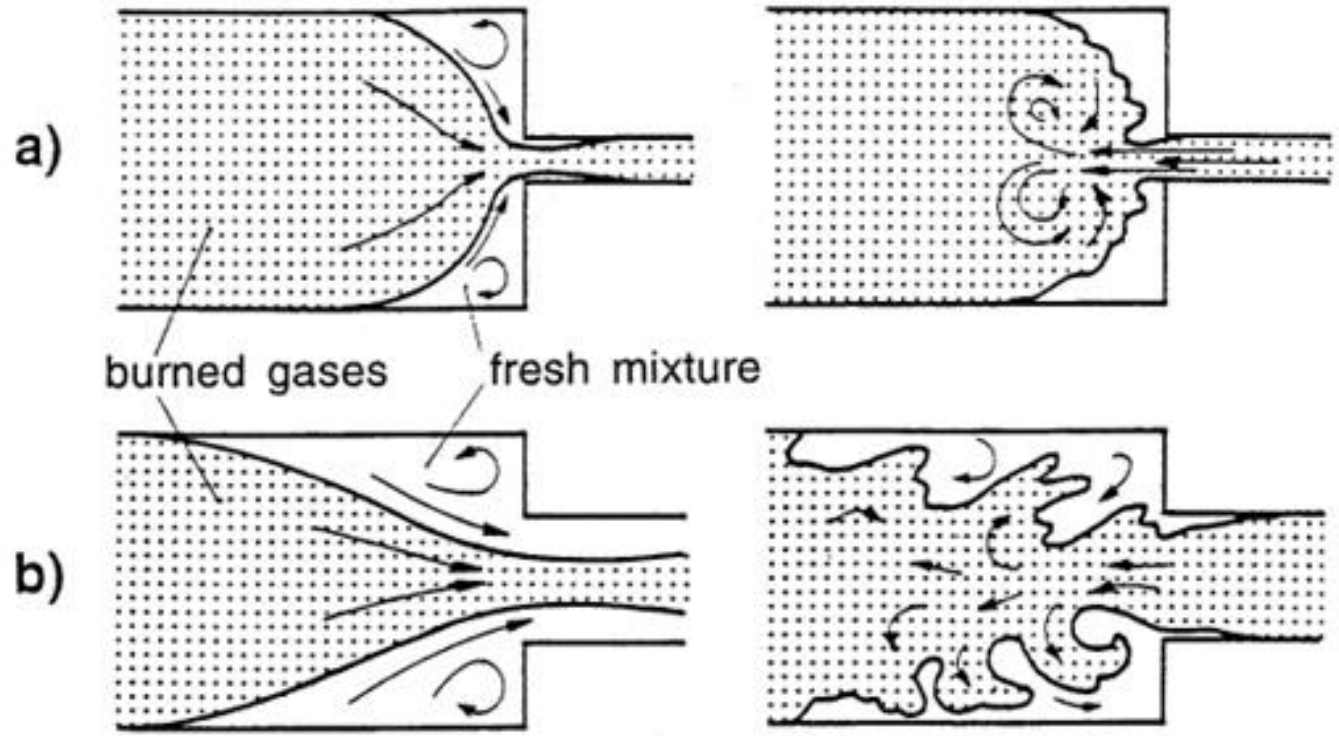


Explosion severity
Peculiarities of vented deflagrations
Flame distortion by vent ducts



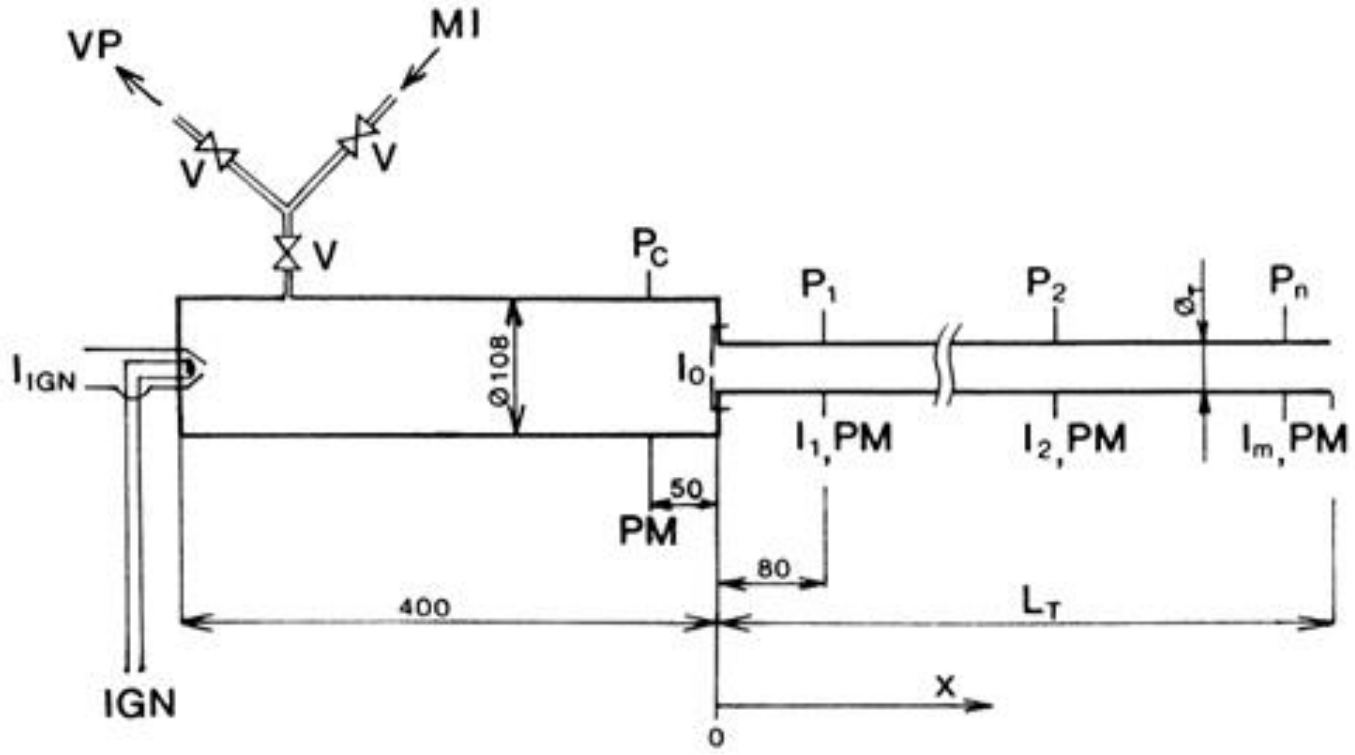
Flow pattern inside a vent duct [48–50].

Explosion severity
Peculiarities of vented deflagrations
Flame distortion by vent ducts



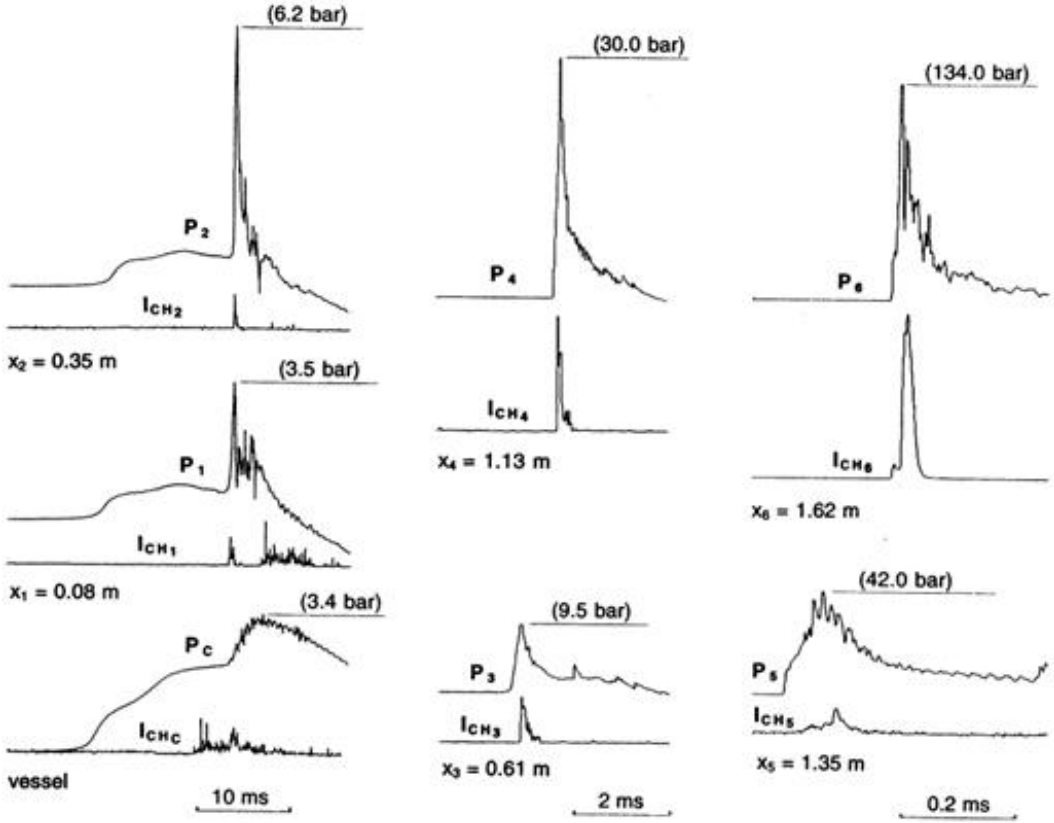
Flow patterns in vessel before and after combustion in the duct, effect of flame front distortion; a) narrow ducts, b) wide ducts. After Ponizy & Leyer (1999) [48, 49].

Explosion severity
Peculiarities of vented deflagrations
Flame distortion by vent ducts



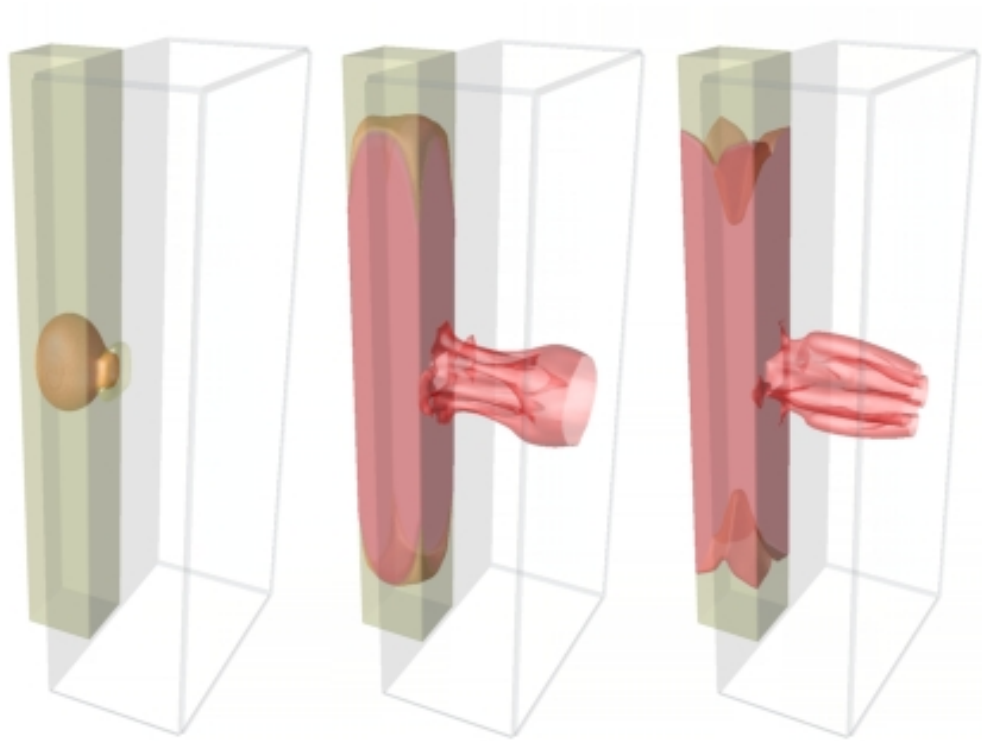
Experimental setup used by Ponizy & Leyer (1999) [48, 49]. IGN, ignition (electrically heated wire); VP, vacuum pump; MI, mixture inlet; V, valves; PM, photomultipliers; PC, P1, P2, . . . Pn, pressure gauges; IIGN, I0, I1, . . . Im, ionization gauges. The tube diameter is 53 mm.

Explosion severity
Peculiarities of vented deflagrations
Flame distortion by vent ducts



Deflagration to detonation transition (detonation onset at 1.7 m from duct entrance) [48, 49].

Explosion severity
Peculiarities of vented deflagrations



From: [51].

- **Enclosure geometry/aspect ratio**
- **Ignition location**
- **Varying pressure and temperature**
- **Varying turbulence**
- **Changes in flame shape**
- **Flame stretch and flame curvature**
- **Darrieu-Landau instability**
- **Thermo-diffusive instability**
- **Raleigh-Taylor instability**
- **Richtmeyer-Meshkov instability**
- **Flame distortion at outflow boundaries**
- **Vent cover inertia**

Laminar burning velocity/flame thickness: effect of pressure/temperature

Objective:
Find an expression for the pressure and temperature dependence of the laminar burning velocity and the laminar flame thickness

Governing equations:

$$\frac{\partial \rho}{\partial t} + \nabla \cdot (\rho \boldsymbol{v}) = 0 \tag{22}$$

$$\frac{\partial (\rho \boldsymbol{v})}{\partial t} + \nabla \cdot (\rho \boldsymbol{v}\boldsymbol{v}) = -\nabla p + \nabla \cdot \boldsymbol{\tau} + \sum_{i=1}^{N} \rho Y_i \boldsymbol{g} \tag{23}$$

$$\frac{\partial (\rho Y_i)}{\partial t} + \nabla \cdot (\rho \boldsymbol{v} Y_i) = -\nabla \cdot [\rho Y_i \boldsymbol{V}_i] + \dot{w}_i \tag{24}$$

$$\begin{aligned} \frac{\partial (\rho h)}{\partial t} + \nabla \cdot (\rho \boldsymbol{v} h) &= \frac{\partial p}{\partial t} + \boldsymbol{v} \cdot \nabla p + \boldsymbol{\tau} : \nabla \boldsymbol{v} - \nabla \cdot [\lambda \nabla T] + \nabla \cdot \boldsymbol{q} \\ &+ \nabla \cdot \left[\sum_{i=1}^{N} \rho Y_i h_i \boldsymbol{V}_i + \mathrm{R}T \sum_{i=1}^{N} \sum_{j=1}^{N} \left(\frac{X_j \alpha_i}{\mathcal{M}_i \mathcal{D}_{ij}} \right) (\boldsymbol{V}_i - \boldsymbol{V}_j) \right] + \sum_{i=1}^{N} \rho Y_i \boldsymbol{g} \cdot \boldsymbol{V}_i \end{aligned} \tag{25}$$

$$\frac{p}{\rho} = \frac{\gamma - 1}{\gamma} \sum_{i=1}^{N} Y_i \left[h_{f_i}^{\circ} + \int_{T^{\circ}}^{T} \mathrm{C}_{\mathrm{P}i}(T)\, dT \right] \tag{26}$$

$$\text{where} \quad \boldsymbol{\tau} = \mu \left[\nabla \boldsymbol{v} + (\nabla \boldsymbol{v})^{\dagger} \right] + \left(\kappa - \tfrac{2}{3}\mu \right) [\nabla \cdot \boldsymbol{v}]\, \boldsymbol{I} \tag{27}$$

$$\text{and} \quad \boldsymbol{q} = \epsilon \sigma T^4 \tag{28}$$

Assumptions:

- **Steady state**
- **Uniform pressure field**
- **Neglect viscous dissipation in energy equation**
- **Neglect effect of body forces in momentum and energy equation**
- **Neglect Dufour effect in energy equation**
- **Keep Soret effect in species and energy equation**

Step 1: **Make use of the fact that $h = \sum Y_i h_i$ to restate equations (24) and (25) as:**

$$\nabla \cdot [\rho Y_i (\boldsymbol{v} + \boldsymbol{V}_i)] = \dot{w}_i \tag{29}$$

$$\nabla \cdot \left[\sum_{i=1}^{N} \rho Y_i h_i (\boldsymbol{v} + \boldsymbol{V}_i) - \lambda \nabla T \right] = 0 \tag{30}$$

Step 2: Use

$$h_i = h_{f_i}^{\circ} + \int_{T^{\circ}}^{T} \mathrm{C_{P}}_i \, dT \tag{31}$$

to rewrite equation (30) as

$$\nabla \cdot \left[\sum_{i=1}^{N} \rho Y_i (\boldsymbol{v} + \boldsymbol{V}_i) h_{f_i}^{\circ} + \sum_{i=9}^{N} \rho Y_i (\boldsymbol{v} + \boldsymbol{V}_i) \int_{T^{\circ}}^{T} \mathrm{C_{P}}_i \, dT - \lambda \nabla T \right] = 0 \tag{32}$$

and apply equation (29) to the first term of the left hand side to obtain

$$\nabla \cdot \left[\rho \boldsymbol{v} \sum_{i=6}^{N} \int_{T^{\circ}}^{T} Y_i \mathrm{C_{P}}_i \, dT + \rho \sum_{i=1}^{N} \boldsymbol{V}_i \int_{T^{\circ}}^{T} Y_i \mathrm{C_{P}}_i \, dT - \lambda \nabla T \right] = - \sum_{i=1}^{N} h_{f_i}^{\circ} \dot{w}_i \tag{33}$$

Step 3: Assume a background fluid so that

$$\rho Y_i \boldsymbol{V}_i = -\rho \mathbb{D} \nabla Y_i \tag{34}$$

Since

$$\mathrm{C_P} = \sum Y_i \mathrm{C_P} \tag{35}$$

it is possible to rewrite equation (33) as

$$\nabla \cdot \left[\rho \boldsymbol{v} \int_{T^\circ}^{T} \mathrm{C_P}\, dT + \rho \mathbb{D} \sum_{i=1}^{N} (\nabla Y_i) \int_{T^\circ}^{T} Y_i \mathrm{C_P}_i\, dT - \rho \mathbb{D} \frac{\lambda}{\rho \mathrm{C_P} \mathbb{D}} \mathrm{C_P} \nabla T \right] = -\sum_{i=1}^{N} h_{f_i}^{\circ} \dot{w}_i \tag{36}$$

and because of the equality,

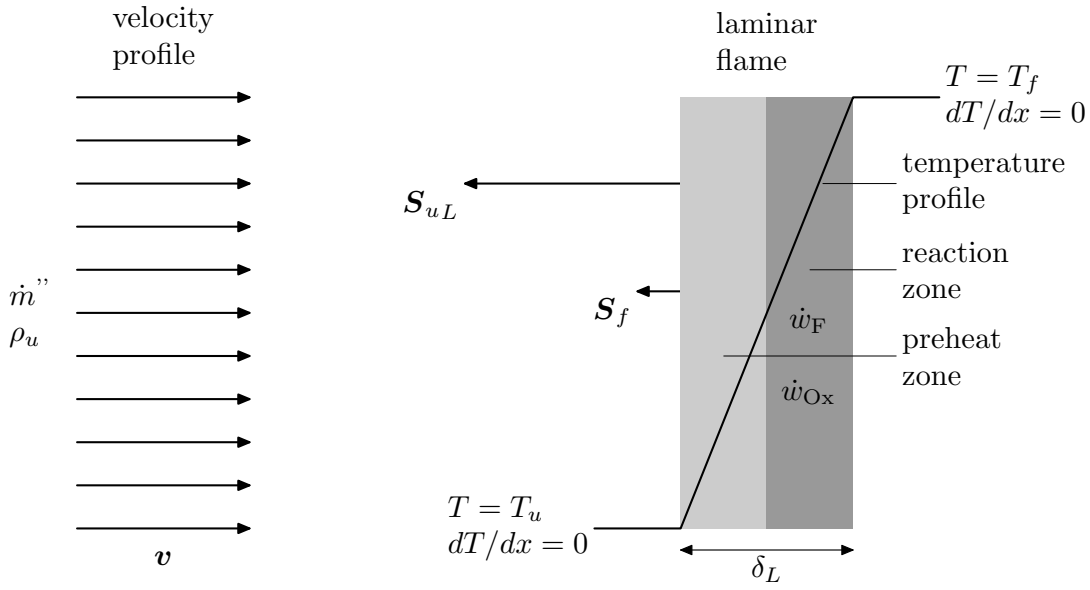
$$\nabla \int_{T^\circ}^{T} \mathrm{C_P}\, dT = \nabla \sum_{i=1}^{N} Y_i \int_{T^\circ}^{T} \mathrm{C_P}_i\, dT = \sum_{i=1}^{N} (\nabla Y_i) \int_{T^\circ}^{T} \mathrm{C_P}_i\, dT + \sum_{i=1}^{N} Y_i \nabla \int_{T^\circ}^{T} \mathrm{C_P}_i\, dT \tag{37}$$

$$= \sum_{i=1}^{N} (\nabla Y_i) \int_{T^\circ}^{T} \mathrm{C_P}_i\, dT + \sum_{i=1}^{N} Y_i \mathrm{C_P}_i \nabla T = \sum_{i=6}^{N} (\nabla Y_i) \int_{T^\circ}^{T} \mathrm{C_P}_i\, dT + \mathrm{C_P} \nabla T \tag{38}$$

equation (36) may be rewritten as

$$\boxed{\nabla \cdot \left[\rho \boldsymbol{v} \int_{T^\circ}^{T} \mathrm{C_P}\, dT + \rho \mathbb{D} \nabla \int_{T^\circ}^{T} \mathrm{C_P}\, dT - \rho \mathbb{D} \left[\mathrm{Le} - 1 \right] \mathrm{C_P} \nabla T \right] = -\sum_{i=1}^{N} h_{f_i}^{\circ} \dot{w}_i} \tag{39}$$

Step 4:



Assume unity Lewis number in equation (39): $$\nabla \cdot \left[\rho \boldsymbol{v} \int_{T^\circ}^{T} \mathrm{C_P}\, dT + \rho \mathbb{D} \nabla \int_{T^\circ}^{T} \mathrm{C_P}\, dT \right] = -\sum_{i=1}^{N} h_{f_i}^\circ \dot{w}_i \qquad (40)$$

If $\mathrm{Le} = 1$ then $\rho\mathbb{D}$ may be replaced by $\lambda/\mathrm{C_P}$! From figure with simplified flame structure: $\rho_u \boldsymbol{v} = \rho_u \boldsymbol{S}_{uL} = \dot{m}'' =$ constant.

Finally $$\boxed{\dot{m}'' \mathrm{C_P} \nabla T + \nabla \cdot [\lambda \nabla T] = -\sum_{i=1}^{N} h_{f_i}^\circ \dot{w}_i} \qquad (41)$$

Step 5:

Express the combustion reaction in terms of a mass balance:

$$1\,\text{kg Fuel} + \nu\,\text{kg Oxidizer} \longrightarrow (\nu+1)\,\text{kg Products} \tag{42}$$

Then

$$-\dot{w}_{\text{F}} = -\frac{1}{\nu}\dot{w}_{\text{Ox}} = \frac{1}{\nu+1}\dot{w}_{\text{Pr}} \tag{43}$$

and hence,

$$\begin{aligned}\sum_{i=1}^{N} h^{\circ}_{f_i}\dot{w}_i &= h^{\circ}_{f_{\text{F}}}\dot{w}_{\text{F}} + h^{\circ}_{f_{\text{Ox}}}\dot{w}_{\text{Ox}} + h^{\circ}_{f_{\text{Pr}}}\dot{w}_{\text{Pr}} \\ &= \left(h^{\circ}_{f_{\text{F}}} + \nu\, h^{\circ}_{f_{\text{Ox}}} - (\nu+1)\, h^{\circ}_{f_{\text{Pr}}}\right)\dot{w}_{\text{F}} \\ &= \Delta_c H\, \dot{w}_{\text{F}}\end{aligned} \tag{44}$$

where $\Delta_c H$ denotes the fuel's heat of combustion. Equation (39) may then be restated as:

$$\boxed{\dot{m}^{"}\text{C}_{\text{P}}\nabla T + \nabla\cdot[\lambda\nabla T] = -\Delta_c H\dot{w}_i} \tag{45}$$

Step 6:

Integrate the one-dimensional form of equation (45) from $x \to -\infty$ to $x \to \infty$ for the simplified flame structure,

$$\dot{m}^{"}\text{C}_{\text{P}}\frac{dT}{dx} + \frac{d}{dx}\left(\lambda\frac{dT}{dx}\right) = -\Delta_c H\,\dot{w}_{\text{F}} \tag{46}$$

subjected to the boundary conditions,

$$x\to-\infty: \quad T = T_u \qquad x\to\infty: \quad T = T_f \tag{47}$$

and the subsidiary conditions,

$$x\to-\infty: \quad \frac{dT}{dx} = 0 \qquad x\to\infty: \quad \frac{dT}{dx} = 0 \tag{48}$$

Inside the flame zone,

$$x \in \delta_L: \quad \frac{dT}{dx} = \frac{T_f - T_u}{\delta_L} \tag{49}$$

Integration of equation (46) gives:

$$\dot{m}^{"}\text{C}_{\text{P}}\,T\big|_{T_u}^{T_f} + \lambda\,\frac{\partial T}{\partial x}\bigg|_{dT/dx=0}^{dT/dx=0} = -\Delta_c H \int_{-\infty}^{\infty}\dot{w}_{\text{F}}\,dx \tag{50}$$

Step 7:

Apply a change of variables to the right hand side of equation (50) on the basis of the assumed temperature profile (49):

$$\frac{dT}{dx} = \frac{T_f - T_u}{\delta_L} \qquad \Longleftrightarrow \qquad dx = \frac{\delta_L}{T_f - T_u} dT \tag{51}$$

Hence,

$$\dot{m}^{"} \mathrm{C_P} \left(T_f - T_u\right) = -\frac{\delta_L \Delta_c H}{T_f - T_u} \int_{T_u}^{T_f} \dot{w}_\mathrm{F} dT = -\delta_L \Delta_c H \overline{\dot{w}}_\mathrm{F} \tag{52}$$

or, equivalently,

$$\boxed{\dot{m}^{"} \mathrm{C_P} \left(T_f - T_u\right) + \delta_L \, \Delta_c H \, \overline{\dot{w}}_\mathrm{F} = 0} \tag{53}$$

$\Longrightarrow$ A single *algebraic* equation with two unknowns:

- the mass flux $\dot{m}^{"} \left(\equiv \rho_u S_{uL}\right)$,
- and the laminar flame thickness δ_L.

Step 8:

Find a second algebraic equation by integrating equation (46) from $x \to -\infty$ to $x \to \delta_L/2$, subjected to the boundary conditions,

$$x \to -\infty : \quad T = T_u \qquad x = \frac{\delta_L}{2} : \quad T = \frac{T_u + T_f}{2} \tag{54}$$

and the subsidiary conditions,

$$x \to -\infty : \quad \frac{dT}{dx} = 0 \qquad x \to \frac{\delta_L}{2} : \quad \frac{dT}{dx} = \frac{T_f - T_u}{\delta_L} \tag{55}$$

Integration of equation (41) results in

$$\dot{m}^{"} \mathrm{C_P} \, T \Big|_{T_u}^{(T_u + T_f)/2} + \lambda \, \frac{\partial T}{\partial x} \bigg|_{dT/dx = 0}^{(T_f - T_u)/\delta_L} = -\Delta_c H \int_{-\infty}^{\delta_L/2} \dot{w}_\mathrm{F} \, dx \tag{56}$$

and hence,

$$\boxed{\tfrac{1}{2} \mathrm{C_P} \dot{m}^{"} \left(T_f - T_u\right) - \lambda \frac{T_f - T_u}{\delta_L} = 0} \tag{57}$$

since $\dot{w}_\mathrm{F}$ is practically zero in the preheat zone.

Step 9:

Solve equations (53) and (57) for S_{uL} and δ_L:

$$S_{uL} = \left[-2\frac{\lambda}{\rho_u \mathrm{C_P}} \frac{\Delta_c H}{\mathrm{C_P}\left(T_f - T_u\right)} \frac{\overline{\dot{w}}_\mathrm{F}}{\rho_u} \right]^{\frac{1}{2}} \tag{58}$$

$$\delta_L = \left[-2\frac{\lambda}{\rho_u \mathrm{C_P}} \frac{\mathrm{C_P}\left(T_f - T_u\right)}{\Delta_c H} \frac{\rho_u}{\overline{\dot{w}}_\mathrm{F}} \right]^{\frac{1}{2}} \tag{59}$$

Express the heat of combustion of the fuel as

$$\Delta_c H = (\nu + 1)\mathrm{C_P}(T_f - T_u) \tag{60}$$

and substitute this into equations (58) and (59):

$$S_{uL} = \left[-2\frac{\lambda}{\rho_u \mathrm{C_P}} (\nu + 1) \frac{\overline{\dot{w}}_\mathrm{F}}{\rho_u} \right]^{\frac{1}{2}} \tag{61}$$

$$\delta_L = \left[-2\frac{\lambda}{\rho_u \mathrm{C_P}} \frac{1}{\nu + 1} \frac{\rho_u}{\overline{\dot{w}}_\mathrm{F}} \right]^{\frac{1}{2}} \tag{62}$$

Step 10:

Assume a generalized overall reaction,

$$\sum_{i=1}^{N} \nu_i^{'} \mathrm{M}_i \longrightarrow \sum_{i=1}^{N} \nu_i^{''} \mathrm{M}_i \tag{63}$$

with a an overall reaction order $n = \sum_{i=1}^{N} \nu_i^{'}$

Mass consumption rate of each individual species:

$$\frac{d\left(\rho Y_i / \mathcal{M}_i\right)}{dt} = \left(\nu_i^{''} - \nu_i^{'}\right) B T^m \exp\left(-\frac{\mathrm{E_a}}{\mathrm{R}T}\right) \prod_{j=1}^{N} \left(\frac{\rho Y_j}{\mathcal{M}_j}\right)^{\nu_j^{'}} \tag{64}$$

$$\Longrightarrow \qquad \overline{\dot{w}}_\mathrm{F} \propto \rho^n B T^m \exp\left(-\frac{\mathrm{E_a}}{\mathrm{R}T}\right) \prod_{j=1}^{N} \left(Y_j / \mathcal{M}_j\right)^{\nu_j^{'}} \tag{65}$$

Since

$$\rho_u \propto T_u^{-1} P \tag{66}$$

and most of the combustion occurs in the reaction zone,

$$\overline{\dot{w}}_\mathrm{F} \propto T_f^{-n} P^n T_f^m \exp\left[-\frac{\mathrm{E_a}}{\mathrm{R}T_f}\right] \tag{67}$$

Step 11:

Substitute equations (66) and (67) into equations (61) and (62) to obtain:

$$\frac{S_{uL}}{S_{uL}^{\circ}} \propto \sqrt{\frac{\lambda(T_u)}{\lambda(T_{u0})}} \frac{T_u}{T_{u0}} \left(\frac{P}{P_0}\right)^{\frac{n-2}{2}} \left(\frac{T_f}{T_f^{\circ}}\right)^{-\frac{n}{2}} \left(\frac{T_f}{T_f^{\circ}}\right)^{\frac{m}{2}} \exp\left[-\frac{\mathrm{E_a}}{2\mathrm{R}}\left(\frac{1}{T_f}-\frac{1}{T_f^{\circ}}\right)\right] \tag{68}$$

$$\frac{\delta_L}{\delta_L^{\circ}} \propto \sqrt{\frac{\lambda(T_u)}{\lambda(T_{u0})}} \left(\frac{P}{P_0}\right)^{-\frac{n}{2}} \left(\frac{T_f}{T_f^{\circ}}\right)^{\frac{n}{2}} \left(\frac{T_f}{T_f^{\circ}}\right)^{-\frac{m}{2}} \exp\left[+\frac{\mathrm{E_a}}{2\mathrm{R}}\left(\frac{1}{T_f}-\frac{1}{T_f^{\circ}}\right)\right] \tag{69}$$

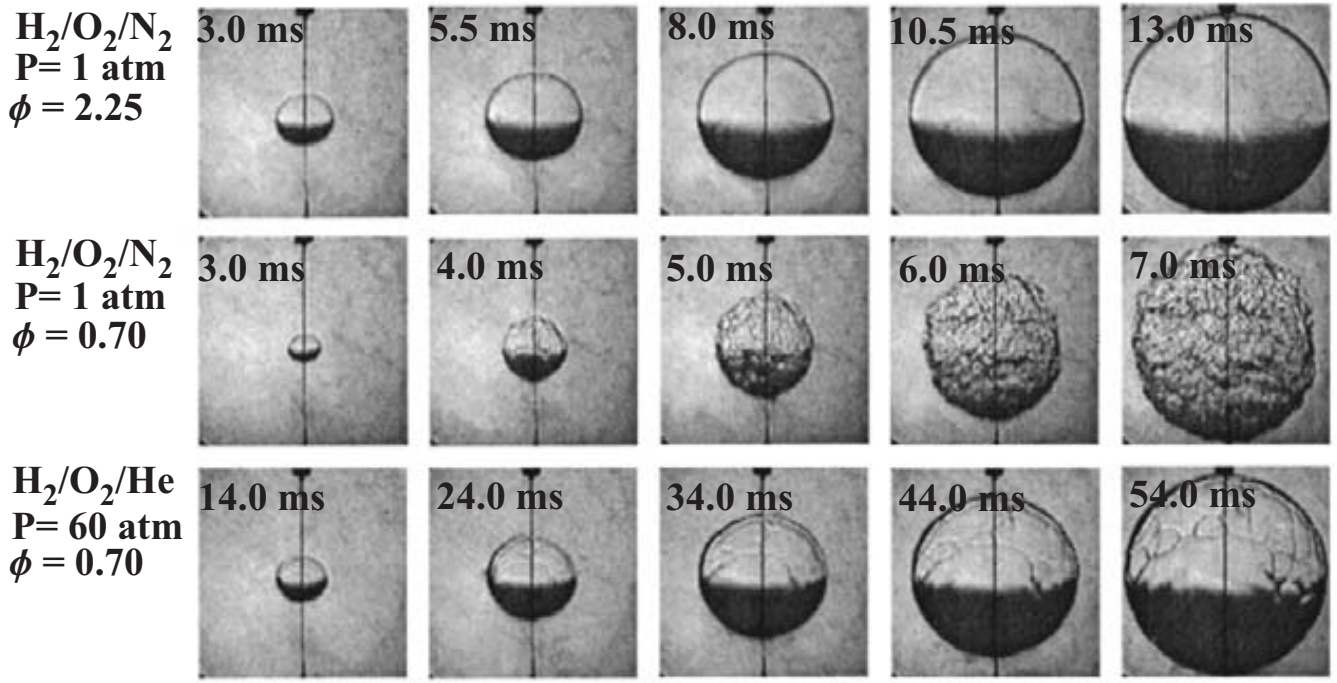
where S_{uL}°, δ_L° and T_f° are the laminar burning velocity, the laminar flame thickness and the flame temperature of the unburnt mixture at a reference state P_0 and T_{u0}.

When the variation in T_u is caused by adiabatic compression, equations (68) and (69) can be approximated by:

$$\frac{S_{uL}}{S_{uL}^{\circ}} = \left(\frac{P}{P_0}\right)^{c+\frac{\gamma-1}{\gamma}-1+\alpha} \tag{70}$$

$$\frac{\delta_L}{\delta_L^{\circ}} = \left(\frac{P}{P_0}\right)^{c-\alpha} \tag{71}$$

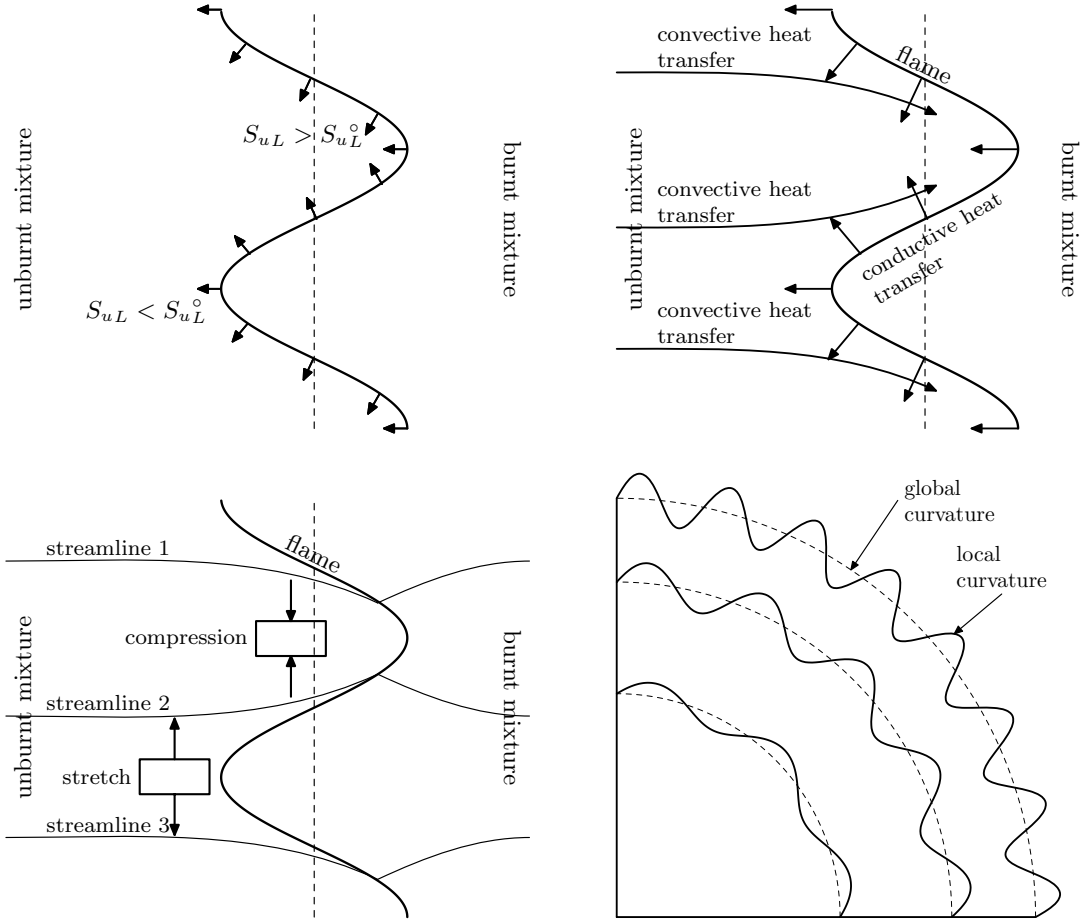
Laminar burning velocity: effect of flame morphology



Flame morphology of propagating hydrogen-air flames.

From: Tse S.D., Zhu D.L., and Law C.K. Morphology and burning rates of expanding spherical flames in H2/O2/inert mixtures up to 60 atmospheres. In Proceedings of the Twenty-Eighth Symposium (International) on Combustion, pages 1793-1800, Pittsburgh, 2000. The Combustion Institute.

Laminar burning velocity: effect of flame stretch and flame curvature



Effect of flame stretch and flame curvature on the laminar burning velocity.

Laminar burning velocity: effect of flame stretch and flame curvature

Stretch rate of a surface element in a strained fluid:

$$\dot{s} = \frac{1}{A}\frac{dA}{dt} \tag{72}$$

Universal expression which relates the stretch rate of a flame surface element to the velocity field, $\boldsymbol{v}$, of a non-uniform flow-field:

$$\dot{s} = \underbrace{-\boldsymbol{nn}{:}\nabla\boldsymbol{v} + \nabla\cdot\boldsymbol{v}}_{\dot{s}_s} + \underbrace{S_{uL}^{\circ}\nabla\cdot\boldsymbol{n}}_{\dot{s}_c} \tag{73}$$

When a planar laminar flame with a thickness δ_L° is distorted into a bulge of size Λ, the local laminar burning velocity at each point can be related to the local stretch rate as

$$\frac{S_{uL}^{\circ} - S_{uL}}{S_{uL}^{\circ}} = \frac{\mathcal{L}}{S_{uL}^{\circ}}\left(\frac{1}{A}\frac{dA}{dt}\right) + \mathcal{O}\left(\epsilon^2\right) \tag{74}$$

where $\epsilon = \delta_L^{\circ}/\Lambda$. When $\Lambda \gg \delta_L^{\circ}$, ϵ is a small number so that:

$$S_{uL}^{\circ} - S_{uL} = \mathcal{L}\left(\frac{1}{A}\frac{dA}{dt}\right) + \mathcal{O}\left(\epsilon^2\right) \tag{75}$$

$$= \mathcal{L}\dot{s} + \mathcal{O}\left(\epsilon^2\right) \tag{76}$$

Laminar burning velocity: effect of flame stretch and flame curvature

Express $\mathcal{L}\dot{s}$ as a linear combination of quantities that account for the separate effects of the strain rate, flame curvature, pressure, etc., each having its own Markstein length:

$$\mathcal{L}\dot{s} \equiv \mathcal{L}_s\dot{s}_s + \mathcal{L}_c\dot{s}_c + \ldots \tag{77}$$

$$\implies S_{uL}^{\circ} - S_{uL} = \left(\mathcal{L}_s\dot{s}_s + \mathcal{L}_c\dot{s}_c + \ldots\right) + \mathcal{O}\left(\epsilon^2\right) \tag{78}$$

Combine equations (73), (76) and (78):

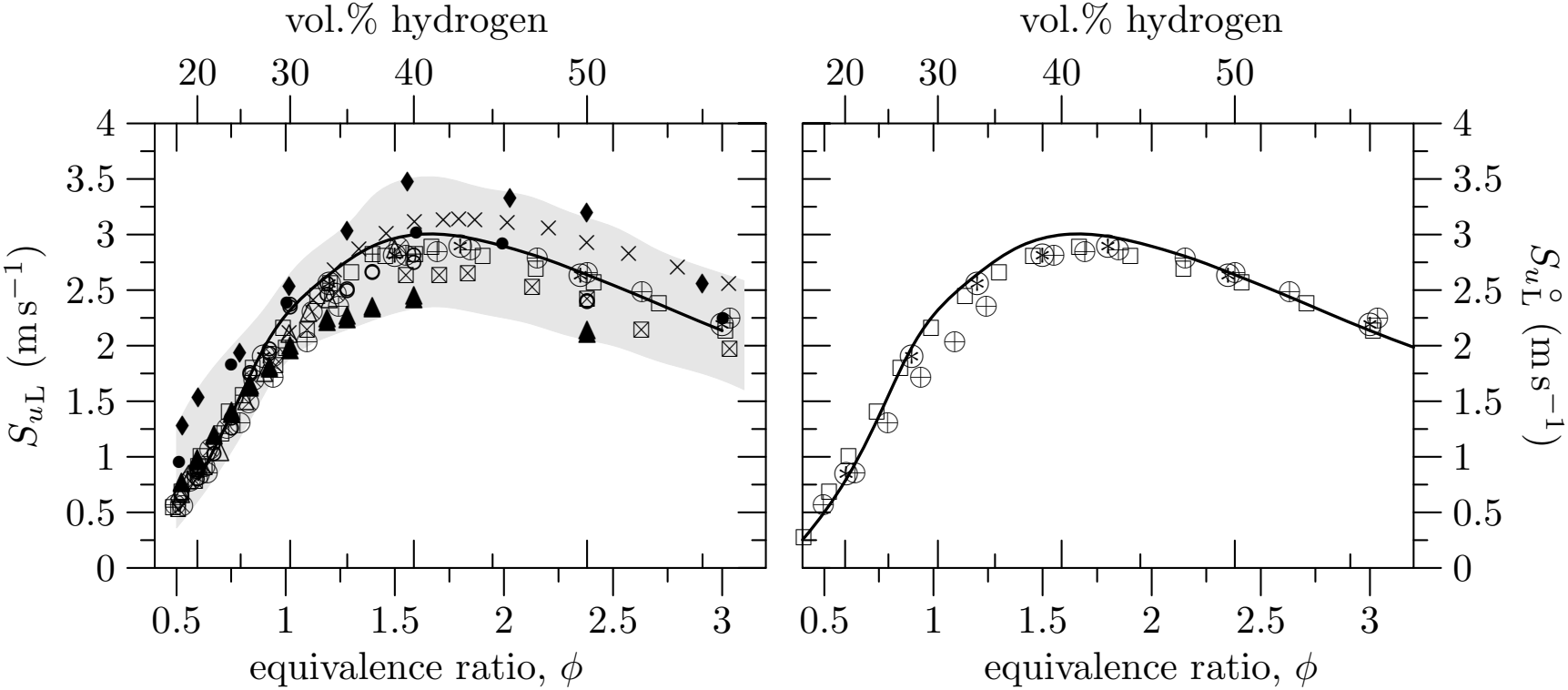
$$S_{uL} = \mathcal{L}_s\left[\boldsymbol{nn}{:}\nabla\boldsymbol{v} - \nabla\cdot\boldsymbol{v}\right] + \left[1 - \mathcal{L}_c\nabla\cdot\boldsymbol{n}\right]S_{uL}^{\circ} \tag{79}$$

$$= \mathcal{L}_s\left[\boldsymbol{nn}{:}\nabla\boldsymbol{v} - \nabla\cdot\boldsymbol{v}\right] + \left[1 + \frac{\mathcal{L}_c}{\kappa_1+\kappa_2}\right]S_{uL}^{\circ} \tag{80}$$

$$= \mathcal{L}_s\left[\boldsymbol{nn}{:}\nabla\boldsymbol{v} - \nabla\cdot\boldsymbol{v}\right] + \left[1 + \frac{\mathcal{L}_c}{\mathcal{R}}\right]S_{uL}^{\circ} \tag{81}$$

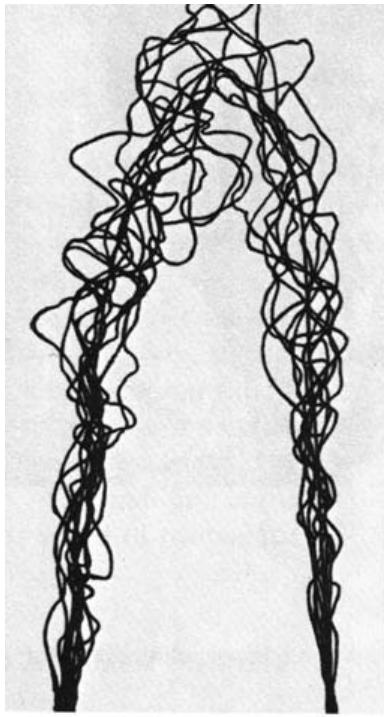
The quantities denoted by $\mathcal{L}_s$ and $\mathcal{L}_c$ are called Markstein lengths.

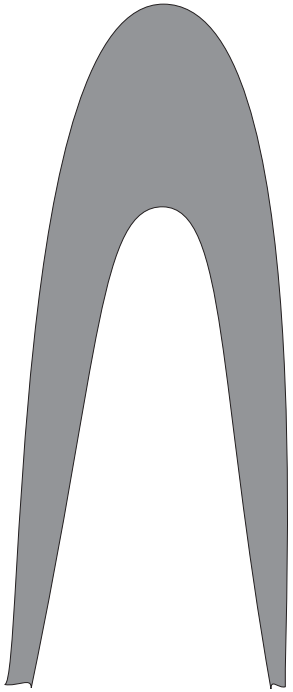
Unstretched laminar burning velocity

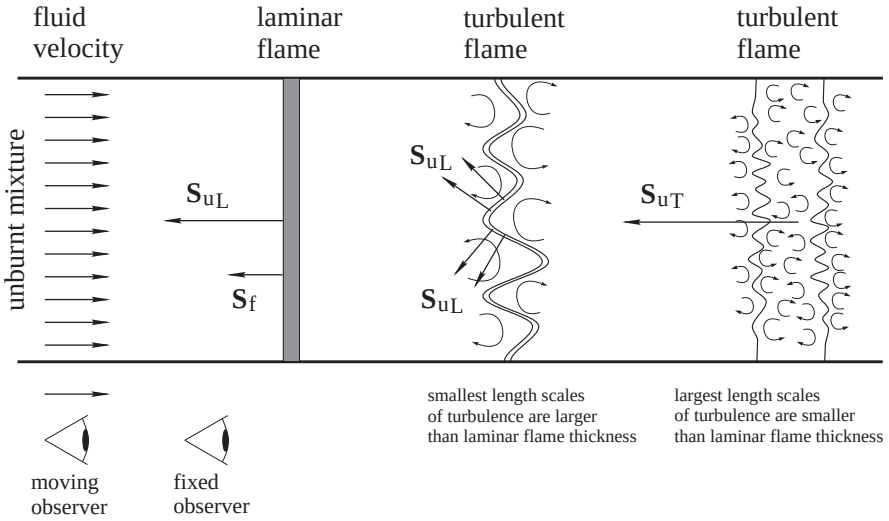


Unstretched laminar burning velocity of hydrogen-air mixtures as a function of equivalence ratio at T_0=293.15–298.15 K and P_0=1 bar. solid line: computed data by Marinov, Westbrook, & Pitz (1996) [52], (▫) Dowdy, Smith & Taylor (1990) [53], (⊛) Kwon & Faeth (2001) [54], (⊕) Tse, Zhu & Law (2000) [55], (●) Dahoe (2005) [7].

Turbulent burning velocity: flame-turbulence interaction







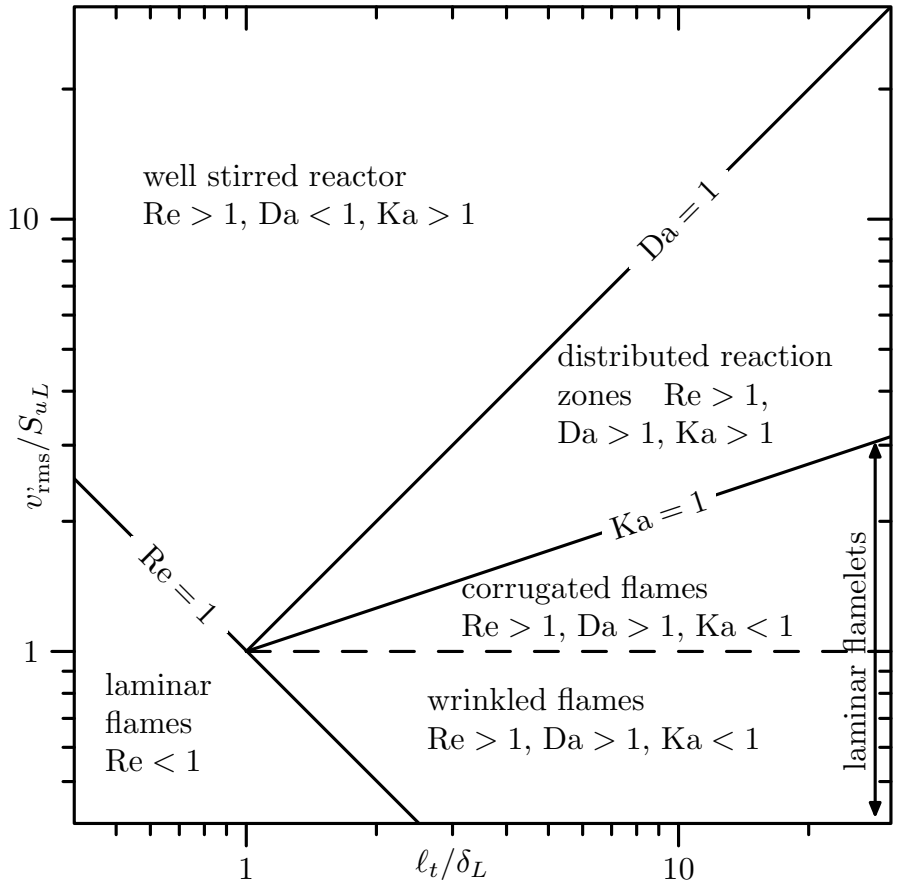
$$S_{u\mathrm{T}} = f(S_{u\mathrm{L}}, v'_{\mathrm{rms}})$$

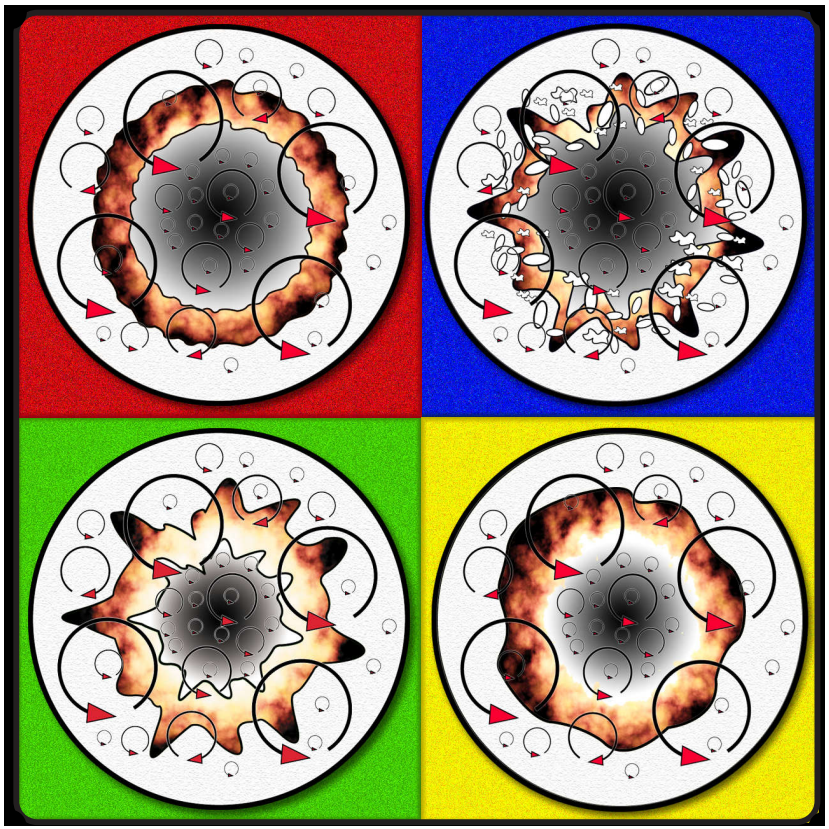
$$S_{u\mathrm{T}} = f(S_{u\mathrm{L}}, v'_{\mathrm{rms}}, \ell_t)$$

$$S_{u\mathrm{T}} = f(S_{u\mathrm{L}}, \delta_{\mathrm{L}}, v'_{\mathrm{rms}}, \ell_t)$$

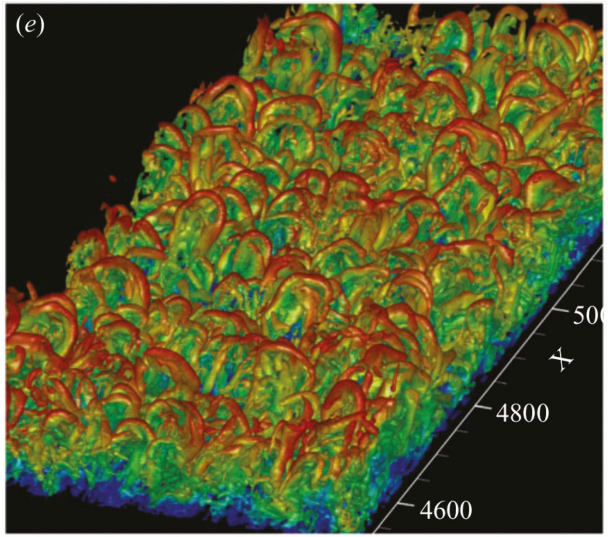
$$\begin{cases} S_{u\mathrm{T}} & = f(S_{u\mathrm{L}}, \delta_{\mathrm{L}}, v'_{\mathrm{rms}}, \ell_t) \\ \delta_{\mathrm{T}} & = g(S_{u\mathrm{L}}, \delta_{\mathrm{L}}, v'_{\mathrm{rms}}, \ell_t) \end{cases}$$

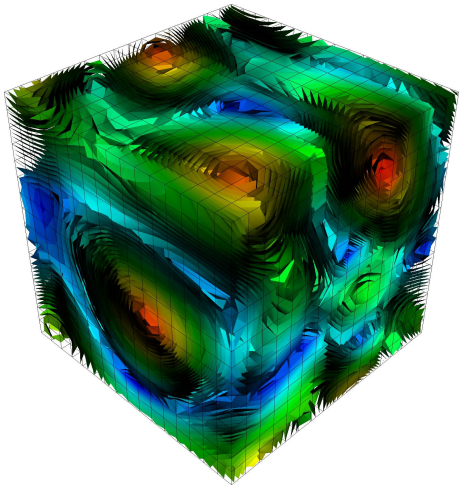
Turbulent burning velocity: combustion regimes



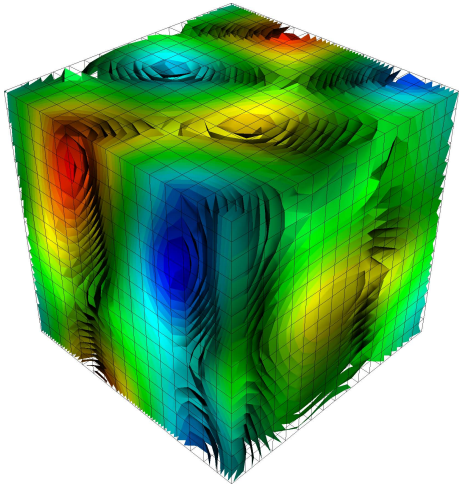


Turbulent burning velocity: turbulence scales





Velocity field



Pressure field

Generic scales:

$$\mathcal{U} \qquad \mathcal{L} \qquad \mathcal{T} = \mathcal{L}/\mathcal{U}$$

Integral scales:

$$\mathcal{U} = v_t \qquad \mathcal{L} = \ell_t \qquad \mathcal{T} = \tau_t = \ell_t/v_t$$

Kolmogorov microscales:

$$\mathcal{U} = v_K \qquad \mathcal{L} = \ell_K \qquad \mathcal{T} = \tau_K = \ell_K/v_K$$

Turbulent burning velocity: correlations

From: Dahoe A.E., Skjold T., Roekaerts D.J.E.M., Pasman H.J., Eckhoff R.K., Hanjalic K., and Donze M. On the application of the Levenberg-Marquardt method in conjunction with an explicit Runge-Kutta and an implicit Rosenbrock method to assess burning velocities from confined deflagrations. *Flow, Turbulence and Combustion*, 91:281–317, 2013 [40].

Model	Ref.
(82) $\frac{S_{uT}}{S_{uL}} = 1 + \frac{v'_{\rm rms}}{S_{uL}}$	[56, 57]
Note: Analysis of instantaneous laminar flame area within a turbulent flame brush. Instantaneous laminar flame area is assumed to increase linearly with $v'_{\rm rms}$.	
(83) $\frac{S_{uT}}{S_{uL}} = \sqrt{1 + \left(\frac{v'_{\rm rms}}{S_{uL}}\right)^2}$	[58, 59]
Note: Analysis of instantaneous laminar flame area within a turbulent flame brush. Distorted laminar flame is assumed to consist of conical bulges. Effect of turbulence taken into account by surface area ratio between cone mantle and cone base.	
(84) $\frac{S_{uT}}{S_{uL}} = 1 + \frac{v'_{\rm rms}}{S_{uL}}$ Same as (82).	[60]
(85) $\frac{S_{uT}}{S_{uL}} = 1 + \sqrt{\frac{5}{12}}\frac{v'_{\rm rms}}{S_{uL}}$ (86) $\frac{S_{uT}}{S_{uL}} = 1 + \sqrt{2}\left(\frac{v'_{\rm rms}}{S_{uL}}\right)^{\frac{1}{2}}$	
Note: Time-scale analysis of r.m.s. displacement [61] within interaction time between flame element and turbulent eddy. Eqn. (84): weak turbulence ($\ell_t/v'_{\rm rms} \gg \delta_l/S_{uL}$) Eqn. (85): intermediate turbulence ($\ell_t/v'_{\rm rms} \approx \delta_l/S_{uL}$). Eqn. (86): strong turbulence ($\ell_t/v'_{\rm rms} \ll \delta_l/S_{uL}$).	

(87) $$\frac{S_{uT}}{S_{uL}} = \sqrt{1 + \left(\frac{2v'_{\text{rms}}}{S_{uL}}\right)^2}$$ [62]

Note: Analysis of intersection between eddies and laminar flame. Eddies assumed to have diameter ℓ_t and a sinusoidal velocity profile characterised by v'_{rms} [63].

(88) $$\frac{S_{uT}}{S_{uL}} = 1 + C\left(\frac{v'_{\text{rms}}}{S_{uL}}\right)^2$$ [64]

Note: Analysis interaction of laminar flame with isotropic turbulence [63, 64].

(89) $$\frac{S_{uT}}{S_{uL}} = 1 + \left(\frac{v'_{\text{rms}}}{S_{uL}}\right)^2$$ [65]

Note: Analysis of the longitudinal displacement of the reactive-diffusive zone by turbulence in an Eulerian frame of reference.

(90) $$\frac{S_{uT}}{S_{uL}} = \left\{\frac{1}{2}\left[1 + \left[1 + C\left(\frac{v'_{\text{rms}}}{S_{uL}}\right)^2\right]^{\frac{1}{2}}\right]\right\}^{\frac{1}{2}}$$ [66]

Note: An extension of model (89) with thermal expansion taken into account [67].

(91) $$\frac{S_{uT}}{S_{uL}} = C\left(\frac{v'_{\text{rms}}}{S_{uL}}\right)^n \qquad C = 3.5,\ n = 0.7$$ [68]

Note: Analysis of flame-turbulence interaction. Turbulence characterised by single velocity scale and single length scale [67].

(92) $$\frac{S_{uT}}{S_{uL}} = f(K) \qquad \text{where} \qquad K = C\text{Re}_{\ell_t}^{-\frac{1}{2}}\left(\frac{v'_{\text{rms}}}{S_{uL}}\right)^2$$ [69]

Note: C=0.157. Two-eddy theory. Rate of burning equal to product of rate of eddy decay and amount of mixture that reacts chemically during eddy lifetime. Localized reaction rate within an eddy is expressed by laminar burning velocity [69]. K is the Karlovitz stretch factor [70].

(93) $$\frac{S_{uT}}{S_{uL}} = C\left(\frac{v'_{\text{rms}}}{S_{uL}}\right) \qquad C = 2.1$$ [71]

Note: Monte Carlo solution of a modelled transport equation for the joint probability density function (pdf) of velocity and reaction progress variable [71].

(94) $$\frac{S_{uT}}{S_{uL}} = \mathrm{Re}_{\ell_K}^{\frac{3}{2}} \left(\frac{v'_{\mathrm{rms}}}{S_{uL}}\right)^{\frac{1}{2}}$$ [72]

Note: Analysis of exchanges of state (burned or unburned) between adjacent fluid elements along a discretized line element in the streamwise direction [72].

(95) $$\frac{S_{uT}}{S_{uL}} = \left\{\beta\left[1 - \left(1 - \beta^{-1}\right)\exp\left(-\alpha\frac{v'_{\mathrm{rms}}}{S_{uL}}\right)\right]\right\}^{D-2}$$ [73]

Note: Fractal modelling of laminar flame surface with fractal dimension $D = 2.32$–2.40 [73–76], outer cutoff $\ell_o{=}\ell_t$, and inner cutoff $\ell_i{=}\ell_K$. $\mathrm{Re}_{\ell_t}{=}\rho v'_{\mathrm{rms}}\ell_t/\mu$, $\alpha{=}(A_t/\mathrm{Re}_{\ell_t})^{1/4}$ and $\beta{=}(A_t/\mathrm{Re}_{\ell_t}^3)^{1/4}$. $A_t{=}0.37$ from turbulent pipe flow data [69, 73, 77].

(96) $$\frac{S_{uT}}{S_{uL}} = \frac{v'_{\mathrm{rms}}}{S_{uL}}$$ [78]

Note: Fractal modelling of laminar flame surface in turbulent flow. Flame surface: outer cutoff $\ell_o{=}\ell_t$ and inner cutoff equal to Gibson length scale, $\ell_i{=}\ell_G$. [79].

(97) $$\frac{S_{uT}}{S_{uL}} = \exp\left[v'^2_{\mathrm{rms}}/S_{uT}^{\,2}\right]$$ [80, 81]

Note: Analysis of very thin reaction zone in a turbulent flow field [80]. Flame represented by scalar field $G(\boldsymbol{x}, t)$ which propagates according to [82, 83] $\partial G/\partial t + \boldsymbol{v}\cdot\nabla G = S_{uL}\,|\nabla G|$. Ref. [80] derives (97) by dynamic re-normalisation group analysis to G-equation. Ref. [81] derives (97) from two distinct expressions for turbulent flame brush thickness while assuming exponential growth of interface between parcels of reactants and products.

(98) $$\frac{S_{uT}}{S_{uL}} = 1 + C\left(v'_{\mathrm{rms}}/S_{uL}^{\,1/2}\right) \qquad C = 5.3$$ [84]

Note: Curve fit to experimental burner data (turbulence by perforated plate) [84].

(99) $$\frac{S_{uT}}{S_{uL}} = 1 + C\mathrm{Re}_{\ell_t}^{\frac{1}{4}} \left(\frac{v'_{\mathrm{rms}}}{S_{uL}}\right)^{\frac{1}{2}} = 1 + C\mathrm{Re}_{\delta_L}^{\frac{1}{4}} \mathrm{Da}^{\frac{1}{4}} \left(\frac{v'_{\mathrm{rms}}}{S_{uL}}\right)^{\frac{3}{4}}$$ [67]

Note: $C = \sqrt[4]{2/15} \approx 0.6$. Application of two distinct expressions for the turbulent flame brush thickness in conjunction with an estimate of the mean distance the flame must travel to consume the mixture between dissipative vortex tubes and the relationship $\lambda_T/\ell_t = \sqrt{15}\mathrm{Re}_{\ell_t}^{-1/2}$ [85, 86]. The Taylor microscale, λ_T, is the spacing between the vortex tubes. Curve-fitting to more than 200 data points for 15 mixtures reported by eight different research groups gave a value of $C = 0.62$ [67].

(100) $$\frac{S_{uT}}{S_{uL}} = 1 + S_{uL}^{1/4} \left(\frac{v'_{\mathrm{rms}}}{S_{uL}}\right) = 1 + \left(\frac{\delta_L v_{\mathrm{rms}}}{\ell_t}\right)^{\frac{1}{4}} \mathrm{Da}^{\frac{1}{4}} \left(\frac{v'_{\mathrm{rms}}}{S_{uL}}\right)$$ [87]

Note: Curve fit to experimental turbulent burning velocities of methane-air, hydrogen-air and methane-hydrogen-air mixtures in fan-stirred vessels (65 l spherical bomb and 1 m^3 cylindrical vessel).

(101) $$\frac{S_{uT}}{S_{uL}} = C\mathrm{Le}^{-0.3}\mathrm{Re}_{\ell_t}^{0.15} \left(\frac{v'_{\mathrm{rms}}}{S_{uL}}\right)^{0.4} \qquad C = 1.534$$ [70]

Note: Curve fit to 1650 experimental data points by 20 different groups [70, 88].

(102) $$\frac{S_{uT}}{S_{uL}} = 1 + C\mathrm{Da}^{\frac{1}{4}} \left(\frac{v'_{\mathrm{rms}}}{S_{uL}}\right) \qquad C = 0.51$$ [89]

Note: Analysis of flame front motion from solution of Favre-averaged governing equations in spherical coordinates with Bray-Moss-Libby formalism as closure model [90–92] and a model for local combustion failure [89].

(103) $$\frac{S_{uT}}{S_{uL}} = 1 + \left(\frac{v'_{\mathrm{rms}}}{S_{uL}}\right)^{1/2} = 1 + \left(\frac{\ell_t}{\delta_L}\right)^{\frac{1}{4}} \mathrm{Da}^{\frac{1}{4}} \left(\frac{v'_{\mathrm{rms}}}{S_{uL}}\right)^{\frac{3}{4}}$$ [93]

Note: Experimental analysis of a downward propagating premixed methane-air flame through a nearly isotropic turbulent flow field in a tube [93].

(104) $$\frac{S_{uT}}{S_{uL}} = 1 + C\left(\frac{\ell_t}{\delta_L}\right)^{1/4}\left(\frac{v'_{\text{rms}}}{S_{uL}}\right)^{3/4} = 1 + C\text{Da}^{\frac{1}{4}}\left(\frac{v'_{\text{rms}}}{S_{uL}}\right)$$ [94]

Note: $C = \sqrt[4]{2/15} \approx 0.6$. Application of a model originating from Refs. [67, 95] to upward propagating potato starch dust-air flames in a tube [94, 96].

(105) $$\frac{S_{uT}}{S_{uL}} = 1 + C'\text{Da}^{a'}\left(\frac{v'_{\text{rms}}}{S_{uL}}\right)^{b'}$$ [40]

Note: Dimensional analysis. Simplification of equation (145).

Turbulent burning velocity: Damköhler's correlation

Equate mass flux, $\dot{m}$, through cross sectional area of flame brush, A_T to mass flow of unburnt mixture through wrinkled laminar flame area, A_L:

$$\dot{m} = \rho_u A_T S_{uT} = \rho_u A_L S_{uL} \tag{106}$$

$$\Rightarrow \frac{S_{uT}}{S_{uL}} = \frac{A_L}{A_T} \tag{107}$$

Damköhler approximated the ratio of the area of wrinkled laminar flame and the cross section of the turbulent flame brush by

$$\frac{A_L}{A_T} = \frac{S_{uL} + v'_{\text{rms}}}{S_{uL}} = 1 + \frac{v'_{\text{rms}}}{S_{uL}} \tag{108}$$

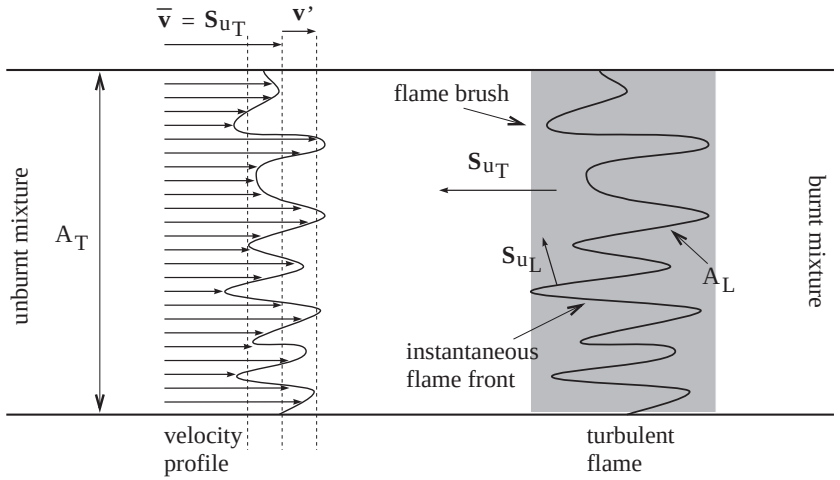
Substitution into equation (107) leads to

$$\boxed{\frac{S_{uT}}{S_{uL}} = 1 + \frac{v'_{\text{rms}}}{S_{uL}}} \tag{109}$$

In the limit $v'_{\text{rms}} \gg S_{uL}$, equation (109) implies that the turbulent burning velocity becomes independent of the laminar burning velocity

$$S_{uT} \sim v'_{\text{rms}} \tag{110}$$

This is known as Damköhler's hypothesis.



Turbulent burning velocity: Schelkin's correlation

Schelkin assumed:

• Turbulence creates conical bulges in a laminar flame.

• Increased flame surface is proportional to the average cone area divided by the average cone base.

• If the radius of the cone base and the apothem are denoted by R and h, then the surface area of the cone base and the cone mantle are equal to πR^2 and $\pi R\sqrt{R^2+h^2}$.

• When a circular element of a planar laminar flame is bulged into a cone, the surface area increases by a factor $\sqrt{R^2+h^2}/R$.

• Diameter of the cone base is proportional to the average length scale of the turbulence, $R \propto \frac{1}{2}\ell_t$.

• Diameter of the cone base is proportional to the average length scale of the turbulence, $R \propto \frac{1}{2}\ell_t$ and that the apothem scales as $h \propto v'_{\rm rms}\ell_t/S_{uL}$.

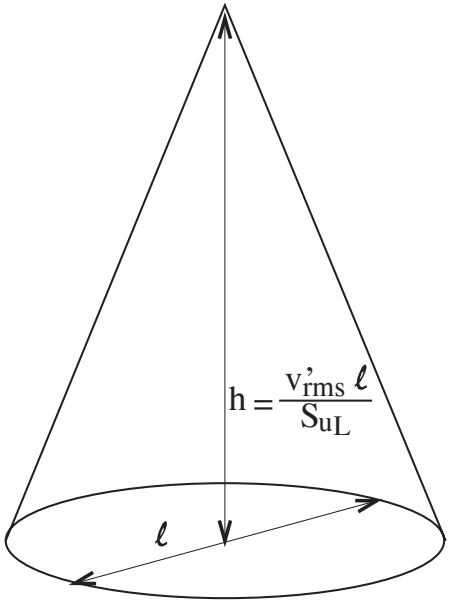
• Apothem to be proportional to the average fluctuating velocity $v'_{\rm rms}$ and the time during which an element of the flame interacts with an eddy, ℓ_t/S_{uL}.

These assumptions lead to

$$\frac{A_L}{A_T} = \frac{\sqrt{R^2+h^2}}{R} = \sqrt{1+\left(\frac{2v'_{\rm rms}}{S_{uL}}\right)^2} \qquad (111)$$

and substitution into equation (107) gives:

$$\boxed{\frac{S_{uT}}{S_{uL}} = \sqrt{1+\left(\frac{2v'_{\rm rms}}{S_{uL}}\right)^2}} \qquad (112)$$



Turbulent burning velocity: Karloviz's correlations

Define a turbulence macro velocity scale, a turbulence macro time scale and a turbulence macro length scale:

$$v_t = v'_{\text{rms}} = (\overline{v'^2})^{\frac{1}{2}}$$

$$\tau_t = \int_0^\infty \rho(\tau) d\tau \qquad \text{where} \qquad \rho(\tau) = \frac{\overline{v'(t)v'(t+\tau)}}{\overline{v'^2(t)}}$$

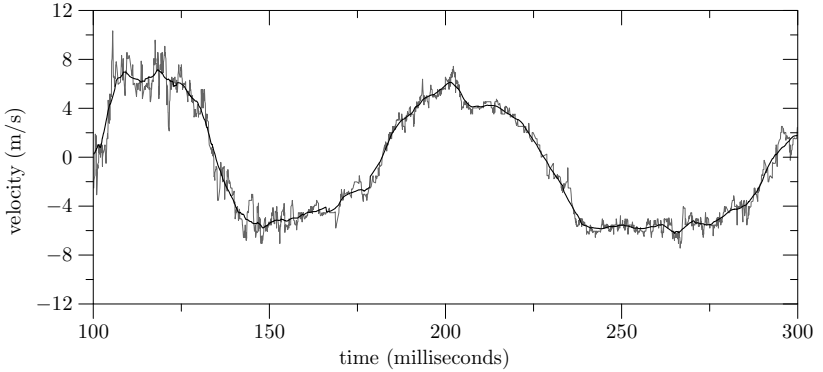
$$\ell_t = v_t \tau_t = v'_{\text{rms}} \tau_t$$

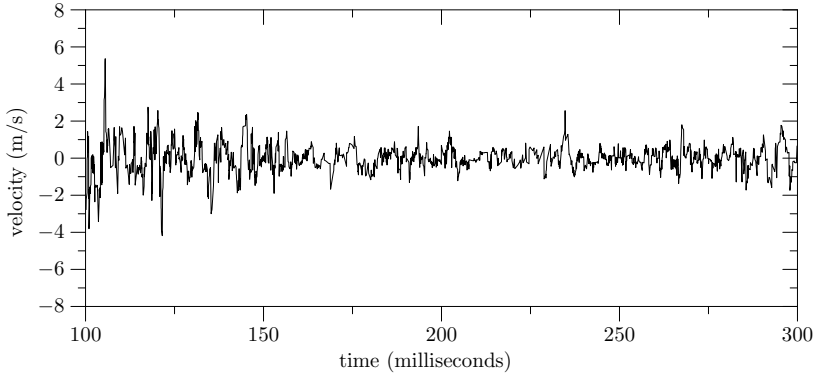
Karlovitz assumed that an additional velocity produced by the turbulent diffusion, ${S_u}^t$, has to be added to the laminar burning velocity:

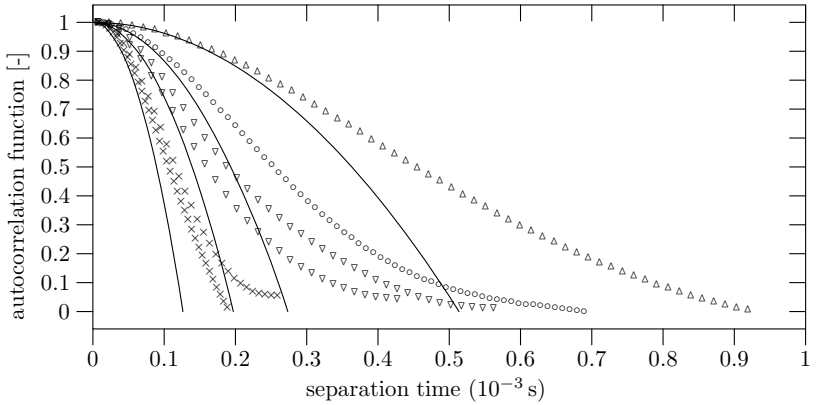
$$S_{uT} = S_{uL} + {S_u}^t \tag{113}$$

The additional velocity is taken into account by dividing the root-mean-square displacement due to the turbulence by the average time interval during which a flame element interacts with an eddy, $\mathcal{T} = \ell_t / S_{uL}$:

$${S_u}^t = \frac{(\overline{x'^2})^{\frac{1}{2}}}{\mathcal{T}} \tag{114}$$







Karloviz's correlations for the turbulent burning velocity

The root-mean-square displacement and root-mean-square velocity are interrelated through:

$$\frac{d\overline{x'^2}}{dt} = 2\,\overline{v'^2}\int_0^t \rho(\tau)\,d\tau = 2\,(v'_{\rm rms})^2\int_0^t \rho(\tau)\,d\tau \qquad (115)$$

Weak turbulence: $v'_{\rm rms} \ll S_{uL}$. Hence $\mathcal{T}\,(\equiv \ell_t/S_{uL}) \ll \tau_t\,(\equiv \ell_t/v'_{\rm rms})$. Consequently, $\rho(\tau) \approx 1$ if $t \leq \mathcal{T}$ so that the root-mean-square displacement within the interaction time between a flame element and a turbulent eddy becomes (by integrating equation (115)): $(\overline{x'^2})^{\frac{1}{2}} = v'_{\rm rms}\mathcal{T}$

$$\Longrightarrow {S_u}^t = \frac{(\overline{x'^2})^{\frac{1}{2}}}{\mathcal{T}} = \frac{v'_{\rm rms}\mathcal{T}}{\mathcal{T}} = v'_{\rm rms} \qquad (116)$$

Substitution into equation (113) and division by S_{uL} results in

$$\boxed{\frac{S_{uT}}{S_{uL}} = 1 + \frac{v'_{\rm rms}}{S_{uL}}} \qquad (117)$$

Strong turbulence: $\mathcal{T}\,(\equiv \ell_t/S_{uL}) \gg \tau_t\,(\equiv \ell_t/v'_{\rm rms})$. The integral on the right hand side of equation (115) assumes a definite value which is equal to the time scale of the turbulence, τ_t. This leads to

$$(\overline{x'^2})^{\frac{1}{2}} = \sqrt{2\ell_t v'_{\rm rms}\mathcal{T}} \qquad (118)$$

and

$${S_u}^t = \frac{(\overline{x'^2})^{\frac{1}{2}}}{\mathcal{T}} = \frac{\sqrt{2\ell_t v'_{\rm rms}\mathcal{T}}}{\ell_t/S_{uL}} = \sqrt{2S_{uL}v'_{\rm rms}} \qquad (119)$$

Insertion into equation (113) and division by S_{uL} yields:

$$\boxed{\frac{S_{uT}}{S_{uL}} = 1 + \sqrt{2}\left(\frac{v'_{\rm rms}}{S_{uL}}\right)^{\frac{1}{2}}} \qquad (120)$$

Intermediate turbulence: $\mathcal{T}\,(\equiv \ell_t/S_{uL}) \approx \tau_t\,(\equiv \ell_t/v'_{\rm rms})$, the root-mean-square displacement depends on the shape of the correlation function. If the shape of the correlation function is approximated by an osculation parabola, where τ_m denotes the Taylor microscale,

$$\rho(\tau) = 1 - \frac{1}{2}\frac{\tau^2}{{\tau_m}^2} \qquad (121)$$

the integral in (115) may be solved for the variance of the displacement to give

$$\overline{x'^2} = \overline{v'^2}\left[\tfrac{1}{2}\mathcal{T}^2 - \tfrac{1}{12}(\mathcal{T}^4/\tau_m^2)\right] \approx \overline{v'^2}\left[\tfrac{1}{2}\mathcal{T}^2 - \tfrac{1}{12}\mathcal{T}^2\right] \approx \tfrac{5}{12}\overline{v'^2}\mathcal{T}^2 \qquad (122)$$

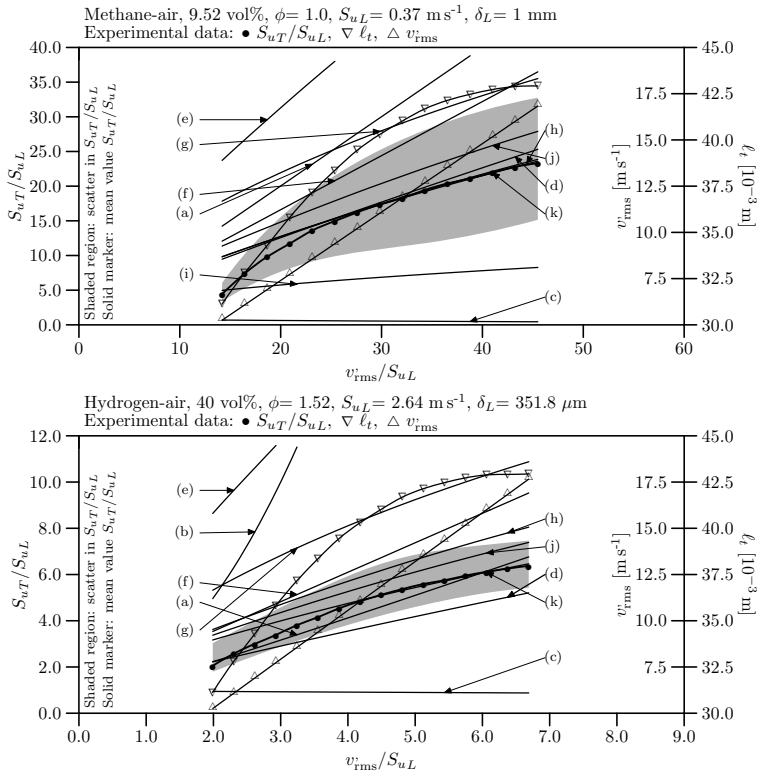
Consequently,

$${S_u}^t = \frac{(\overline{x'^2})^{\frac{1}{2}}}{\mathcal{T}} = \frac{\sqrt{\frac{5}{12}}v'_{\rm rms}\mathcal{T}}{\mathcal{T}} = \sqrt{\tfrac{5}{12}}v'_{\rm rms} \qquad (123)$$

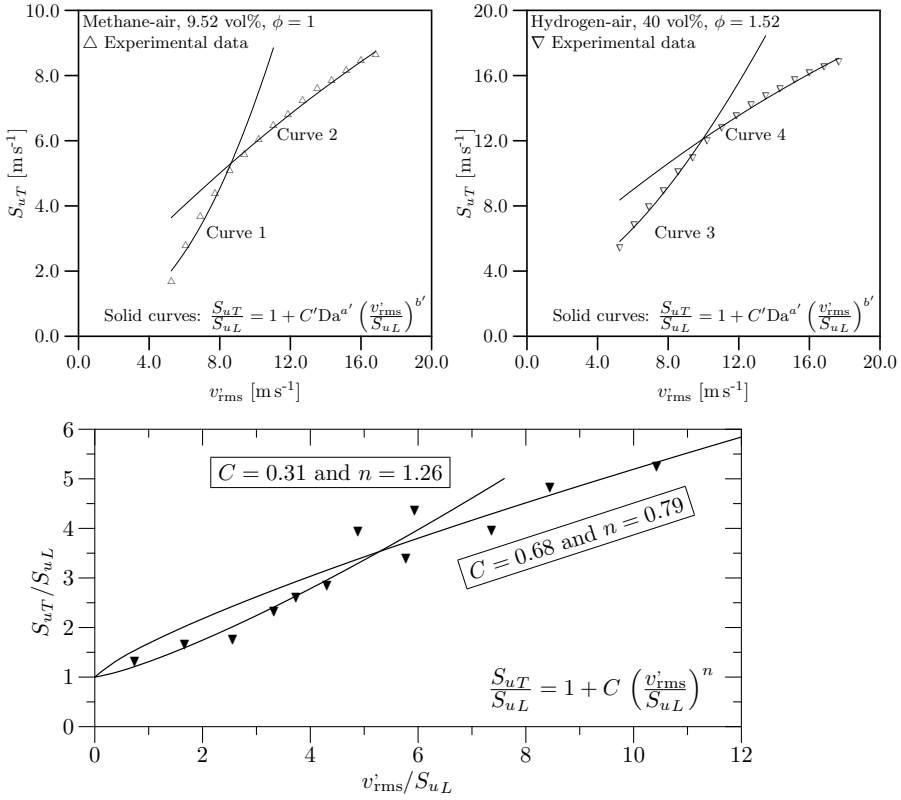
and

$$\boxed{\frac{S_{uT}}{S_{uL}} = 1 + \sqrt{\tfrac{5}{12}}\frac{v'_{\rm rms}}{S_{uL}}} \qquad (124)$$

Turbulent burning velocity: correlations
Comparison with experimental data



Key: (a) eqn (83), (b) eqn (89), (c) eqn (95), (d) eqn (97), (e) eqn (99), (f) eqn (100), (g) eqn (101), (h) eqn (102), (i) eqn (103), (j) eqn (104), (k) eqn (146). From [40].



Cornstarch-air.

Borghi Diagram: Dimensionless Groups

Governing equations:

$$\frac{\partial \rho}{\partial t} + \nabla \cdot (\rho \boldsymbol{v}) = 0 \tag{125}$$

$$\frac{\partial (\rho \boldsymbol{v})}{\partial t} + \nabla \cdot (\rho \boldsymbol{v}\boldsymbol{v}) = -\nabla \cdot p + \nabla \cdot \boldsymbol{\tau} + \sum_{i=1}^{N} \rho Y_i \boldsymbol{g} \tag{126}$$

$$\frac{\partial (\rho Y_i)}{\partial t} + \nabla \cdot (\rho \boldsymbol{v} Y_i) = \nabla \cdot (\rho \mathbb{D}_i \nabla Y_i) + \dot{w}_i \tag{127}$$

$$\frac{\partial (\rho h)}{\partial t} + \nabla \cdot (\rho \boldsymbol{v} h) = \frac{\partial p}{\partial t} + \boldsymbol{v} \cdot \nabla p + \boldsymbol{\tau} \colon \nabla \boldsymbol{v} + \nabla \cdot (\lambda \nabla T) - \nabla \cdot \boldsymbol{q} - \sum_{i=1}^{N} \rho Y_i \boldsymbol{g} \cdot (\mathbb{D}_i \nabla Y_i) \tag{128}$$

Restate using a length scale, $\mathcal{L}$, a velocity scale, $\mathcal{U}$, and, a chemical time scale, τ_c, so that

$$\frac{\partial \rho^*}{\partial t^*} + \nabla^* \cdot (\rho^* \boldsymbol{v}^*) = 0 \tag{129}$$

$$\frac{\partial (\rho^* \boldsymbol{v}^*)}{\partial t^*} + \nabla^* \cdot (\rho^* \boldsymbol{v}^* \boldsymbol{v}^*) = -\left(\frac{\rho \mathcal{U}^2}{p}\right) \nabla^* p^* \tag{130}$$

$$+ \left(\frac{\rho \mathcal{U}^2}{p}\right) \left(\frac{\mu}{\rho \mathcal{U} \mathcal{L}}\right) \nabla^* \cdot \boldsymbol{\tau}^* + \left(\frac{\mathcal{L} g}{\mathcal{U}^2}\right) \sum_{i=1}^{N} \rho^* Y_i \boldsymbol{g}^* \tag{131}$$

$$\frac{\partial (\rho^* Y_i)}{\partial t^*} + \nabla^* \cdot (\rho^* \boldsymbol{v}^* Y_i) = \left(\frac{\mu}{\rho \mathcal{U} \mathcal{L}}\right) \left(\frac{\rho \mathbb{D}_i}{\mu}\right) \nabla^{*\,2} Y_i + \left(\frac{\rho \mathcal{U}^2}{p}\right) \left(\frac{\mathcal{L}/\mathcal{U}}{\tau_c}\right) \dot{w}_i^* \tag{132}$$

$$\frac{\partial (\rho^* h^*)}{\partial t^*} + \nabla^* \cdot (\rho^* \boldsymbol{v}^* h^*) = \left(\frac{\rho \mathcal{U}^2}{p}\right) \left(\frac{\mathcal{U}^2}{\mathrm{C_P} T_0}\right) \left[\frac{\partial p^*}{\partial t^*} + \boldsymbol{v}^* \cdot \nabla^* p^*\right] \tag{133}$$

$$+ \left(\frac{\rho \mathcal{U}^2}{p}\right) \left(\frac{\mu}{\rho \mathcal{U} \mathcal{L}}\right) \left(\frac{\mathcal{U}^2}{\mathrm{C_P} T_0}\right) \boldsymbol{\tau}^* \colon \nabla^* \boldsymbol{v}^* + \left(\frac{\rho \mathcal{U}^2}{p}\right) \left(\frac{\mu}{\rho \mathcal{U} \mathcal{L}}\right) \left(\frac{\lambda}{\mu \mathrm{C_P}}\right) \nabla^{*\,2} T^* \tag{134}$$

$$- \left(\frac{\rho \mathcal{U}^2}{p}\right) \left(\frac{q_0}{\rho \mathcal{U} \mathrm{C_P} T_0}\right) \nabla^* \cdot \boldsymbol{q}^* - \left(\frac{\mu}{\rho \mathcal{U} \mathcal{L}}\right) \left(\frac{\mu}{\rho \mathbb{D}_i}\right) \left(\frac{\mathcal{L} g}{\mathcal{U}^2}\right) \sum_{i=1}^{N} Y_i \rho^* \boldsymbol{f}_i^* \cdot \nabla^* Y_i \tag{135}$$

Borghi Diagram: Dimensionless Groups

So that finally:

$$\frac{\partial \rho^*}{\partial t^*} + \nabla^* \cdot (\rho^* \boldsymbol{v}^*) = 0 \tag{136}$$

$$\frac{\partial (\rho^* \boldsymbol{v}^*)}{\partial t^*} + \nabla^* \cdot (\rho^* \boldsymbol{v}^* \boldsymbol{v}^*) = -\mathrm{Ma}^2 \nabla^* p^* + \frac{\mathrm{Ma}^2}{\mathrm{Re}} \nabla^* \cdot \boldsymbol{\tau}^* + \frac{1}{\mathrm{Fr}} \sum_{i=1}^{N} \rho^* Y_i \boldsymbol{g}^* \tag{137}$$

$$\frac{\partial (\rho^* Y_i)}{\partial t^*} + \nabla^* \cdot (\rho^* \boldsymbol{v}^* Y_i) = \frac{1}{\mathrm{Re}\,\mathrm{Sc}_i} \nabla^{*\,2} Y_i + \mathrm{Ma}^2 \mathrm{Da}\, \dot{w}_i^* \tag{138}$$

$$\begin{aligned} \frac{\partial (\rho^* h^*)}{\partial t^*} + \nabla^* \cdot (\rho^* \boldsymbol{v}^* h^*) = \mathrm{Ma}^2 \mathrm{Ec} \left[\frac{\partial p^*}{\partial t^*} + \boldsymbol{v}^* \cdot \nabla^* p^* \right] + \frac{\mathrm{Ma}^2 \mathrm{Ec}}{\mathrm{Re}} \boldsymbol{\tau}^* : \nabla^* \boldsymbol{v}^* \\ + \frac{\mathrm{Ma}^2}{\mathrm{Re}\,\mathrm{Pr}} \nabla^{*\,2} T^* - \frac{\mathrm{Ma}^2}{\mathrm{Bz}} \nabla^* \cdot \boldsymbol{q}^* - \frac{1}{\mathrm{Re}\,\mathrm{Sc}_i\,\mathrm{Fr}} \sum_{i=1}^{N} \rho^* Y_i \boldsymbol{f}_i^* \cdot \nabla^* Y_i \end{aligned} \tag{139}$$

Turbulent burning velocity and flame thickness
Dimensional analysis

Express the departure of the turbulent velocity from the laminar burning velocity, S_{uT} - S_{uL}, as a function of the laminar burning velocity, S_{uL}, the laminar flame thickness, δ_L, the root-mean-square value of the velocity fluctuations, v'_{rms}, the macro length scale of the turbulence, ℓ_t, the density, ρ, the dynamic viscosity, μ, the diffusion coefficient, $\mathbb{D}$, the thermal conductivity, λ, and the specific heat, C_P:

$$S_{uT} - S_{uL} = f\left(S_{uL}, \delta_L, v'_{\text{rms}}, \ell_t, \rho, \mu, \mathbb{D}, \lambda, \text{C}_\text{P}\right) \tag{140}$$

$$= D'\left(S_{uL}\right)^a \left(\delta_L\right)^b \left(v'_{\text{rms}}\right)^c \left(\ell_t\right)^d \left(\rho\right)^e \left(\mu\right)^f \left(\mathbb{D}\right)^g \left(\lambda\right)^h \left(\text{C}_\text{P}\right)^i \tag{141}$$

Invoke the dimensions of the quantities involved as

$$\frac{m}{s} = \left(\frac{m}{s}\right)^a (m)^b \left(\frac{m}{s}\right)^c (m)^d \left(\frac{kg}{m^3}\right)^e \left(\frac{kg}{m\,s}\right)^f \left(\frac{m^2}{s}\right)^g \left(\frac{kg\,m}{s^3\,K}\right)^h \left(\frac{m^2}{s^2\,K}\right)^i \tag{142}$$

$$\iff \begin{cases} m: & 1 = a + b + c + d - 3e - f + 2g + h + 2i \\ s: & -1 = -a - c - f - g - 3h - 2i \\ kg: & 0 = e + f + h \\ K: & 0 = -h - i \end{cases} \tag{143}$$

and solve to obtain

$$a = 1 - c - f - g - h, \quad b = -d - f - g - h, \quad e = -f - h, \quad i = -h \tag{144}$$

Substitution into equation (141) gives

$$\frac{S_{uT}-S_{uL}}{S_{uL}} = D'\left(\frac{S_{uL}\delta_L}{\mathbb{D}}\right)^{-g}\left(\frac{\mu}{\rho\mathbb{D}}\right)^{f-g}\left(\frac{\lambda}{\rho \mathrm{C_P}\mathbb{D}}\right)^{h-g}\left(\frac{v'_{\mathrm{rms}}/\ell_t}{S_{uL}/\delta_L}\right)^{d-c}\left(\frac{v'_{\mathrm{rms}}}{S_{uL}}\right)^{c}$$

$$\Longrightarrow \quad \boxed{\frac{S_{uT}}{S_{uL}} = 1 + D'\mathrm{Bo}^{c'}\mathrm{Sc}^{d'}\mathrm{Le}^{e'}\mathrm{Da}^{a'}\left(\frac{v'_{\mathrm{rms}}}{S_{uL}}\right)^{b'}} \tag{145}$$

$$\Longrightarrow \quad \boxed{\frac{S_{uT}}{S_{uL}} = 1 + C'\mathrm{Da}^{a'}\left(\frac{v'_{\mathrm{rms}}}{S_{uL}}\right)^{b'}} \tag{146}$$

where Bo denotes the Bodenstein number, Sc the Schmidt number, Le the Lewis number, and, Da the Damköhler number. Notice that Le = Sc/Pr where Pr denotes the Prandtl number.
A similar analysis can also be made for the turbulent flame thickness:

$$\delta_T - \delta_L = f\left(S_{uL}, \delta_L, v'_{\mathrm{rms}}, \ell_t, \rho, \mu, \mathbb{D}, \lambda, \mathrm{C_P}\right) \tag{147}$$

$$= D''\left(S_{uL}\right)^a\left(\delta_L\right)^b\left(v'_{\mathrm{rms}}\right)^c\left(\ell_t\right)^d\left(\rho\right)^e\left(\mu\right)^f\left(\mathbb{D}\right)^g\left(\lambda\right)^h\left(\mathrm{C_P}\right)^i \tag{148}$$

so that

$$\frac{m}{s} = \left(\frac{m}{s}\right)^a(m)^b\left(\frac{m}{s}\right)^c(m)^d\left(\frac{kg}{m^3}\right)^e\left(\frac{kg}{m\,s}\right)^f\left(\frac{m^2}{s}\right)^g\left(\frac{kg\,m}{s^3\,K}\right)^h\left(\frac{m^2}{s^2\,K}\right)^i \tag{149}$$

$$\Longleftrightarrow \quad \begin{cases} m: & 1 = a+b+c+d-3e-f+2g+h+2i \\ s: & 0 = -a-c-f-g-3h-2i \\ kg: & 0 = e+f+h \\ K: & 0 = -h-i \end{cases} \tag{150}$$

and henceforth

$$a = -c-f-g-h, \quad b = 1-d-f-g-h, \quad e = -f-h, \quad i = -h \tag{151}$$

Substitution into equation (148) leads to

$$\frac{\delta_T - \delta_L}{\delta_L} = D'' \left(\frac{S_{uL}\delta_L}{\mathbb{ID}}\right)^{-g} \left(\frac{\mu}{\rho \mathbb{ID}}\right)^{f-g} \left(\frac{\lambda}{\rho \mathrm{C_P} \mathbb{ID}}\right)^{h-g} \left(\frac{v'_{\mathrm{rms}}/\ell_t}{S_{uL}/\delta_L}\right)^{d-c} \left(\frac{v'_{\mathrm{rms}}}{S_{uL}}\right)^{d}$$

$$\implies \quad \boxed{\frac{\delta_T}{\delta_L} = 1 + D''\mathrm{Bo}^{c''}\mathrm{Sc}^{d''}\mathrm{Le}^{e''}\mathrm{Da}^{a''}\left(\frac{v'_{\mathrm{rms}}}{S_{uL}}\right)^{b''}} \tag{152}$$

$$\implies \quad \boxed{\frac{\delta_T}{\delta_L} = 1 + C''\mathrm{Da}^{a''}\left(\frac{v'_{\mathrm{rms}}}{S_{uL}}\right)^{b''}} \tag{153}$$

Together, equations (145) and (152) constitute a more detailed turbulent flame propagation model with twelve constants: a', a'', b', b'', c', c'', d', d'', e', e'', D' and D''.

Detonations: Hugoniot Curve – Hugoniot Relations

- Relationships exist between the variables on the two sides of a shock wave. These are known as the Hugoniot relations.
- The Hugoniot relations establish the connection between eight quantities: four variables on the left (low pressure) side of the shock wave (p_0, h_0, ρ_0, v_0) and four variables on the right (high pressure) side $(p_\infty, h_\infty, \rho_\infty, v_\infty)$.
- These variables are the solution to the inviscid conservation equations for mass, momentum, and energy for waves in a steady, constant area flow.
- There are three Hugoniot relations connecting eight quantities (four on either side of the shock wave).

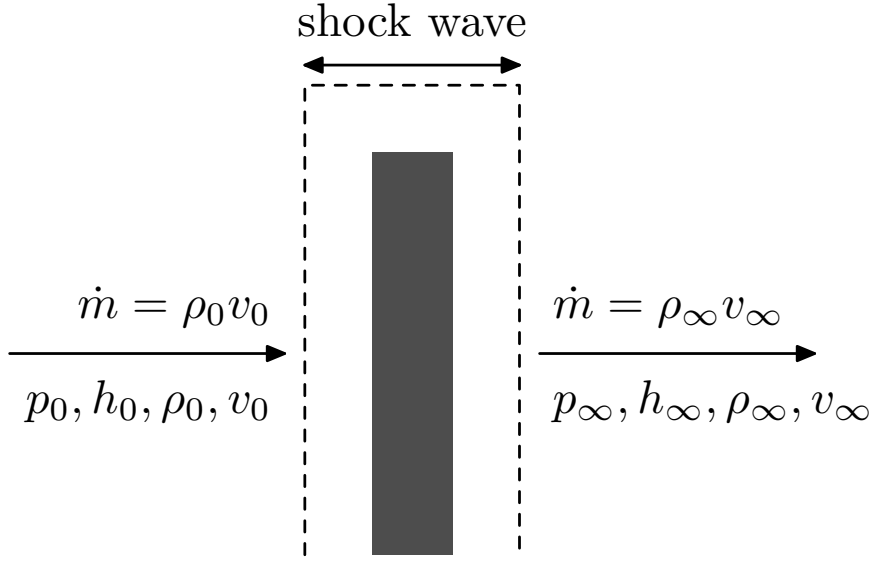


Figure 1: Simplified shock wave structure.

The Hugoniot relations are:

$$\rho_0 v_0 = \rho_\infty v_\infty \equiv \dot{m} \tag{154}$$

$$p_0 + \rho_0 v_0^2 = p_\infty + \rho_\infty v_\infty^2 \tag{155}$$

$$h_0 + \frac{v_0^2}{2} = h_\infty + \frac{v_\infty^2}{2} \tag{156}$$

Detonations: Hugoniot Curve – Rankine-Hugoniot Relation

Equations (154) to (156) may be combined into the Rankine-Hugoniot relation

$$\frac{\gamma-1}{\gamma}\left(\frac{p_\infty}{\rho_\infty}-\frac{p_0}{\rho_0}\right)-\frac{p_\infty-p_0}{2}\left(\frac{1}{\rho_\infty}+\frac{1}{\rho_0}\right)=-(h_\infty-h_1) \tag{157}$$

The difference between a detonation and the shock in an inert gas is in the form of h_∞ .
In a shock the chemical composition remains unchanged, whereas in a detonation the chemical composition changes so that energy is released. Chemical equilibrium is attained after the gas passes through the wave.

- A plot of p_∞ versus $1/\rho_\infty$ for a given value of $(p_0, 1/\rho_0)$ and the heat release $-(h_\infty - h_1)$ is called the Hugoniot curve.
- The Hugoniot curve is the locus of all possible solutions of equations (154) to (156), or equivalently, equation (157).
- The point $(p_0, 1/\rho_0)$ is called the origin of the Hugoniot plot.
- There are two Chapman-Jouget points. They arise from drawing tangents to the Hugoniot curve through the origin of the Hugoniot plot $(p_0, 1/\rho_0)$.

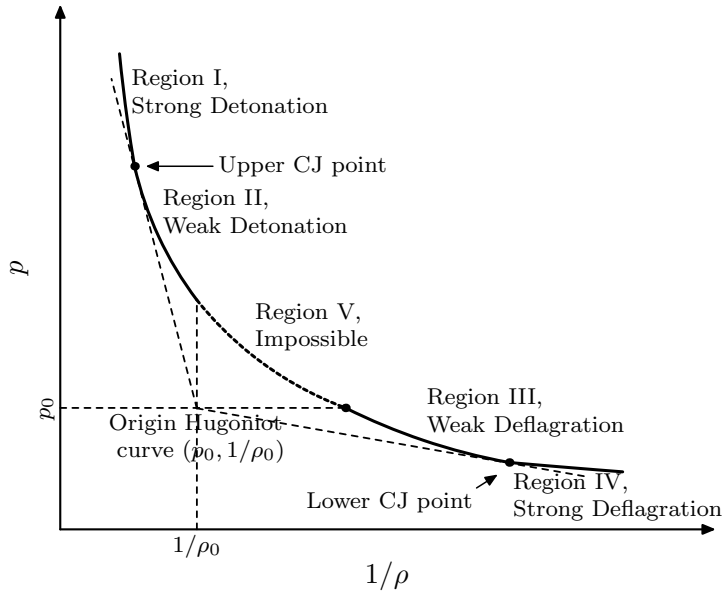


Figure 2: The Rankine-Hugoniot diagram.

Detonations: Hugoniot Curve – Rayleigh-line Relation

Equations (154) and (155) may be combined into the Rayleigh-line relation

$$\rho_0^2 v_0^2 = \frac{p_\infty - p_0}{1/\rho_0 - 1/\rho_\infty} \equiv \dot{m}^2 \tag{158}$$

The Rayleigh-line relation is a criterion to identify regimes within the Hugoniot curve where deflagration and detonation are possible.

- Region I, strong detonation regime.
- Region II, weak detonation regime.
- Region III, weak deflagration regime.
- Region IV, strong deflagration regime.
- In region V, it is seen that $1/\rho_0 - 1/\rho_\infty < 0$ and in $p_0 - p_\infty > 0$. The Rayleigh-line relation implies imaginary values for v_0 (i.e. impossible for deflagration or detonation to exists).

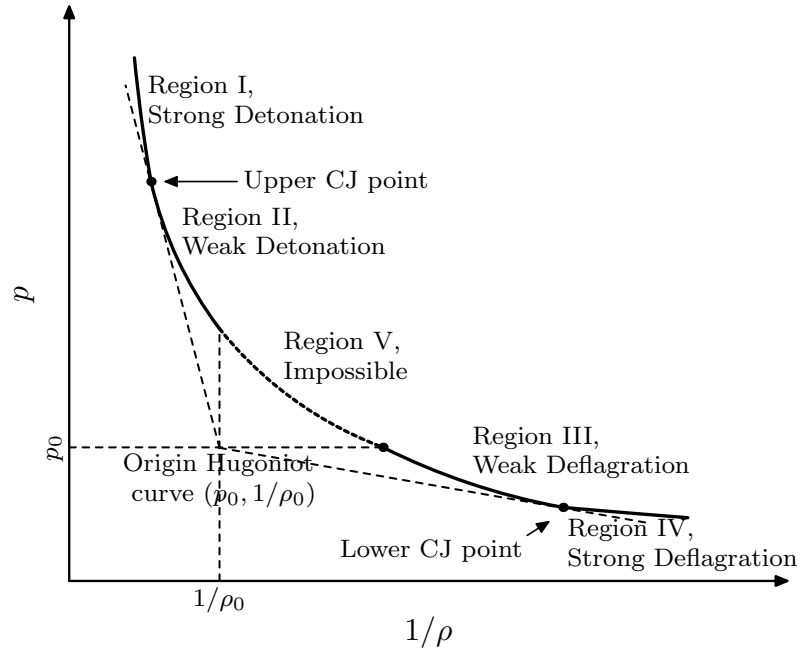


Figure 2: The Rankine-Hugoniot diagram.

Deflagrations are subsonic combustion waves:

- Typical deflagrations propagate at speeds on the order of 1-100 $\mathrm{m\,s^{-1}}$.
- Across a deflagration, the pressure decreases while the volume increases: $p_\infty < p_0$ and $1/\rho_\infty > 1/\rho_0$.
- For deflagrations, the structure of the wave, and turbulent and diffusive processes, determine the propagation speed.

Detonations are supersonic combustion waves:

- Typical detonation waves propagate at a velocity on the order of 2000 $\mathrm{m\,s^{-1}}$.
- Across a detonation, the pressure increases while the volume decreases: $p_\infty > p_0$ and $1/\rho_\infty < 1/\rho_0$.
- For detonations in stoichiometric hydrogen and hydrocarbon fuel-air mixtures: $p_\infty/p_0 = 15 - 20$. For detonations, gas dynamic considerations are sufficient to determine the solution. Chapman (1899) [97] and Jouguet (1905) [98] proposed that detonations travel at one particular velocity, which is the minimum velocity for all the solutions on the detonation branch (the Chapman-Jouget velocity).
- Zeldovich (1940) [99], von Neumann (1943) [100] and Döring (1943) [101] postulated independently that a detonation is a combustion wave being sustained by a shock wave.

Detonations: Hugoniot Curve – Chapman-Jouget Points

Differentiate the Rankine-Hugoniot relation (157) with respect to ρ_∞ to obtain:

$$\frac{1}{\rho_\infty}\left(\frac{\gamma}{\gamma-1}\right)\frac{dp_\infty}{d(1/\rho_\infty)}+\left(\frac{\gamma}{\gamma-1}\right)p_\infty-\frac{1}{2}(p_\infty-p_0)-\frac{1}{2}\frac{dp_\infty}{d(1/\rho_\infty)}\left(\frac{1}{\rho_\infty}+\frac{1}{\rho_0}\right)=0 \tag{159}$$

and hence:

$$\frac{dp_\infty}{d(1/\rho_\infty)}=\frac{(p_\infty-p_0)-\left(\frac{2\gamma}{\gamma-1}\right)p_\infty}{\left(\frac{2\gamma}{\gamma-1}\right)\frac{1}{\rho_\infty}-\left(\frac{1}{\rho_\infty}+\frac{1}{\rho_0}\right)} \tag{160}$$

The slopes at the Chapman-Jouget points are:

$$\left.\frac{dp_\infty}{d(1/\rho_\infty)}\right|_{\mathrm{CJ}}=\frac{p_\infty-p_0}{(1/\rho_\infty)-(1/\rho_0)} \tag{161}$$

From (160) and (161):

$$\frac{p_\infty-p_0}{(1/\rho_\infty)-(1/\rho_0)}=-\gamma\rho_\infty p_\infty-p_0 \tag{162}$$

The Rayleigh-line is tangent to the Hugoniot curve at the Chapman-Jouget points. From (162) and the Rayleigh-line relation (158):

$$v_\infty^2=\frac{\gamma p_\infty}{(\rho_\infty)}=c_\infty^2 \quad \text{or} \quad |v_\infty|=c_\infty \tag{163}$$

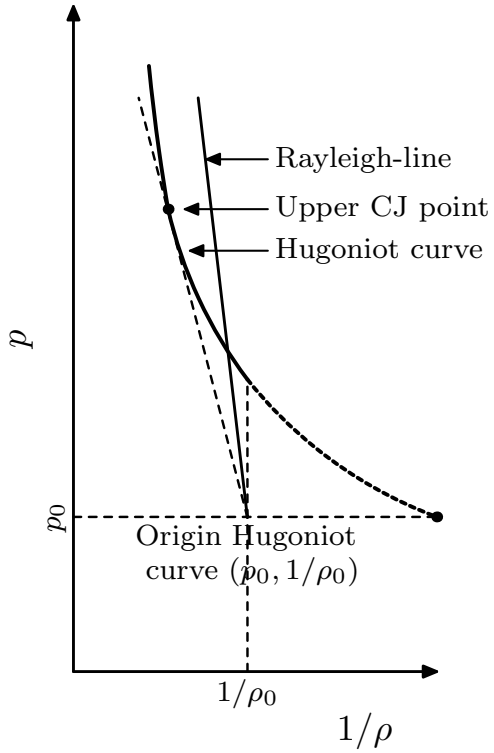


Figure 3: The upper Chapman-Jouget point and the tangency condition between the Rayleigh-line and the Hugoniot curve.

Equation (163) implies that the Mach number behind the shock wave is unity ($\mathrm{Ma}_\infty = 1$) at the Chapman-Jouget points.

Detonations: Hugoniot Curve – Chapman-Jouget Points

Experimentally observed conditions of pressure (p_∞), temperature (T_∞), and velocity (v_∞) at the upper Chapman-Jouget point. Initial conditions $p_0 = 1\,\mathrm{bar}$ and $T_0 = 291\,\mathrm{K}$. After: Hirschfelder, Curtiss & Bird (1967) [102].

Explosive mixture	pressure p_∞ (bar)	temperature T_∞ (K)	velocity v_∞ ($\mathrm{m\,s^{-1}}$)
$(2\,H_2 + O_2)$	18.1	3583	2819
$(2\,H_2 + O_2) + 5\,O_2$	14.1	2620	1700
$(2\,H_2 + O_2) + 5\,N_2$	14.4	2685	1822
$(2\,H_2 + O_2) + 4\,H_2$	16.0	2976	3527
$(2\,H_2 + O_2) + 5\,He_2$	16.3	3097	3160
$(2\,H_2 + O_2) + 5\,Ar_2$	16.3	3097	1700

Detonation Wave Velocity – Iterative Calculation Procedure

A procedure for estimating the Chapman-Jouget velocity from the thermodynamic properties of the unreacted mixture may be derived as follows. The sonic velocity behind a detonation wave is:

$$c_\infty = \sqrt{\left[\frac{\partial p_\infty}{\partial \rho_\infty}\right]_s} \tag{164}$$

Because $u_\infty = c_\infty$ at the upper Chapman-Jouget point, the condition of mass conservation (154) across the shock wave and equation (164) lead to:

$$u_0 = \frac{1}{\rho_0} c_\infty \rho_\infty = \frac{1}{\rho_0}\sqrt{\rho_\infty^2 \left[\frac{\partial p_\infty}{\partial \rho_\infty}\right]_s} = \frac{1}{\rho_0}\sqrt{-\left[\frac{\partial p_\infty}{\partial (1/\rho_\infty)}\right]_s} \tag{165}$$

Differentiation of the isentropic relation for the burned gas,

$$p_\infty \left(\frac{1}{\rho_\infty}\right)^{\gamma_\infty} = \text{constant} \quad \Longrightarrow \quad -\left[\frac{\partial p_\infty}{\partial (1/\rho_\infty)}\right]_s = \frac{\gamma_\infty p_\infty}{1/\rho_\infty} \tag{166}$$

and substitution into equation (165) gives

$$\boxed{u_0 = p_\infty \frac{1/\rho_0}{1/\rho_\infty}\sqrt{\gamma_\infty p_\infty \frac{1}{\rho_\infty}} = \frac{\rho_\infty}{\rho_0}\sqrt{\gamma_\infty R_\infty T_\infty}} \quad \text{or} \quad \boxed{\rho_0^2 u_0^2 = \gamma_\infty p_\infty \rho_\infty} \tag{167}$$

after application of the ideal gas law.

Derive an equivalent Rankine-Hugoniot relation by combining Kirckhoff's law with the ideal gas law,

$$\frac{p}{\rho} = \frac{\gamma - 1}{\gamma} \sum_{i=1}^{N} Y_i \left[h_{f_i}^{\circ} + \int_{T^{\circ}}^{T} \mathrm{C_{P}}_i(T)\, dT \right] \quad \Longrightarrow \quad h = h^{\circ} + \left(\frac{\gamma}{\gamma - 1} \right) \frac{p}{\rho} \tag{168}$$

and substituting this into the conventional Rankine-Hugoniot relation (157):

$$h_{\infty} - h_0 = \frac{1}{2}(p_{\infty} - p_0) \left(\frac{1}{\rho_{\infty}} + \frac{1}{\rho_0} \right) \tag{169}$$

Because $h = e + (p/\rho)$,

$$h_{\infty} - h_0 = (e_{\infty} - e_0)(p_{\infty} - p_0) \left(\frac{p_{\infty}}{\rho_{\infty}} + \frac{p_0}{\rho_0} \right) \tag{170}$$

so that (169) becomes

$$e_{\infty} - e_0 = \frac{1}{2}(p_{\infty} - p_0) \left(\frac{1}{\rho_{\infty}} + \frac{1}{\rho_0} \right) - \left(\frac{p_{\infty}}{\rho_{\infty}} + \frac{p_0}{\rho_0} \right) \tag{171}$$

$$\boxed{e_{\infty} - e_0 = \frac{1}{2}(p_{\infty} - p_0) \left(\frac{1}{\rho_0} - \frac{1}{\rho_{\infty}} \right)} \tag{172}$$

Substitute equation (167) into the Rayleigh-line relation (158):

$$\frac{1}{\rho_\infty} + \frac{1}{\rho_0} = -\frac{p_\infty - p_0}{\gamma_\infty p_\infty \rho_\infty} \tag{173}$$

and combine this result with equation (172) to obtain

$$\boxed{e_\infty - e_0 = \frac{p_\infty^2 - p_0^2}{\gamma_\infty p_\infty \rho_\infty}} \tag{174}$$

Multiply equation (173) by $(p_\infty + p_0)$ to have

$$\boxed{(p_\infty - p_0)\left(\frac{1}{\rho_\infty} + \frac{1}{\rho_0}\right) = \frac{(p_\infty^2 - p_0^2)}{\gamma_\infty p_\infty \rho_\infty}} \tag{175}$$

Equations (172), (174) and (175) form the design basis of an iterative procedure to determine the Chapman-Jouget velocity from the thermodynamic properties of the unreacted mixture.

For a detonation wave $p_\infty \gg p_0$ so that equations (174) and (175) may be rewritten into an approximate Rankine-Hugoniot relation (176) and an approximate Rayleigh-line relation (177):

$$\boxed{e_\infty - e_0 \approx \frac{p_\infty^2 - p_0^2}{\gamma_\infty p_\infty \rho_\infty} = \frac{R_\infty T_\infty}{2\gamma_\infty}} \tag{176}$$

$$\boxed{\left(\frac{\rho_\infty}{\rho_0}\right)^2 \left(1 + \frac{1}{\gamma_\infty} - \frac{R_0 T_0}{R_\infty T_\infty}\right)\left(\frac{\rho_\infty}{\rho_0}\right) - \frac{R_0 T_0}{R_\infty T_\infty} = 0} \tag{177}$$

The iterative procedure to determine the Chapman-Jouget velocity from the thermodynamic properties of the unreacted mixture is as follows.

1. Assume p_∞.
2. Assume T_∞.
3. Calculate the equilibrium composition based on p_∞ and T_∞.
4. From the equilibrium composition, determine γ_∞, R_∞ and e_∞.
5. Verify whether γ_∞, R_∞ and e_∞ at the assumed temperature T_∞ satisfies the approximate Rankine-Hugoniot relation (176).
   - If equation (176) is satisfied, proceed to step 6.
   - If not, then reassume a new p_∞ and return to step 2.
6. Solve the approximate Rayleigh-line relation (177) for ρ_∞/ρ_0.
7. Find p_∞ from the equation of state, e.g. the ideal gas law

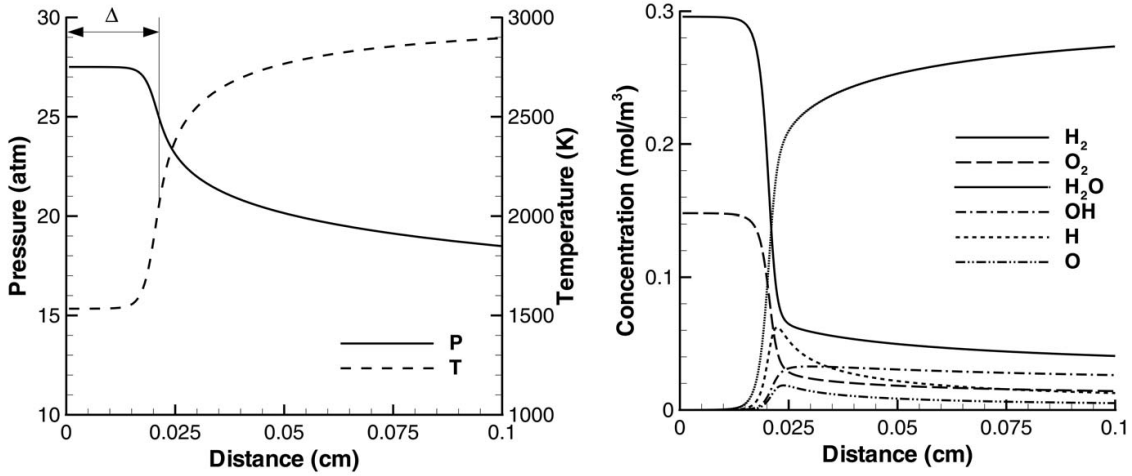
$$p_\infty = \left(\frac{\rho_\infty}{\rho_0}\right)\left(\frac{R_\infty T_\infty}{R_0 T_0}\right) p_0 \qquad (178)$$

   - If the calculated p_∞ equals the assumed p_∞, the iteration sequence has completed. Proceed to step 8.
   - If not, then return to step 1 and assume a new p_∞.
8. Calculate the Chapman-Jouget velocity, v_∞, from equation (167).

ONE-DIMENSIONAL DETONATION WAVE STRUCTURE
The Zeldovich-von Neumann-Döring Theory

The simplest model of the structure of a detonation wave (the ZND structure) consists of a shock wave coupled to a reaction zone. Zeldovich (1940), von Neumann (1943) and Döring (1943) were the first who postulated this view.

- The shock wave compresses and heats up the gas, which reacts after an induction period.
- The reaction triggers a volumetric expansion of the gas, which drives the shock wave.

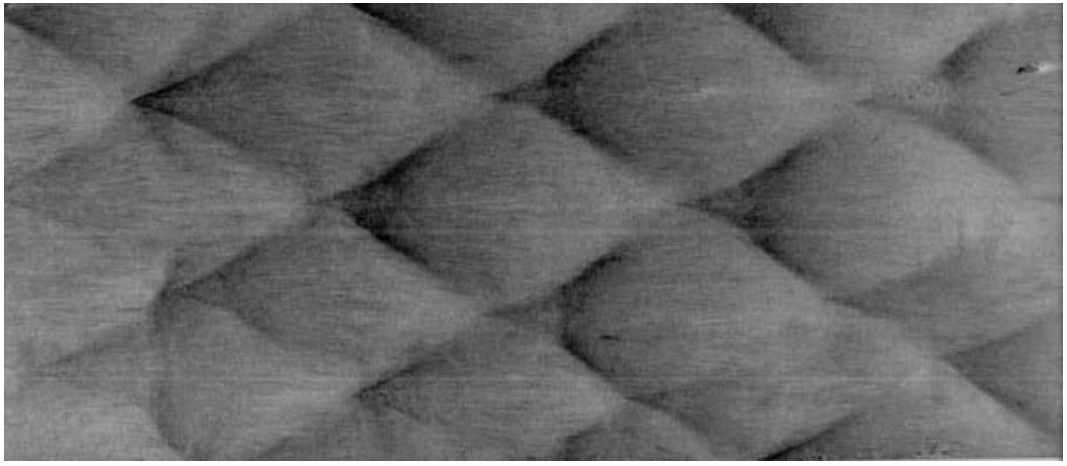


ZND profile of a detonation wave in stoichiometric hydrogen-air mixture ignited at 1 bar and 300 K. Δ denotes the induction zone length.

MULTI-DIMENSIONAL DETONATION WAVE STRUCTURE

Detonation waves have a multidimensional structure.

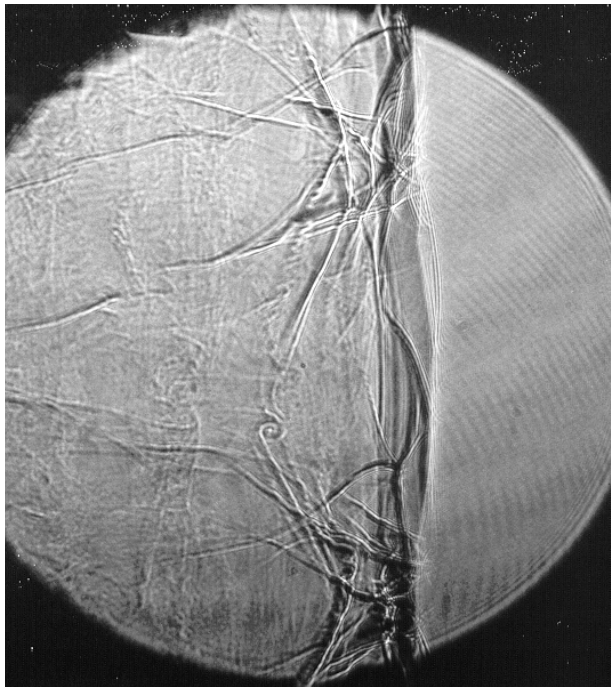
- They consist of a leading shock waves, triple points, and transverse waves.
- The wave structure has a cellular pattern.
- The structure of a detonation wave is correlated with the induction length.
- The cellular structure left behind on sooted foils is a record of the triple point trajectory.
- Empirical correlations exist between cell width and induction length.



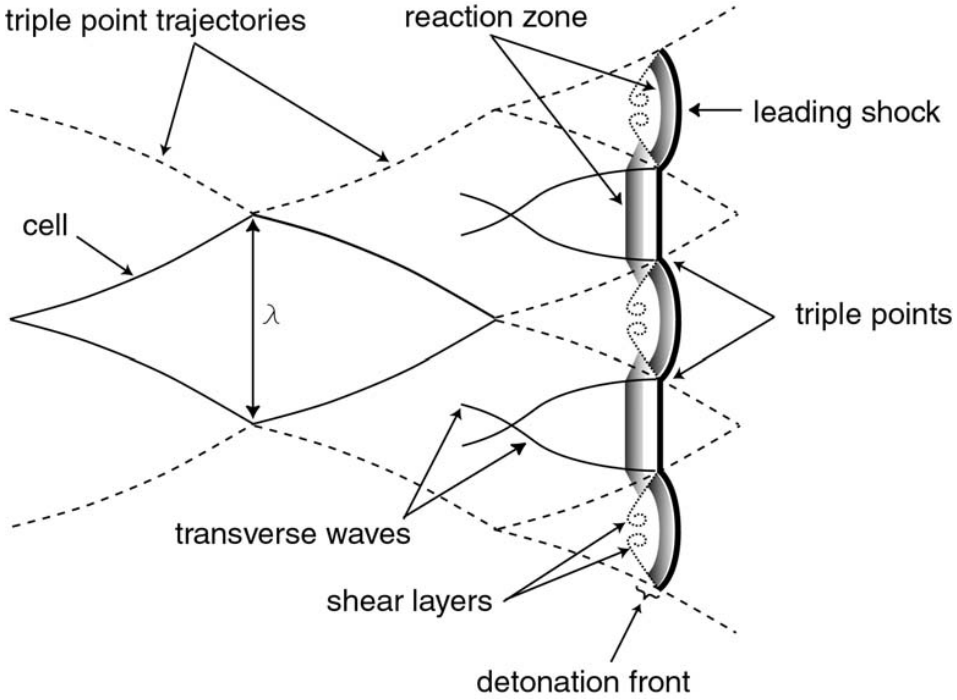
Cellular structure imprinted on a sooted foil record by the detonation of a $2H_2 + O_2 + 17Ar$ mixture, ignited at 20 kPa and 295 K. After Austin (2003) [103].

MULTI-DIMENSIONAL DETONATION WAVE STRUCTURE

a)

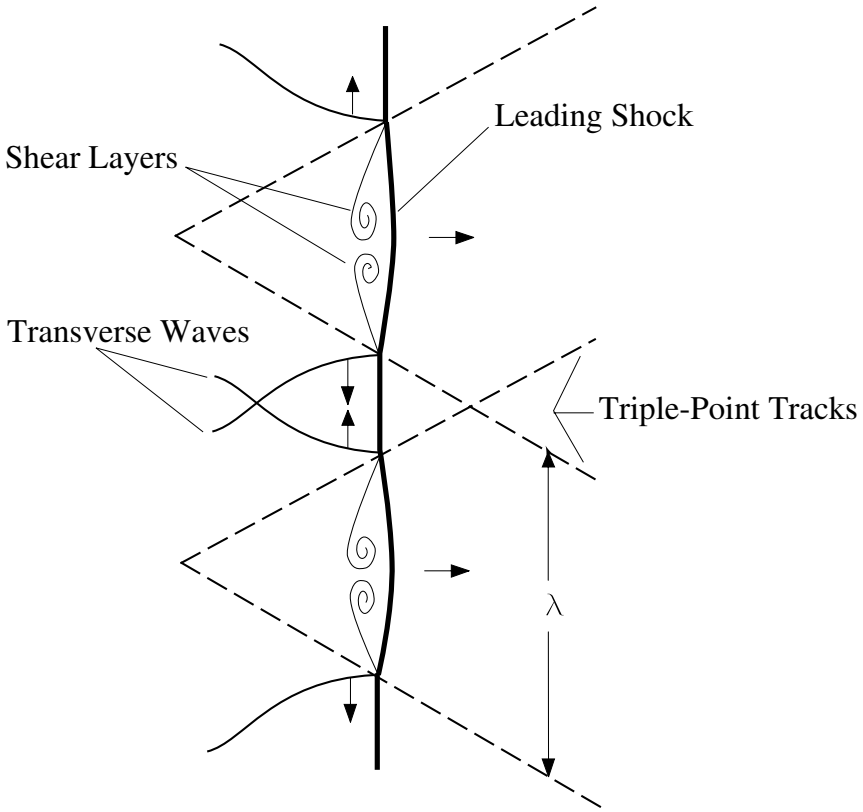


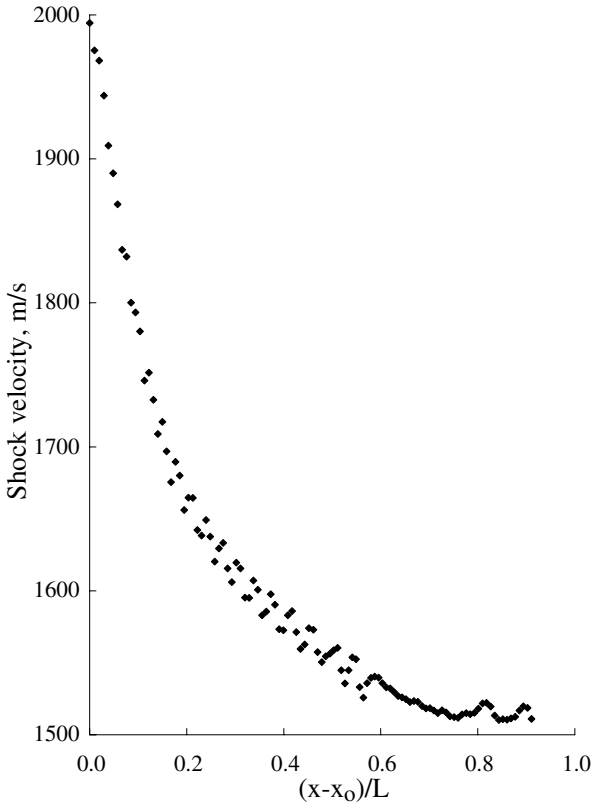
b)



(a) Structure of a detonation wave in a $2H_2 + O_2 + 20Ar$ mixture at 20 kPa and 295 K (after Akbar (1997) [104]).
(b) Formation of the cellular structure on a sooted foil record by a detonation wave (after Winterberger & Shepherd (2004)).

MULTI-DIMENSIONAL DETONATION WAVE STRUCTURE





Morphology of a multi-dimensional detonation front propagating from left to right. After: Austin (2003) [103], Eckett(2000) [105], and Pintgen, Eckett, Austin & Shepherd (2003) [106].

MULTI-DIMENSIONAL DETONATION WAVE STRUCTURE

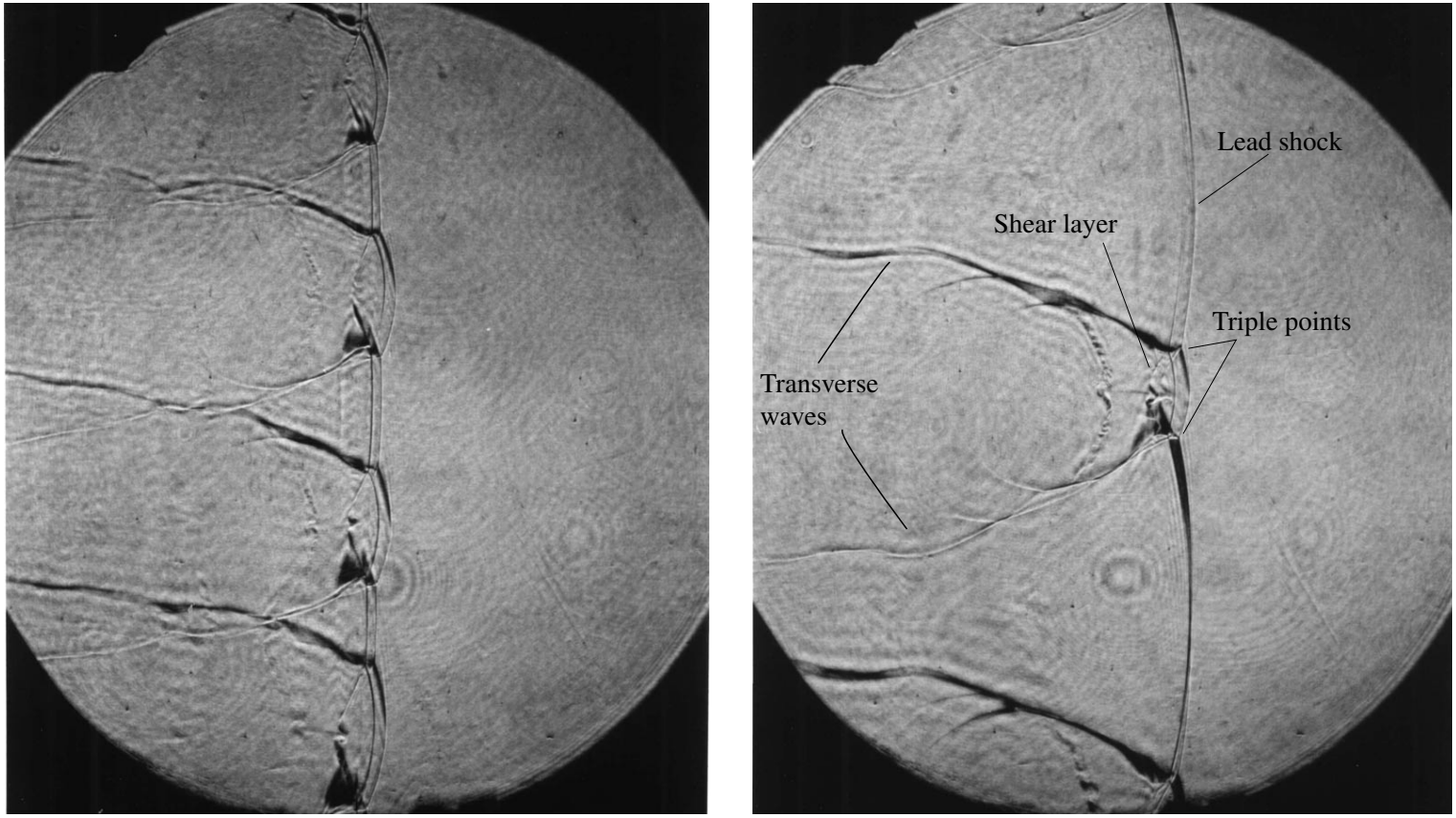
Morphology of a multi-dimensional detonation front:

- Triple points exist at the junction of the leading shock front and a transverse wave.
- The pattern observed on soot foils is a history of the triple point tracks in the propagating detonation front. Urtiew and Oppenheim (1966) [107] have shown that the tracks are closely related with the triple points on the detonation front.
- The precise physical mechanism by which the tracks are made in the soot layer is still unclear!
- The width of cells that appear on the foil are a measure of the spacing of the transverse waves in the detonation front. This global length scale, referred to as the detonation cell width, λ, can not in general be calculated a priori but may be related to the induction zone length, Δ, by a constant of proportionality ,A. More specifically,

$$\lambda = A\,\Delta \tag{179}$$

- The constant A depends on the fuel-oxidiser-inert type (Westbrook (1982) [108]) and also varies with the equivalence ratio (Shepherd (1986) [109, 110]).
- The induction zone length can be empirically related to dynamic parameters such as the critical initiation energy (Lee (1984) [111]).

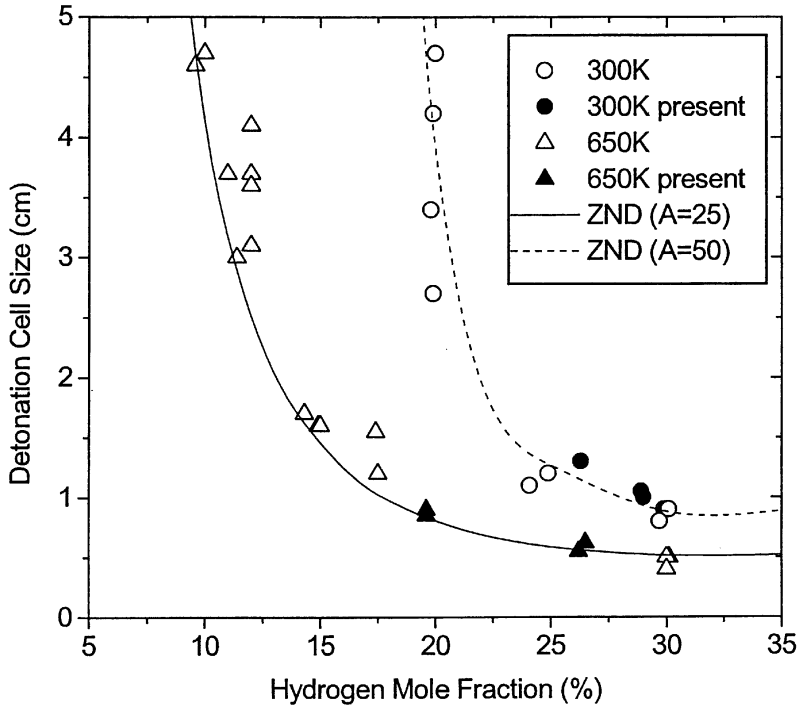
MULTI-DIMENSIONAL DETONATION WAVE STRUCTURE

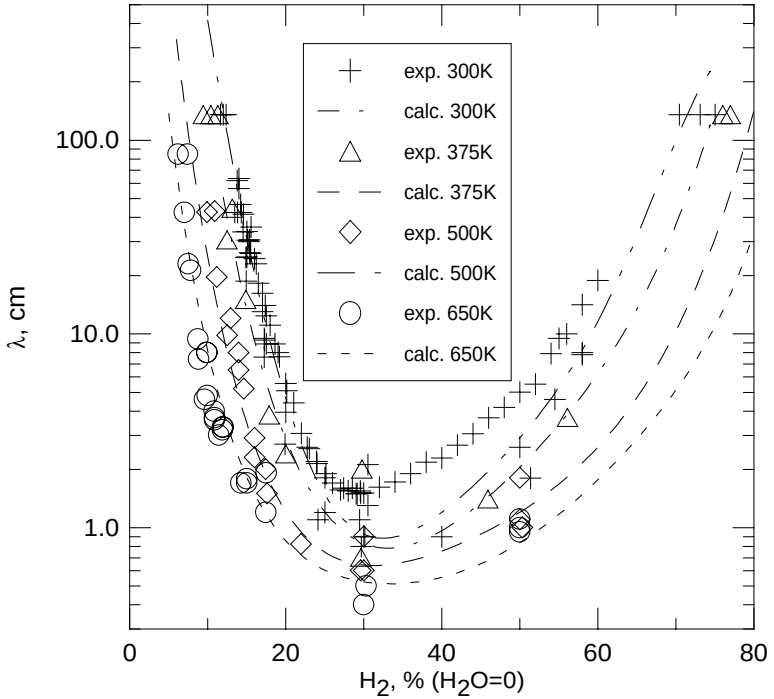


Schlieren images of (left) a $2H_2$-O_2-12Ar detonation, p_0=20 kPa, and (right) a $2H_2$-O_2-17Ar detonation, p_0=20 kPa (after Austin (2003) [103]).

DETONATION CELL SIZE

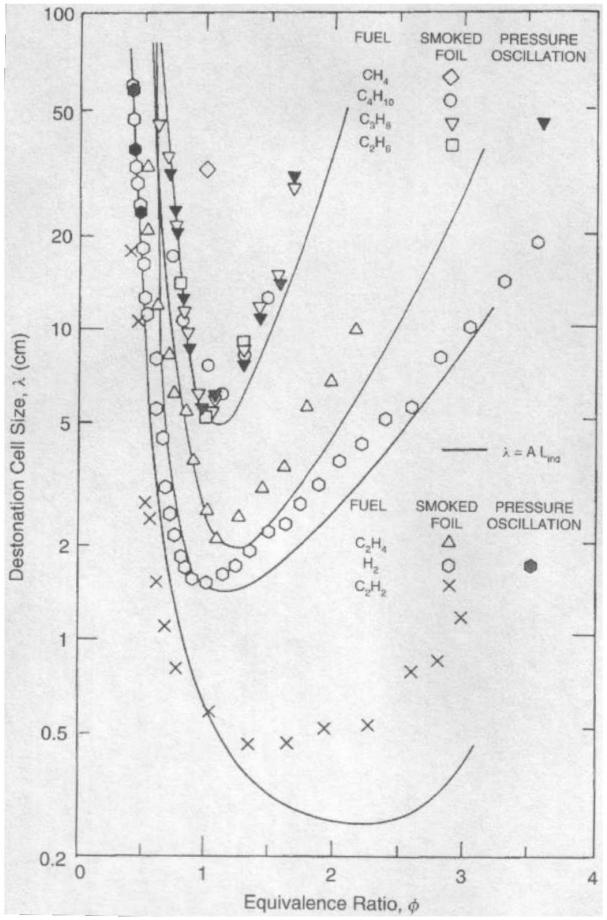
Dependence on composition and temperature





Detonation cell-size for hydrogen-air mixtures at different initial temperatures (after Breitung *et al.*(2000) [112]) and Ciccarelli (2002) [113].

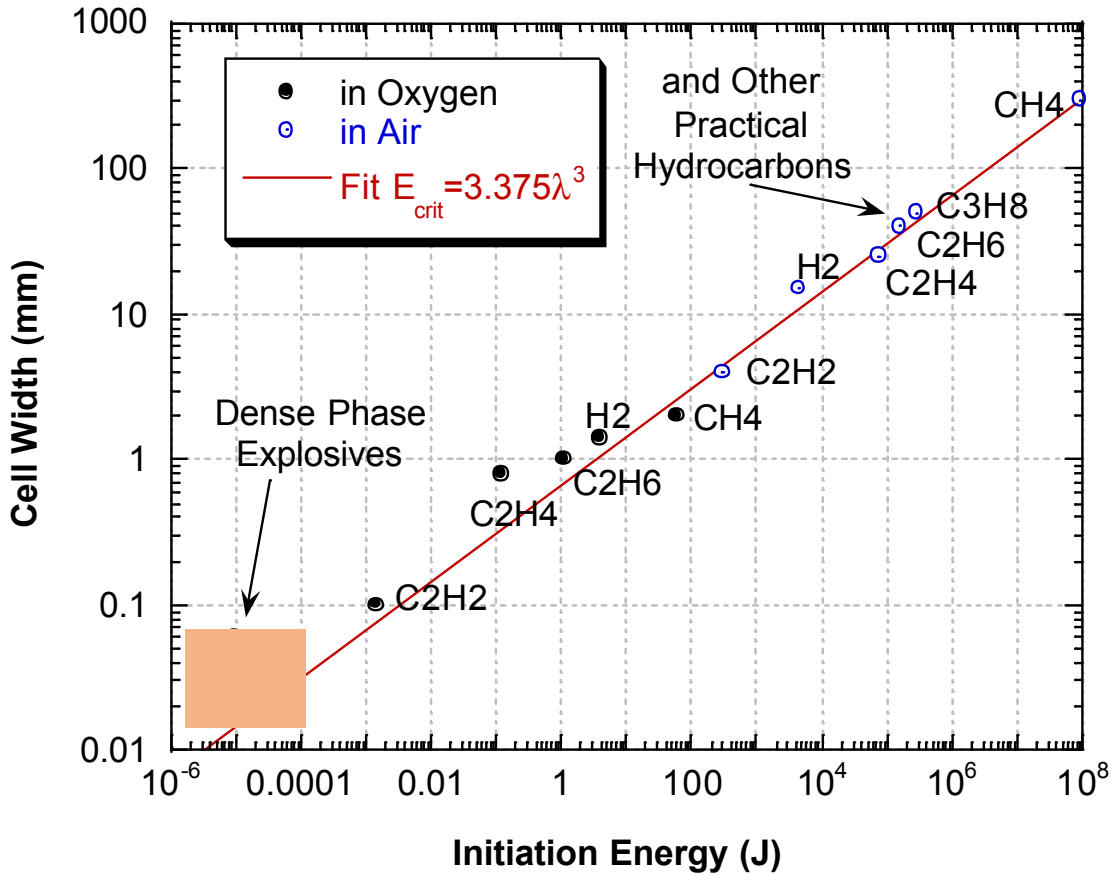
DETONATION CELL SIZE
Comparison between hydrogen and hydrocarbon fuels



Detonation cell-size of different fuels (after Knystautas *et al.* [114]).

RELATIONSHIP BETWEEN DETONATION INITIATION ENERGY AND DETONATION CELL SIZE

Comparison between hydrogen, other fuels, and explosives



Detonation cell-size of different fuels (after Schauer *et al.* [115]).

DETONATION LIMITS

Confined and unconfined detonation limits of hydrogen and other fuels

Detonation limits (vol %) of confined and unconfined mixtures and flammability limits (vol %) in oxygen and air (after Grossel (2002) [116], Kuo (2005) [117], and Nettleton (1987) [118]).

Fuel	Confined detonation limit O_2		Confined detonation limit air		Unconfined detonation limit O_2		Unconfined detonation limit air		Flammability limit O_2		Flammability limit air	
	lower	upper	lower	upper	lower	upper	lower	upper	lower	upper	lower	upper
H_2	15.0	90.0	18.3	58.9					4.0	95.0	4.0	75.0
CH_4			5.7	14							5.3	15
C_2H_6	3.60	46.4	2.87	12.20	11.0	39.0	4.0	9.2	3.0	66.0	3.0	12.4
C_3H_8	2.50	42.5	2.57	7.37	7.0	31.0	3.0	7.0			2.1	9.5
nC_4H_{10}	2.05	38.0	1.98	6.18			2.5	5.2			1.8	8.4
nC_8H_{18}	1.55	17.3	1.45	2.85							0.95	
C_2H_4	4.10	60.0	3.32	14.70	9.2	51.0			2.9	80.0	2.7	36.0
C_3H_6	2.50	50.0	3.55	10.40	6.7	37.0	3.5	8.5	2.1	53.0	2.4	11.0
C_2H_2	2.90	88.8	4.20	50.0	6.7	68.0			2.5	80.0		
CH_3OH	9.50	64.5									6.7	36.0
C_2H_5OH			5.1	9.8							3.3	19.0
$C_2H_5OC_2H_5$	2.6	>40	2.8	4.5	14.7	29.0			2.0	82.0	1.9	36.0
gasoline			1.1	3.3							1.4	7.6
CO	38.0	90.0							15.5	93.3		
NH_3	25.4	75.0							13.5	79		
C_6H_6	1.55	36.0	1.60	5.55							1.3	7.9
xylene	1.05	26.5									1.1	6.4
CH_3COCH_3	3.3	40.0									2.6	13.0

Nomenclature

LATIN SYMBOLS		
C_P	Constant pressure specific heat.	[J kg^{-1} K^{-1}]
$\boldsymbol{g}$	Gravitational force.	[N]
g	Gravitational acceleration g.	[m s^{-2}]
h	Microscopic enthalpy h	[J kg^{-1}]
p	Microscopic pressure.	[Pa]
P	Macroscopic pressure.	[Pa]
P_{max}	Maximum explosion pressure.	[Pa]
$\boldsymbol{q}$	Radiant flux. Radiant fluxes emitted from reaction zones are often described as $\boldsymbol{q} = \epsilon\sigma T^4$ [119, p.646] where σ denotes the Stefan-Boltzmann constant and ϵ is the emissivity.	[W m^{-2}]
r_f	Front boundary of the flame zone.	[m]
r_r	Rear boundary of the flame zone.	[m]
S_u	Burning velocity.	[m s^{-1}]
S_{uL}	Laminar burning velocity.	[m s^{-1}]
S_{uL}°	Laminar burning velocity at reference conditions.	[m s^{-1}]
S_{uT}	Turbulent burning velocity.	[m s^{-1}]
T	Temperature	[K]
$\boldsymbol{v}$	Microscopic velocity.	[m s^{-1}]
$v_{\mathrm{rms}}^{'}$	Root-mean-square value of the velocity fluctuations.	[m s^{-1}]
V_v	Volume explosion vessel	[m^3]

$\dot{w}_i$	Chemical source of the i-th species.	[kg m^{-3} s^{-1}]
Y_i	Mass fraction of the i-th species	[-]
GREEK SYMBOLS		
γ	Specific heat ratio.	[-]
δ	Flame thickness	[m]
δ_L	Laminar flame thickness	[m]
δ_L°	Laminar flame thickness at reference conditions	[m]
δ_T	Turbulent flame thickness	[m]
λ	Thermal conductivity.	[W m^{-1} K^{-1}]
λ_T	Taylor micro length scale	[m]
μ	Dynamic viscosity.	[Pa s]
ν	Kinematic viscosity.	[m^{-2} s]
ρ	Density.	[kg m^{-3}]
τ	$\boldsymbol{\tau} = \mu\left(\nabla\boldsymbol{v} + (\nabla\boldsymbol{v})^\dagger\right) + \left(\kappa - \frac{2}{3}\mu\right)(\nabla\cdot\boldsymbol{v})\,\boldsymbol{I}$ denotes the shear stress tensor. κ denotes the bulk viscosity.	[N m^{-2}]
OTHER SYMBOLS		
$\mathbb{D}_i$	Fickian diffusion coefficient of the i-th species.	[m^2 s^{-1}]
SCALES		
ℓ_G	Gibson length scale	[m]
ℓ_K	Kolmogorov length scale	[m]
ℓ_t	Turbulence macro length scale	[m]
$\mathcal{L}$	Length scale.	[m]
$\mathcal{M}$	Molecular mass.	[kg mol^{-1}]
τ_c	Chemical time scale.	[s]

τ_K	Kolmogorov time scale	[s]
τ_t	Turbulence macro time scale	[s]
υ_K	Kolmogorov velocity scale.	[$\mathrm{m\,s^{-1}}$]
υ_t	Turbulence macro velocity scale.	[$\mathrm{m\,s^{-1}}$]
$\mathcal{U}$	Velocity scale.	[$\mathrm{m\,s^{-1}}$]
DIMENSIONLESS INDEPENDENT VARIABLES AND OPERATORS		
t^*	Physical time t over $\mathcal{L}/\mathcal{U}$.	[-]
∇^*	Nabla operator divided by the reciprocal length scale, $\nabla/\mathcal{L}^{-1}$.	[-]
NONDIMENSIONAL DEPENDENT VARIABLES		
ρ^*	Density ρ divided by $p/\mathcal{U}^2$.	[-]
$\boldsymbol{v}^*$	Velocity $\boldsymbol{v}$ divided by the velocity scale $\mathcal{U}$.	[-]
p^*	Microscopic pressure p divided by $\rho\mathcal{U}^2$.	[-]
$\boldsymbol{\tau}^*$	Shear stress tensor $\boldsymbol{\tau}$, divided by $\mu\mathcal{U}/\mathcal{L}$.	[-]
$\boldsymbol{g}^*$	Gravitational force $\boldsymbol{g}$ divided by the magnitude of the gravitational force g.	[-]
Y_i	Mass fraction of the i-th species.	[-]
$\dot{w}_i^*$	Chemical source $\dot{w}_i$ divided by $\rho(\mathcal{L}/\mathcal{U})/\tau_c$.	[-]
h^*	Enthalpy h divided by $\mathrm{C_P}\,T_0$.	[-]
T^*	Temperature T divided by a refernce temperature T_0.	[-]
$\boldsymbol{q}^*$	Radiant flux $\boldsymbol{q}$ divided by the magnitude of the radiant energy flux q_0 at a reference temperature.	[-]
DIMENSIONLESS GROUPS		
Bo	Bodenstein number, $\mathcal{U}\mathcal{L}/\mathbb{D}$. $\mathrm{Bo} = \mathrm{Re}\,\mathrm{Sc}$. It is the mass transfer analogue to the Peclet number, Pe.	[-]

Bz	Boltzmann number, $\rho\mathcal{U}\mathrm{C_P}T_0/q_0$.	[-]
Da	Damköhler number, $(\mathcal{L}/\mathcal{U})/\tau_c = \ell_t S_{uL}/\upsilon_t\delta_L$.	[-]
Ec	Eckert number, $\mathcal{U}^2/\mathrm{C_P}T_0$.	[-]
Fr	Froude number, $\mathcal{U}^2/g\mathcal{L}$.	[-]
Ka	Karlovitz number, $\tau_c/(\mathcal{L}/\mathcal{U}) = \upsilon_K\delta_L/\ell_K S_{uL}$.	[-]
Le_i	Lewis number of i-th species, $\lambda/\rho\mathrm{C_P}\mathbb{D}_i$. $\mathrm{Le} = \mathrm{Sc}_i/\mathrm{Pr}$.	[-]
Ma	Newtonian Mach number, $\mathcal{U}/\sqrt{p/\rho}$.	[-]
Pe	Peclet number, $\rho\mathrm{C_P}\mathcal{U}\mathcal{L}/\lambda$. $\mathrm{Pe} = \mathrm{Re}\,\mathrm{Pr}$.	[-]
Pr	Prandtl number, $\mu\mathrm{C_P}/\lambda$.	[-]
Re	Reynolds number, $\rho\mathcal{U}\mathcal{L}/\mu$.	[-]
Sc_i	Schmidt number of i-th species, $\mu/\rho\mathbb{D}_i$.	[-]

Bibliography

[1] Ngo T., Mendis P., Gupta A., and Ramsay J. Blast loading and blast effects on structures – An overview. *Electronic Journal of Structural Engineering*, 7:76–91, 2007. Special Issue: Loading on Structures.

[2] Eckhoff R.K. *Dust explosions in the process industries*. Gulf, Amsterdam, third edition, 2003.

[3] Dahoe A.E. Principles of Hydrogen Safety. Knowledge Center for Explosion and Hydrogen Safety. Url: `http://www.explosionsolutions.org/phs/`.

[4] Law C.K. *Combustion Physics*. Cambridge University Press, New York, 2006.

[5] Cashdollar K.L., Zlochower I.A., Green G.M., Thomas R.A., and Hertzberg M. Flammability of methane, propane, and hydrogen gases. *Journal of Loss Prevention in the Process Industries*, 13:327–340, 2000.

[6] Schroeder V. and Holtappels K. Explosion characteristics of hydrogen-air and hydrogen-oxygen mixtures at elevated pressures. Paper presented at the First International Conference on Hydrogen Safety, Pisa, Italy, 8–10 September 2005.

[7] Dahoe A.E. Laminar burning velocities of hydrogen-air mixtures from closed vessel gas explosions. *Journal of Loss Prevention in the Process Industries*, 18:152–166, 2005.

[8] European Commission. Directive 2014/34/EU of the European Parliament and of the Council of 26 February 2014. On the harmonisation of the laws of the Member States relating to equipment and protective systems intended for use in potentially explosive atmospheres. *Official Journal of the European Union*, L 96:309–356, 2014. ATEX 114.

[9] European Commission. Directive 1999/92/EC of the European Parliament and of the Council of 16 December 1999. On minimum requirements for improving the safety and health protection of workers potentially at risk from explosive atmospheres. *Official Journal of the European Union*, L 23:57–64, 1999. ATEX 153 (formerly ATEX 137).

[10] Health and Safety Executive. Control of Major Accident Hazards (COMAH). Hazardous Area Classification and Control of Ignition Sources. Url: `https://www.hse.gov.uk/comah/sragtech/techmeasareaclas.htm`.

[11] EN 60079-10-2. Explosive atmospheres - Part 10-1: Classification of areas - Explosive gas atmospheres. European Committee for Standardization (CEN), Brussels, Belgium, Europe, 2021.

[12] EN 60079-10-2. Explosive atmospheres - Part 10-2: Classification of areas - Explosive dust atmospheres. European Committee for Standardization (CEN), Brussels, Belgium, Europe, 2015.

[13] NFPA 68. Standard on Explosion Protection by Deflagration Venting, 2013 Edition. National Fire Protection Association, Quincy, MA, United States of America, 2013.

[14] NFPA 654. Standard for the Prevention of Fire and Dust Explosions from the Manufacturing, Processing, and Handling of Combustible Particulate Solids, 2017 Edition. National Fire Protection Association, Quincy, MA, United States of America, 2017.

[15] NFPA 61. Standard for the Prevention of Fires and Dust Explosions in Agricultural and Food Processing Facilities, 2017 Edition. National Fire Protection Association, Quincy, MA, United States of America, 2017.

[16] NFPA 484. Standard for Combustible Metals, 2015 Edition. National Fire Protection Association, Quincy, MA, United States of America, 2015.

[17] NFPA 664. Standard for the Prevention of Fires and Explosions in Wood Processing and Woodworking Facilities, 2017 Edition. National Fire Protection Association, Quincy, MA, United States of America, 2017.

[18] NFPA 655. Standard for Prevention of Sulfur Fires and Explosions, 2017 Edition. National Fire Protection Association, Quincy, MA, United States of America, 2017.

[19] EN 13237. Potentially explosive atmospheres. Terms and definitions for equipment and protective systems intended for use in potentially explosive atmospheres, 2012 Edition. European Committee for Standardization (CEN), Brussels, Belgium, Europe, 2012.

[20] EN 1437. Explosion suppression systems, 2005 Edition. European Committee for Standardization (CEN), Brussels, Belgium, Europe, 2005.

[21] EN 14491. Dust explosion venting protective systems, 2012 Edition. European Committee for Standardization (CEN), Brussels, Belgium, Europe, 2012.

[22] EN 14797. Explosion venting devices, 2006 Edition. European Committee for Standardization (CEN), Brussels, Belgium, Europe, 2006.

[23] EN 13673-1. Determination of the maximum explosion pressure and the maximum rate of pressure rise of gases and vapours - Part 1: Determination of the maximum explosion pressure, 2003 Edition. European Committee for Standardization (CEN), Brussels, Belgium, Europe, 2003. European Standard, Prepared by Technical Committee CEN/TC 305 *Potentially explosive atmospheres - Explosion prevention and protection.*

[24] EN 13673-2. Determination of the maximum explosion pressure and the maximum rate of pressure rise of gases and vapours - Part 2: Determination of the maximum rate of explosion pressure rise, 2005 Edition. European Committee for Standardization (CEN), Brussels, Belgium, Europe, 2005. European Standard, Prepared by Technical Committee CEN/TC 305 *Potentially explosive atmospheres - Explosion prevention and protection.*

[25] EN 14034-1. Determination of explosion characteristics of dust clouds - Part 1: Determination of the maximum explosion pressure $p_{\max}$ of dust clouds, 2004 Edition. European Committee for Standardization (CEN),

Brussels, Belgium, Europe, 2004. European Standard, Prepared by Technical Committee CEN/TC 305 *Potentially explosive atmospheres - Explosion prevention and protection.*

[26] EN 14034-1. Determination of explosion characteristics of dust clouds - Part 1: Determination of the maximum explosion pressure $p_{\max}$ of dust clouds, 2011 Edition. European Committee for Standardization (CEN), Brussels, Belgium, Europe, 2011. European Standard, Prepared by Committee EXL/23 *Explosion and fire precautions in industrial and chemical plant.* Amendment July 2011. Amends and replaces EN 14034-1:2004.

[27] EN 14034-2. Determination of explosion characteristics of dust clouds - Part 2: Determination of the maximum explosion rate of explosion pressure rise $(dp/dt)_{\max}$ of dust clouds. 2006 Edition. European Committee for Standardization (CEN), Brussels, Belgium, Europe, 2006. European Standard, Prepared by Technical Committee CEN/TC 305 *Potentially explosive atmospheres - Explosion prevention and protection.*

[28] EN 14034-3. Determination of explosion characteristics of dust clouds - Part 3: Determination of the lower explosion limit LEL of dust clouds, 2006 Edition. European Committee for Standardization (CEN), Brussels, Belgium, Europe, 2006. European Standard, Prepared by Technical Committee CEN/TC 305 *Potentially explosive atmospheres - Explosion prevention and protection.*

[29] EN 14034-4. Determination of explosion characteristics of dust clouds - Part 4: Determination of the limiting oxygen concentration LOC of dust clouds, 2004 Edition. European Committee for Standardization (CEN), Brussels, Belgium, Europe, 2004. European Standard, Prepared by Technical Committee CEN/TC 305 *Potentially explosive atmospheres - Explosion prevention and protection.*

[30] ISO 6184-1. Explosion Protection Systems - Part 1: Determination of explosion indices of combustible dusts in air. The International Organization for Standardization (ISO), 1985.

[31] Dunn S. Hydrogen futures: toward a sustainable energy system. *International Journal of Hydrogen Energy*, 27:235–264, 2002.

[32] Dahoe A.E. and Molkov V.V. On the development of an international curriculum on hydrogen safety engineering and its implementation into educational programmes. *International Journal of Hydrogen Energy*, 32:1113–1120, 2007.

[33] Van den Berg M. Explosieveiligheid en de energietransitie. Veiligheidsregio Rotterdam-Rijnmond, June 2023.

[34] Tang M.J. and Baker Q.A. A new set of blast curves from vapor cloud explosion. *Process Safety Progress*, 18:235–240, 1999.

[35] Baker W.E., Cox P.A., Westine P.S., Kulesz J.J., and Strehlow R.A. *Explosion Hazards and Evaluation*, volume 5 of *Fundamental studies in engineering*. Elsevier Scientific Publishing Company, New York, 1983.

[36] Casal J. *Evaluation of the effects and consequences of major accidents in industrial plants*. Industrial Safety Series. Elsevier, Amsterdam, 2008.

[37] Dahoe A.E. *Dust Explosions: a Study of Flame Propagation*. PhD thesis, Delft University of Technology, Delft, The Netherlands, May 2000.

[38] Dahoe A.E. and de Goey L.P.H. On the determination of the laminar burning velocity of closed vessel explosions. *Journal of Loss Prevention in the Process Industries*, 16:457–478, 2003.

[39] Miller J.A., Mitchell R.E., Smooke M.D., and Kee R.J. Toward a comprehensive chemical kinetic mechanism for the oxidation of acetylene: comparison of model predictions with results from flame and shock tube experiments. In *Proceedings of the Nineteenth Symposium (International) on Combustion*, pages 181–196, Pittsburgh, 1982. The Combustion Institute.

[40] Dahoe A.E., Skjold T., Roekaerts D.J.E.M., Pasman H.J., Eckhoff R.K., Hanjalic K., and Donze M. On the application of the Levenberg-Marquardt method in conjunction with an explicit Runge-Kutta and an implicit Rosenbrock method to assess burning velocities from confined deflagrations. *Flow, Turbulence and Combustion*, 91:281–317, 2013.

[41] Lewis B. and von Elbe G. *Combustion, Flames and Explosions of Gases*. Academic Press, third edition, 1987.

[42] Dahoe A.E., Zevenbergen J.F., Lemkowitz S.M., and Scarlett B. Dust explosions in spherical vessels: the role of flame thickness in the validity of the 'cube-root-law'. *Journal of Loss Prevention in the Process Industries*, 9(1):33–44, 1996.

[43] Bradley D. and Mitcheson A. The venting of gaseous explosions in spherical vessels. I – Theory. *Combustion and Flame*, 32:221–236, 1978.

[44] Bradley D. and Mitcheson A. The venting of gaseous explosions in spherical vessels. II – Theory and experiment. *Combustion and Flame*, 32:237–255, 1978.

[45] Bartknecht W. *Dust Explosions: Course, Prevention, Protection*. Springer Verlag, 1989. Translation of *Staubexplosionen* by R.E. Bruderer, G.N. Kirby and R. Siwek.

[46] VDI 2263 Blatt 1. Druckentlastung von Staubexplosionen. Verein Deutcher Ingenieure (VDI), 2002. English translation: Pressure venting of dust explosions.

[47] Tamanini F. Scaling parameters for vented gas and dust explosions. *Journal of Loss Prevention in the Process Industries*, 14:455–461, 2001.

[48] Ponizy B. and Leyer J.C. Flame dynamics in a vented vessel connected to a duct: I. Mechanism of vessel-duct interaction. *Combustion and Flame*, 116:259–271, 1999.

[49] Ponizy B. and Leyer J.C. Flame dynamics in a vented vessel connected to a duct: II. Influence of ignition site, membrane rupture, and turbulence. *Combustion and Flame*, 116:272–281, 1999.

[50] Ponizy B. and Veyssiere B. Mitigation of explosions in a vented vessel connected to a duct. *Combustion Science and Technology*, 158:167–182, 2000.

[51] Bauwens C.R., Dorofeev S., and Tamanini F. Effects of aspect ratio and ignition location on vented explosion pressures. In *Proceedings of the Fifth International Seminar on Fire and Explosion Hazards*, pages 292–301, Edinburgh, United Kingdom, 23–27 April 2007. University of Edinburgh.

[52] Marinov N.M., Westbrook C.K., and Pitz W.J. Detailed and Global Chemical Kinetics Model for Hydrogen. In S.H. Chan, editor, *Transport Phenomena in Combustion*, volume 1, pages 118–129, Washington, DC, 1996. Taylor & Francis.

[53] Dowdy D.R., Smith D.B., S.C. Taylor, and Williams A. The use of expanding spherical flames to determine burning velocities and stretch effects in hydrogen-air mixtures. In *Proceedings of the Twenty-Third Symposium (International) on Combustion*, pages 325–332, Pittsburgh, 1990. The Combustion Institute.

[54] Kwon O.C. and Faeth G.M. Flame/stretch interactions of premixed hydrogen-fueled flames: measurements and predictions. *Combustion and Flame*, 124:590–610, 2001.

[55] Tse S.D., Zhu D.L., and Law C.K. Morphology and burning rates of expanding spherical flames in H_2/O_2/inert mixtures up to 60 atmospheres. In *Proceedings of the Twenty-Eighth Symposium (International) on Combustion*, pages 1793–1800, Pittsburgh, 2000. The Combustion Institute.

[56] Damköhler G. Der Einfluss der Turbulenz auf die Flammengeschwindigkeit in Gasgemischen. *Zeitschrift für Elektrochemie*, 46:601–626, 1940.

[57] Damköhler G. The effect of turbulence on the flame velocity in gas mixtures. Technical Memorandum NACA TM 1112, National Advisory Committee for Aeronautics, Washington, 1947.

[58] Schelkin K.I. On combustion in a turbulent flow. *Soviet Physics – Technical Physics*, 13:520–530, 1943.

[59] Schelkin K.I. On combustion in a turbulent flow. NACA Technical Memorandum 1110, National Advisory Committee for Aeronautics, Washington, Feruary 1947. Original: Jour. Tech. Phys. (USSR), vol. 13, nos. 9–10, 1943, pp. 520–530.

[60] Karlovitz B., Denniston D.W., and Wells F.E. Investigation of turbulent flames. *Journal of Chemical Physics*, 19(5):541–547, 1951.

[61] Taylor G.I. Diffusion by continuous movements. *Proceedings of the London Mathematical Society*, 20:196–212, 1922.

[62] Leason D.B. Turbulence and flame propagation in premixed gases. *Fuel*, 30:233–239, 1951.

[63] Andrews G.E., Bradley D., and Lwakabamba S. B. Turbulence and turbulent flame propagation – A critical appraisal. *Combustion and Flame*, 24:285–304, 1975.

[64] Tucker M. Interaction of a free flame front with a turbulence field. Technical Note NACA TN 3407, National Advisory Committee for Aeronautics, Washington, March 1955.

[65] Clavin P. and Williams F.A. Theory of premixed-flame propagation in large-scale turbulence. *Journal of Fluid Mechanics*, 90:589–604, 1979.

[66] Clavin P. and Williams F.A. Effects of molecular diffusion and of thermal expansion on the structure and dynamics of premixed flames in turbulent flows of large scale and low turbulence. *Journal of Fluid Mechanics*, 116:251–282, 1982.

[67] Gülder Ö.L. Turbulent premixed flame propagation models for different combustion regimes. In *Proceedings of the Twenty-Third Symposium (International) on Combustion*, pages 743–750, Pittsburgh, 1990. The Combustion Institute.

[68] Klimov A.M. Premixed turbulent flames – interplay of hydrodynamic and chemical phenomena. *Progress in Astronautics and Aeronautics*, 88:133–146, 1983.

[69] Abdel-Gayed R.G., Ali-Khishali K.J., and Bradley D. Turbulent burning velocity and flame straining in explosions. *Proceedings of the Royal Society of London, Series A: Mathematical and Physical Sciences*, 391:393–414, 1984.

[70] Bradley D., Lau A.K.C., and Lawes M. Flame stretch as a determinant of turbulent burning velocity. *Philosophical Transactions of the Royal Society of London, Series A: Mathematical and Physical Sciences*, 338:359–387, 1992.

[71] Pope S.B. and Anand M.S. Flamelet and distributed combustion in premixed turbulent flames. In *Proceedings of the Twentieth Symposium (International) on Combustion*, pages 403–410, Pittsburgh, 1984. The Combustion Institute.

[72] Kerstein A.R. Pair-exchange model of turbulent premixed flame propagation. In *Proceedings of the Twenty-First Symposium (International) on Combustion*, pages 1281–1289, Pittsburgh, 1986. The Combustion Institute.

[73] Gouldin F.C. An application of fractals to modeling premixed turbulent flames. *Combustion and Flame*, 68:249–266, 1987.

[74] Lovejoy S. The area-perimeter relation for rain and cloud areas. *Science*, 216:185–187, 1982.

[75] Hentschel H.G.E. and Procaccia I. Relative diffusion in turbulent media: the fractal dimension of clouds. *Physical Review A*, 29:1461–1470, 1984.

[76] Sreenivasan K.R. and Meneveau C. The fractal facets of turbulence. *Journal of Fluid Mechanics*, 173:357–186, 1986.

[77] Abdel-Gayed R.G. and Bradley D. Derivation of turbulent transport coefficients from turbulent parameters in isotropic turbulence. *Journal of Fluids Engineering, Transactions of the ASME*, 99:732–736, 1977.

[78] Peters N. Laminar flamelet concepts in turbulent combustion. In *Proceedings of the Twenty-First Symposium (International) on Combustion*, pages 1231–1250, Pittsburgh, 1988. The Combustion Institute.

[79] Peters N. Length scales in laminar and turbulent flames. *Progress in Astronautics and Aeronautics*, 135:155–182, 1991.

[80] Yakhot V. Propagation velocity of premixed turbulent flames. *Combustion Science and Technology*, 60:191–214, 1988.

[81] Kerstein A.R. Simple derivation of Yakhot's turbulent premixed flamespeed formula. *Combustion Science and Technology*, 60:163–165, 1988.

[82] Poinsot T. and Veynante D. *Theoretical and numerical combustion.* Edwards, Philadelphia, second edition, 2005.

[83] Kerstein A.R., Ashurst W., and Williams F.A. Field equation for interface propagation in an unsteady homogeneous flow field. *Physical Review A*, 37:2728–2731, 1988.

[84] Liu Y. and Lenze B. The influence of turbulence on the burning velocity of premixed CH4–H2 flames with different laminar burning velocities. In *Proceedings of the Twenty-Second Symposium (International) on Combustion*, pages 747–754, Pittsburgh, 1988. The Combustion Institute.

[85] Tennekes H. and Lumley J.L. *A first course in turbulence.* MIT Press, Cambridge, MA, 1972.

[86] Hinze J.O. *Turbulence.* McGraw-Hill Series in Mechanical Engineering, New York, second edition, 1975.

[87] Leuckel W., Nastoll W., and Zarzalis N. Experimental investigation of the influence of turbulence on the transient premixed flame propagation inside closed vessels. In *Proceedings of the Twenty-Third Symposium (International) on Combustion*, pages 729–734, Pittsburgh, 1990. The Combustion Institute.

[88] Abdel-Gayed R.G., Bradley D., and Lawes M. Turbulent burning velocities: a general correlation in terms of straining rates. *Proceedings of the Royal Society of London, Series A: Mathematical and Physical Sciences*, 414:389–413, 1987.

[89] Zimont V.L. and Lipatnikov A.N. A numerical model of premixed turbulent combustion of gases. *Chemical Physics Reports*, 14:993–1025, 1995.

[90] Bray K.N.C., Libby P.A., and Moss J.B. Flamelet crossing frequencies and mean reaction rates in premixed turbulent combustion. *Combustion Science and Technology*, 41:143–172, 1984.

[91] Bray K.N.C., Libby P.A., and Moss J.B. Unified modelling approach for premixed turbulent combustion – Part I: General formulation. *Combustion and Flame*, 61:87–102, 1985.

[92] Bray K.N.C. and Libby P.A. Passage times and flamelet crossing frequencies in premixed turbulent combustion. *Combustion Science and Technology*, 47:253, 1986.

[93] Shy S.S., Lin W.J., and Wei J.C. An experimental correlation of turbulent burning velocities for premixed turbulent methane-air combustion. *Proceedings of the Royal Society of London, Series A: Mathematical and Physical Sciences*, 456:1997–2019, 2000.

[94] Hamberger P., Schneider H., Jamois D., and Proust C. Correlation of turbulent burning velocity and turbulence intensity for starch dust air mixtures. Proceedings of the Third European Combustion Meeting, 11–13 April 2007, Chania, Greece, 2007.

[95] Bray K.N.C. Studies of the turbulent burning velocity. *Proceedings of the Royal Society of London, Series A: Mathematical and Physical Sciences*, 431:315–335, 1990.

[96] Schneider H. and Proust C. Determination of turbulent burning velocities of dust air mixtures with the open tube method. *Journal of Loss Prevention in the Processes Industries*, 20:470–476, 2007.

[97] Chapman D.L. On the rate of explosion in gases. *Physics of Fluids*, 47:90–104, 1899.

[98] Jouguet E. On the propagation of chemical reactions in gases. *Journal de Mathematiques Pures et Appliquees*, 1:347–425, 1906.

[99] Zeldovich Ya.B. On the theory of the propagation of detonation in gaseous systems. *Journal of Experimental and Theoretical Physics*, 10:542–568, 1940.

[100] Neumann J. von. Theory of detonation waves. In A.H. Taub, editor, *John von Neumann, Collected Works*, volume 6 of *Theory of games, astrophysics, hydrodynamics and meteorology*. Pergamon, Oxford, 1942.

[101] Döring W. Uber den detonationvorgangin gases. *Ann. Phys. Lpz.*, 43:421–436, 1943.

[102] Hirschfelder J.O., Curtiss C.F., and Bird R.B. *The molecular theory of gases and liquids*. John Wiley & Sons, New York, fourth edition, 1967.

[103] Austin J.M. *The Role of Instability in Gaseous Detonation*. PhD thesis, California Institute of Technology, California, United States of America, May 2003.

[104] Akbar R. *Mach reflection of gaseous detonations*. PhD thesis, Rensselaer Polytechnic Institute, New York, United States of America, August 1997.

[105] Eckett C. A., Quirk J. J., and Shepherd J. E. The role of unsteadiness in direct initiation of gaseous detonations. *Journal of Fluid Mechanics*, 421:147–183, 2000.

[106] Pintgen F., Eckett C.A., Austin J.M., and Shepherd J.E. Direct observations of reaction zone structure in propagating detonations. *Combustion and Flame*, 133:211–229, 2003.

[107] Urtiew P.A. and Oppenheim A.K. Experimental observations of transition to detonation in explosive gas. *Philosophical Transactions of the Royal Society of London, Series A: Mathematical and Physical Sciences*, 295:13–38, 1966.

[108] Westbrook C.K. Chemical-kinetics of hydrocarbon oxidation in gaseous detonation. *Combustion and Flame*, 46:191–216, 1982.

[109] Shepherd J. Chemical kinetics of hydrogen-air-diluent detonations. *Progress in Aeronautics and Astronautics*, 106:263–293, 1986.

[110] Shepherd J., Moen I.O., Murray S., and Thibault P. Analysis of the cellular structure of detonations. In *Proceedings of the Twenty-First Symposium (International) on Combustion*, pages 1649–1658, Pittsburgh, 1986. The Combustion Institute.

[111] Lee J.H.S. Dynamic parameters of gaseous detonations. *Annual Reviews of Fluid Mechanics*, 16:311–336, 1984.

[112] Breitung W., Chan C.K., Dorofeev S.B., Eder A., Gelfand B.E., Heitsch M., Klein R., Malliakos A., Shepherd J.E., Studer E., and Thibault P. Flame acceleration and deflagration to detonation transition in nuclear safety. State-of-the-art report by a group of experts, OECD Nuclear Energy Agency, August 2000.

[113] Ciccarelli G. Critical tube measurements at elevated initial mixture temperatures. *Combustion Science and Technology*, 174:173–183, 2002.

[114] Knystautas R., Lee J.H.S., Moen I.O., and Wagner H.Gh. Direct initiation of spherical detonation by a hot turbulent gas jet. In *Proceedings of the Seventeenth Symposium (International) on Combustion*, pages 1235–1245, Pittsburgh, 1979. The Combustion Institute.

[115] Schauer F.R., Miser C.L., Tucker K.C., Bradley R.P., and Hoke J.L. Detonation initiation of hydrocarbon-air mixtures in a pulsed detonation engine. AIAA-paper 2005-1343, 2005.

[116] Grossel S.S. *Deflagration and detonation flame arresters*. American Institute of Chemical Engineers, Center for Chemical Process Safety, New York, 2002.

[117] Kuo K.K. *Principles of Combustion*. John Wiley & Sons, New York, second edition, 2005.

[118] Nettleton M.A. *Gaseous Detonations: their nature, effects and control*. Chapman and Hall, 1987.

[119] Williams F.A. *Combustion Theory: the fundamental theory of chemically reacting flow systems*. Combustion Science and Engineering Series. The Benjamin/Cummings Publishing Company, Menlo Park, California, second edition, 1985.